A STRUCTURAL ANALYSIS OF SMOOTH-TOPPED CHAOTIC TERRAINS IN SOUTHERN CIRCUM-CHRYSE, MARS

Jonathan Walmsley, BSc. (Hons.)

Submitted in partial fulfillment
of the requirements for the degree of

Master of Science in Earth Sciences

Faculty of Math and Science, Brock University
St. Catharines, Ontario

Abstract

The presence of large outflow channels on Mars shows the importance of water in shaping the surface of the planet over geologic time. Chaotic terrain has been identified as the source region for flood waters responsible for carving out many of these channels. There are still many unanswered questions regarding chaotic terrains on Mars. Using the most up to date CTX, HRSC, and MOLA coverage, DEM and TIN models were used to investigate examples of smooth-topped chaotic terrains which include Hydraotes Chaos, a crater pair in Hydraspis Chaos, Baetis Chaos, and Candor Chaos, all south of Chryse Planitia. The findings of this study suggest that the collapse of chaotic terrains is not regionally controlled. This study also suggests that the largest chaotic terrains do not require external heat sources to form. Finally, there is evidence that chaotic terrain forming events have occurred from the Middle Noachian to the Late Hesperian/Early Amazonian.

Acknowledgements

I would like to express sincere appreciation to Professor Frank Fueten for the multitude of opportunities and the endless assistance he has provided me. I would also like to thank Dr. Bob Stesky for his insights and hours of editorial work and feedback as well as my other committee members Professor Rick Cheel, and Professor Mariek Schmidt. Lastly, I would also like to thank all my friends and family which have supported and guided me through my academic career and will continue to do so for the future.

Table of Contents

List of Figures

Chapter 1

Chapter 2

Chapter 3

Chapter 4

Chapter 5

Chapter 6

Chapter 7

List of Tables

Chapter 1

Chapter 3

Chapter 4

Chapter 5

Chapter 6

Chapter 7

List of Abbreviations

FFC	Fractured-Floor Crater
SLE	Single-Layered Ejecta
MLE	Multi-Layered Ejecta
HRSC	High Resolution Stereo Camera
CTX	Context Camera
MOLA	Mars Orbiter Laser Altimeter
DEM	Digital Elevation Model
PDS	Planetary Data System
AVA	Augmented Visualization of Attitude
TIN	Triangular Irregular Network
ILD	Interior Layered Deposit

Chapter 1.0 **: Introduction**

1.1 Mars

Finding life on other celestial bodies has been and continues to be a driving force in the study of planetary science. The discovery of large outflow channels on Mars during the Mariner 9 mission and their subsequent characterization (Sharp & Malin, 1975) has led to the study of these channels as possible hosts for life. Chaotic terrains on Mars have been interpreted to be the source location for floods which carved out many of these outflow channels (Lucchitta & Ferguson, 1983; Carr, 1987; Ori & Mosangini, 1998; Andrews-Hanna & Phillips, 2007; Harrison & Grimm, 2008; Baker, et al., 2015; Rodriguez, et al., 2015), making them excellent targets of study.

The objective of this study is to answer key questions regarding the collapse and formation of chaotic terrains on Mars; do chaotic terrains require external sources of heating as many authors have suggested, is their collapse controlled by the underlying regional geology, and when did they form. To answer these questions smooth-topped chaotic terrains of each type (primary, secondary, and Fractured-Floor Craters) were chosen to find a link between different chaotic terrains around Valles Marineris and its main outflow channels which debouch into Chryse Planitia. Study sites include Hydraotes Chaos, a crater pair in Hydraspis Chaos, Baetis Chaos, and Candor Chaos (Figure 1-4). Chaotic terrains with smooth-topped mesa blocks were chosen to acquire measurements of surface strike and dip.

1.2 Geological and Climatic Background of Mars

The Martian geologic time scale is divided into three epochs: The Noachian (4.55 - 3.7 Ga), the Hesperian (3.7 - 3.0 Ga), and the Amazonian (~3.0 Ga - Present) (Tanaka & Hartmann, 2012). Relative dating of Martian surfaces is derived from surface crater counting calibrated to impact-crater flux models, and samples taken from Earth's Moon (Tanaka & Hartmann, 2012).

The Noachian (4.55 - 3.7 Ga) was characterized by heavy impact cratering causing the formation of the major basins on Mars like Hellas Basin (Figure 1-1) and the dichotomy boundary (Figure 1-1). Over this time the atmosphere was thought to have been much denser and there were sufficiently warm periods of time for liquid water to exist on the surface (Fanale, et al., 1992). The Tharsis province (Figure 1-1) began forming by the middle Noachian with heavy volcanism occurring (Tanaka, et al., 1992). By the late Noachian, valley networks started forming (Tanaka & Hartmann, 2012). Atmospheric losses were likely substantial, accelerated by a loss in the global magnetosphere, impacts, and hydrodynamic escape, removing most of the Martian atmosphere by the early Hesperian (Fanale, et al., 1992; Catling, 2009).

The Hesperian (3.7 - 3.0 Ga) was a time of major volcanism accompanied by major rifting in Valles Marineris (Figure 1-1) and the surrounding area of Tharsis. The major outflow channels developed during this time, giving evidence for large volumes of surface water. During the Hesperian most of the atmosphere had been lost (Melosh & Vickery, 1989) and therefore surface pressures and temperatures were below freezing, leading to the growth of the global cryosphere (Weiss & Head, 2017).

Initially the Amazonian (~3.0 Ga - Present) still had high rates of volcanism based on the area of the planet covered by volcanic deposits of this age, but these rates declined to their current levels of no active surface volcanism (Tanaka, et al., 1988). Through the Amazonian the climate has been and still is cold and dry, and water ice is limited to the polar ice caps and elsewhere on the planet within the subsurface. Most surface activity has ceased; erosion and deposition are aeolian dominated (Tanaka & Hartmann, 2012).

1.2.1 The Dichotomy Boundary

The dichotomy boundary (Figure 1-1) is a major geologic division between the southern highlands and northern lowlands and can be traced around the planet. The dichotomy likely formed before 4.19 Ga making it one of the oldest features on Mars (Roberts & Zhong, 2006; Frey, 2006). It is approximately elliptical in shape when compensated for Tharsis loading (Andrews-Hanna, et al., 2008). On average the northern lowlands are 3 – 6 km lower in elevation with an estimated crustal thickness of 32 km versus the southern highlands which have a crustal thickness of 58 km (Roberts & Zhong, 2006). The suggested causes of the dichotomy include: a giant impact (Andrews-Hanna, et al., 2008; Marinova, et al., 2008), several impact events (Frey, 2006), or mantle convection/overturn (Roberts & Zhong, 2006).

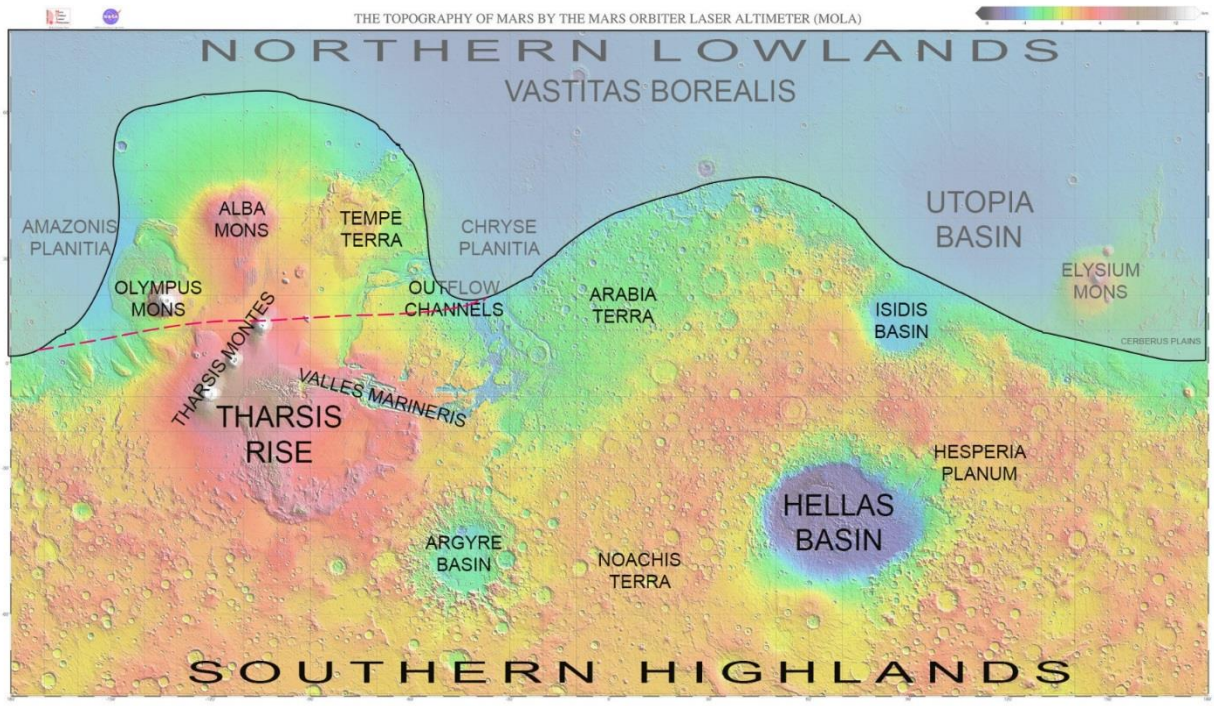

Figure 1-1 Topographic map of the surface of Mars. Major surface features are labelled as well as the Northern Lowlands and Southern Highlands. A rough trace of the Dichotomy (black line) and interpreted boundary (Andrews-Hanna, et al., 2008) under Tharsis (dashed red line). MOLA map: NASA / JPL / GSFC. Map by Emily Lakdawalla

1.2.2 Climate Models of Early Mars

The extensive presence of valley networks and outflow channels on the surface of Mars indicates large volumes of liquid water were present on the surface of Mars between the late Noachian and early Hesperian (Tanaka & Hartmann, 2012). A substantial portion of this water is thought to have been released by catastrophic collapse of chaotic terrains. This requires water to be stored in the subsurface either as water in an aquifer system or as buried ice lenses/sheets. Currently water on the surface of Mars is unstable (susceptible to boiling/freezing) due to the low atmospheric pressure and low surface temperatures. To explain this difference two main climatic models are posited. The first requires long-term warm and wet conditions (Craddock & Howard, 2002; Wordsworth, et al., 2015), while the second assumes a planet which is

frozen and experiences episodic or seasonal melting of snow and ice to provide temporary liquid water at the surface (Wordsworth, et al., 2013; Wordsworth, et al., 2015).

To sustain a warm and wet climate on Mars requires a much thicker atmosphere of 1-2 bar (Phillips, et al., 2001). For reference the current Martian atmospheric pressure is 0.006 bar. This atmosphere would be made up primarily of CO_2 (Wordsworth, et al., 2013; Wordsworth, et al., 2015), much of which would come from volcanic sources. A thicker atmosphere would allow for surface lakes to form producing runoff and drainage systems.

Several recent studies (Wordsworth, et al., 2013; Wordsworth, et al., 2015; Palumbo, et al., 2018) have found that the cold climate model more closely matches the spatial distribution of valley networks and chaotic terrain. In the cold climate model, a northern highlands ice sheet would form and during peak temperatures would allow for melting and run off to occur, producing the adjacent valley networks. This cold climate model allows for accumulation of ice sheets and glaciers, which could be potential sources for buried ice, with melting triggering catastrophic flood events.

1.2.3 Presence of a Global Ocean

Further evidence for large volumes of surface water comes in the form of putative paleo-shorelines used to show the existence of a northern ocean (Parker, et al., 1993; Head, et al., 1999; Clifford & Parker, 2001; Carr & Head, 2003). One of the problems with this theory is the wide variability of the elevation of these shorelines. Modeling by Citron et al. (2018) shows that the emplacement of Tharsis could be mostly responsible

for the deformation of these shorelines. They hypothesize that the Arabia shoreline formed (4.0 Ga) before and during the emplacement of Tharsis while subsequent shorelines represent a decline in ocean volume during late Tharsis emplacement. Figure 1-2 shows the possible extent of the Arabia Ocean accounting for the removal of Tharsis.

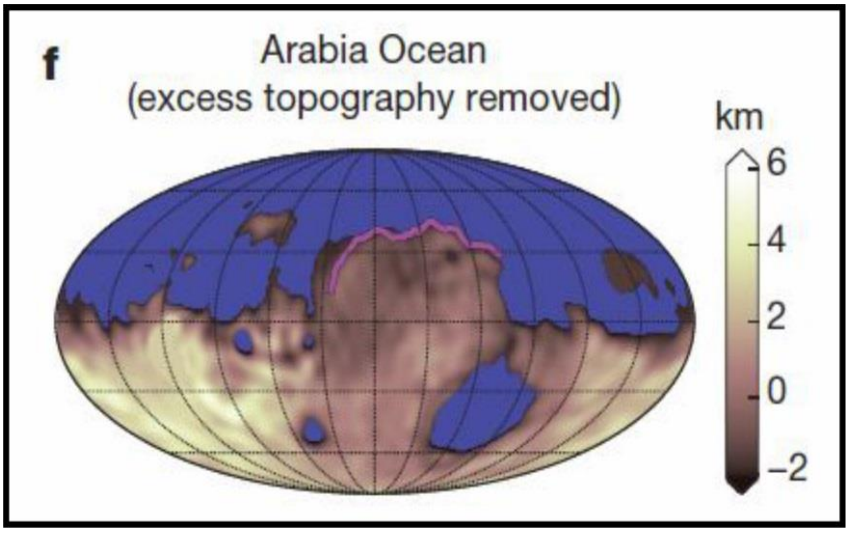

Figure 1-2 Model of the extent of the Arabia Ocean accounting for Tharsis, Elysium, and polar topography. (From Citron et al. 2018)

The emplacement of Tharsis has been cited by Citron et al. (2018) as being the major controlling factor for the decline of the northern ocean. The declining northern ocean produced another, less deformed shoreline, which is called Deuteronilus and was emplaced by 3.6 Ga (Citron, et al., 2018). Figure 1-3 shows the extent of the Deuteronilus ocean based on paleo-shorelines.

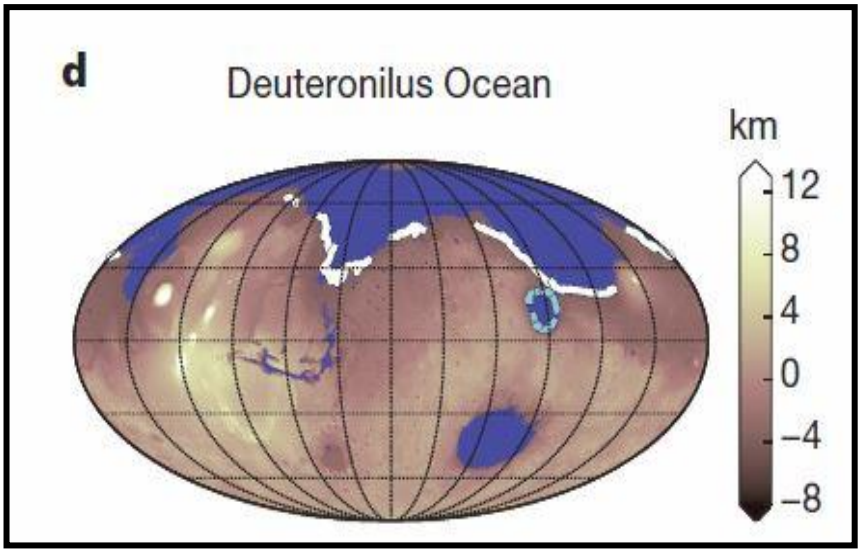

Figure 1-3 Extent of the Deuteronilus Ocean with Martian topography. (From Citron et al. 2018)

1.2.4 The Global Cryosphere

Under the current Martian climate water can not exist on the surface for extended periods meaning the majority of surface water on Mars is frozen. The Martian global cryosphere is the area of subsurface which experiences temperatures below the freezing point of water over a period of at least two years (Clifford, et al., 2010). This area grows and shrinks as the freezing front moves. The general trend of cooling on Mars suggests that this freezing front moves deeper over time, locking up more and more groundwater in the cryosphere. Clifford & Parker (2001) hypothesize that the current global cryosphere thickness is 2.3 – 4.7 km at the equator with newer estimates of ~5 – 9 km (Clifford, et al., 2010) and that it is unlikely that groundwater exists under the cryosphere in the current Martian climate. Several studies have estimated the depth of the ancient global cryosphere and their results are shown below (Table 1-1).

Table 1-1 Summation of previous cryosphere depth estimates.

Author	Cryosphere Depth	Age
Coleman (2005)	700 – 1000 m (Xanthe Terra)	Mid-Upper Hesperian
Andrews-Hanna & Phillips (2007)	1 – 3 km (Equator)	Hesperian (3.7 – 3.0 Ga)
Harrison & Grimm (2008)	2.8 km (Equator)	Hesperian
Weiss & Head (2017)	1.3 km (Equator)	Hesperian - Amazonian

To estimate the thickness of the cryosphere Weiss & Head (2017) used Single-Layered Ejecta (SLE) and Multiple-Layered Ejecta (MLE) crater excavation depths. The transition from SLE to MLE craters is thought to occur as excavation depth reaches below an ice-cemented target (cryosphere). Their evidence suggests an equatorial cryosphere thickness of 1.3 km for the Late Hesperian – Early Amazonian. Their modeling suggests that the thickness of the cryosphere during the Amazonian is much less than previously expected. This is possibly due to a 'supply-limited' cryosphere; where the thickness of the cryosphere depends on the volume of water available in the subsurface. Their results suggest that the global cryosphere reached its maximum thickness 3.0 – 3.3 Ga (Late Hesperian – Early Amazonian, at the latest).

1.3 Chaotic Terrain

Chaotic terrain (Figure 1-4 and 1-5) is a geologic feature which consists of ridges, knobs, and smooth-topped crustal blocks in a basin, interpreted to have collapsed. Chaotic terrain is a unique geologic feature of Mars (Sharp, et al., 1971). Other features called “chaotic terrain” are present on Mercury (Schultz & Gault, 1975) and Europa (Greenberg, et al., 1999); however they are unrelated to Martian chaotic terrain; where Martian chaotic terrain is made of crustal material collapsing due to removal of subsurface material, the “chaotic terrain” on Europa is made from ice and forms in areas where the thin icy shell of the moon is breached by underlying liquid water (Greenberg, et al., 1999), on Mercury “chaotic terrain” is thought to form as a result of strong seismic activity created by impact events (Schultz & Gault, 1975).

Chaotic terrain on Mars was first described by Sharp et al. in 1971 based on Mariner 6 and 7 photography. They described chaotic terrain as “a rough, irregular complex of short ridges, knobs, and irregularly shaped troughs and depressions”. Chaotic terrains on Mars occur in depressions, some of which can be very large like Aurorae Chaos (Figure 1-4), which covers more than 88,000 km^2, while others are contained in craters of <700 km^2. The largest areas of chaotic terrain are dominated by irregular knobs and ridges, while smaller areas like the Hydraspis crater pair (Figure 1-4), contain a mixture of large flat-topped plateau blocks and knobs. These terrains are mainly associated with the large outflow channels on Mars, the largest of which flows out of the eastern end of Valles Marineris eventually emptying into Chryse Planitia. A substantial proportion of chaotic terrain is also located near the Martian dichotomy boundary (Bamberg, et al., 2014). Generally, chaotic terrain is thought to be the source

location for catastrophic flooding (Lucchitta & Ferguson, 1983; Carr, et al., 1987; Ori & Mosangini, 1998; Andrews-Hanna & Phillips, 2007; Harrison & Grimm, 2008; Baker, et al., 2015; Rodriguez, et al., 2015) and has been found to have a “strong link” to the dichotomy boundary (Bamberg, et al., 2014; Roda et al., 2014). Impact craters are the simplest explanation as sinks for water concentrating in some areas and not others given their abundance (Roda et al., 2014).

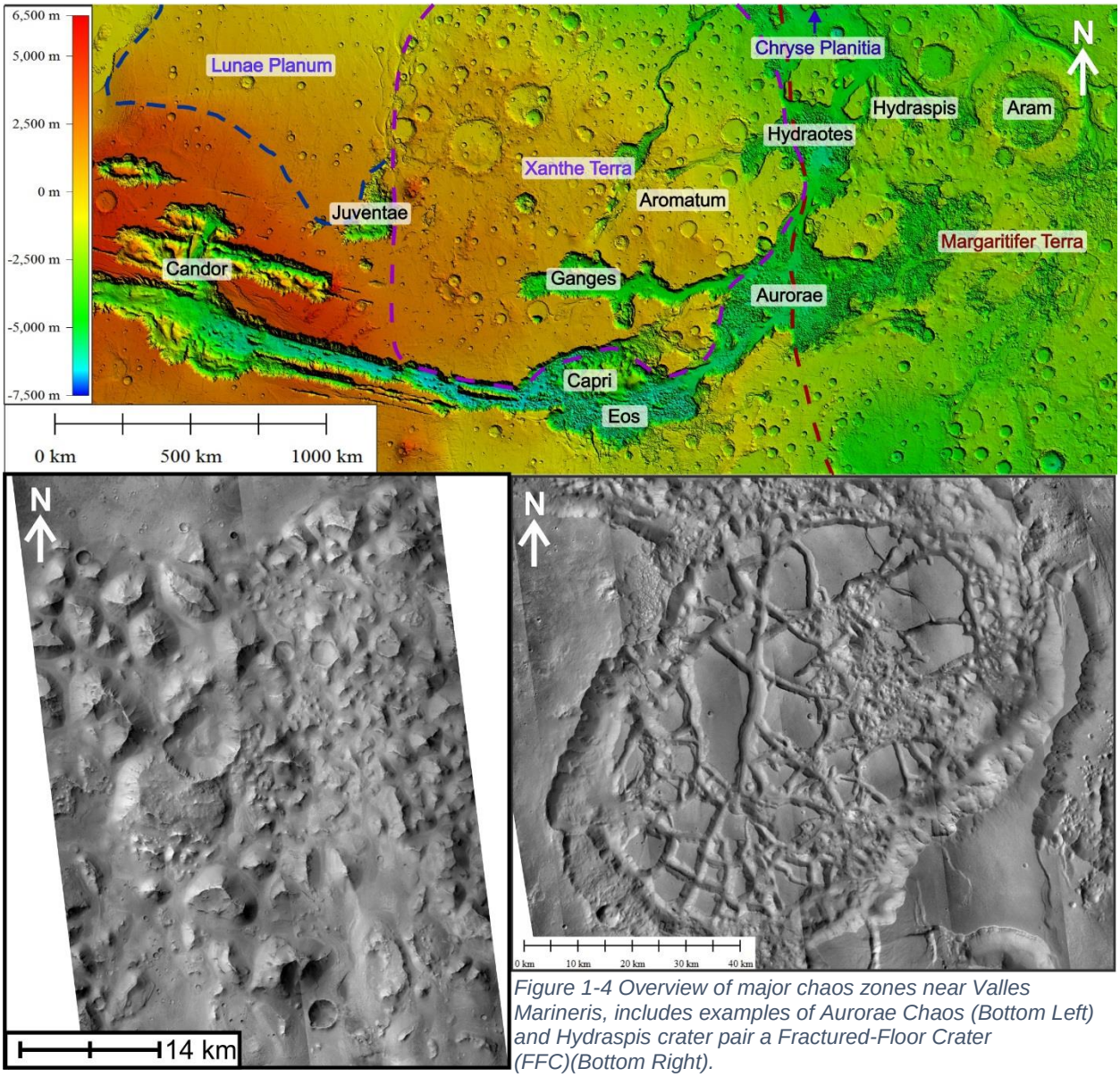

Figure 1-4 Overview of major chaos zones near Valles Marineris, includes examples of Aurorae Chaos (Bottom Left) and Hydraspis crater pair a Fractured-Floor Crater (FFC)(Bottom Right).

The types of chaotic terrains described in the literature are primary chaotic terrains (Ori & Mosangini, 1998), secondary chaotic terrains (Rodríguez, et al., 2011), and Fractured-Floor Craters (FFCs) (Bamberg, et al., 2014). Primary chaotic terrains are those described above, cover a wide range of size with some areas over 88,000 km^2, and others less than 700 km^2, the formation of which produces catastrophic flooding which can erode outflow channels. The largest area of primary chaotic terrain on Mars is located east of Valles Marineris, comprising most of Capri Chasma, Eos Chasma, and Aurorae Chaos.

Secondary chaotic terrain is described in detail by Rodríguez et al. (2011). Secondary chaotic terrains cover a much smaller area than primary chaotic terrains, and they do not result in catastophic flooding. Secondary chaotic terrain (Figure 1-5) is present in the floors of many of the outflow channels which flow into Chyrse Planitia, and as such were likely triggered by catastophic floods generated as a result of the formation of primary chaotic terrains. Their surficial features are similar to primary chaos with mesa and knobs present, but they tend to be much smaller and the depth of collapse (< 1 km (Rodríguez, et al., 2011)) is much less than for the primary chaos (several km).

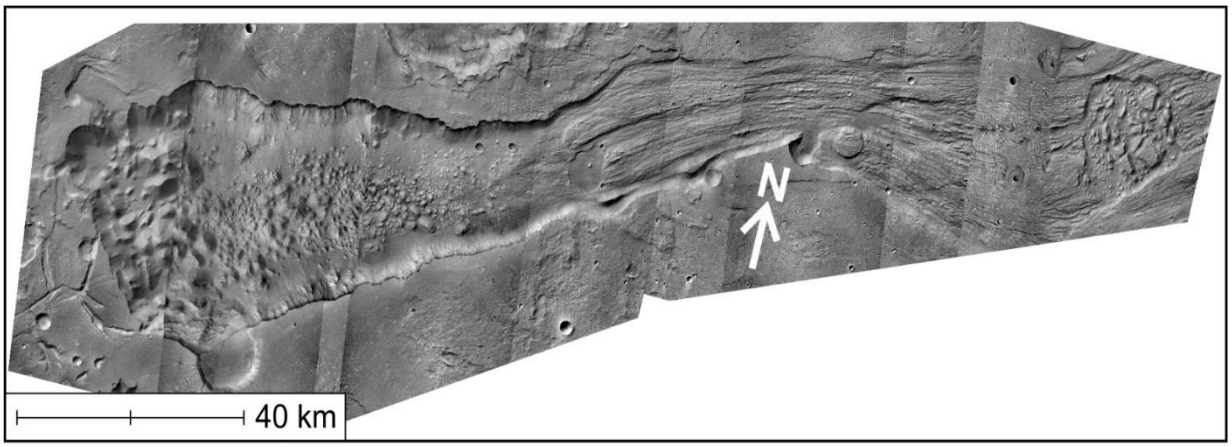

Figure 1-5 Example of a Primary Chaos (Aromatum (Figure 1-4), Left) interpreted to have produced a Secondary Chaos (Iamuna, Right) through flooding and erosion (Coleman, 2005).

Fractured-Floor Craters (FFCs) (Figure 1-4) are craters on Mars which display a similar morphology to primary chaotic terrains, with mesas and knobs in a depression. The main differences between primary chaotic terrains and FFCs are that FFCs can be formed by removal of volcanic material from below, upwelling onto the surface following impact, and FFCs are, by definition, contained within identified craters. The depressions which other primary chaotic terrains form in could be previous craters (Roda, et al., 2016) however this is only a hypothesis. The highest density of FFCs is along the dichotomy boundary (Bamberg, et al., 2014), many of which are also located east of Valles Marineris (Bamberg, et al., 2014), which suggests a link between the dichotomy boundary zone and chaotic terrains.

1.4 Formation of Martian Chaotic Terrain

Several different hypotheses for the formation of chaotic terrains on Mars have been proposed. The models for primary chaotic terrains include pressurized aquifer eruption (Chapman & Tanaka, 2002; Coleman, 2005; Andrews-Hanna & Phillips, 2007), partial melting and release of water involving magmatism (Leask, et al., 2006; Meresse,

et al., 2008), subsurface ice lake destabilization (Zegers, et al., 2010), and release of carbon dioxide or methane gas trapped in clathrates (Rodriguez, et al., 2006; Komatsu, et al., 2000). Many previous studies (Komatsu, et al., 2000; Leask, et al., 2006; Rodriguez, et al., 2006; Meresse, et al., 2008) of chaotic terrain proposed the existence of an intrusive body or other localized heat source to trigger melting and collapse of the terrain. The formation mechanisms for FFCs are generally similar to primary chaotic terrains, requiring subsurface ice/water interaction causing collapse, with the exception of purely intrusive volcanism with no water/ice interaction. Secondary chaotic terrains (Rodríguez, et al., 2011) have a different set of possible formation mechanisms, but in general they require subsurface volatiles being removed, either through excavation, or pressurization. More in-depth descriptions of the possible explanations for chaotic terrains on Mars is given below.

1.4.1 Pressurization of Subsurface Aquifer

Several authors (Chapman & Tanaka, 2002; Coleman, 2005; Andrews-Hanna & Phillips, 2007) have suggested that hydrostatic pressure build up in a confined global aquifer system under the cryosphere causes catastrophic flooding where it breaches the surface. Removal of this water causes collapse of the above terrain forming chaotic terrain. In a confined system pressure can be built up over time either through surface loading or the downward migration of the cryosphere freezing front. Other authors (Harrison & Grimm, 2009) have suggested that this aquifer system is compartmentalized on a local or regional scale and that the distribution of groundwater is heterogeneous.

A model for FFC formation (Sato, et al., 2010; Bamberg, et al., 2014) also includes a confined groundwater aquifer system. Outbursts onto the surface cause a rapid drop in the groundwater table (Sato, et al., 2010; Bamberg, et al., 2014) followed by earth fissuring and seepage erosion which removes material under and away from the area just inside the crater rim (Sato, et al., 2010; Bamberg, et al., 2014).

1.4.2 Magmatic Intrusion

Meresse et al. (2008) proposed a 3-stage model for the development of chaotic terrain in Hydraotes caused by an intrusive body. Stage 1 calls for the emplacement of a sill beneath pre-fractured crust, pre-fracturing being caused by local subsidence or impact cratering. In Stage 2 the sill destabilizes the aquifer causing further subsidence and fracturing as groundwater is released onto the surface. In Stage 3 the removal of subsurface water causes a second collapse. This is followed by a period of surface volcanism as the sill extrudes onto the surface, causing cinder cones to form.

The magmatic intrusion model (Bamberg, et al., 2014) for FFCs requires a volcanic body (sill, dike, laccolith) which exploits the reduction of crustal thickness, causing uplift inside the crater. The uplift drives fracturing of the crater floor and may happen several times (Bamberg, et al., 2014). This process does not produce flooding, however magma can reach the surface producing fresh infilling on the crater floor (Bamberg, et al., 2014).

1.4.3 Subsurface Lake Destabilization

An example of the subsurface lake destabilization model was developed to explain the origins of Aram Chaos contained in Aram Crater (Figure 1-4) by Zegers et al. (2010) and Zeger & Roda (2012) based on an older model suggested by Manker & Johnson (1982). This model assumes a surface mean temperature of -40°C and as a reference point uses a value of 1.4 $Wm^{-1}\ K^{-1}$ for the thermal conductivity of the sediment package and 25 mW m^{-2} for the surface heat flux. To start the model requires a pre-existing depression, in the case of Aram Crater the depression being a large impact crater and therefore an FFC, which fills with a 2 km (at center) sheet of water ice. This ice sheet is subsequently buried, most likely by a mix of aeolian sediments, impact ejecta, and volcanic ashfall (Zegers, et al., 2010). The insulating effect of a sediment cover with a lower thermal conductivity than the surrounding basement causes the lowest parts of the ice to melt. The heat source for their model comes from the heat of formation of Mars, long-lived radioactive isotopes are not taken into account. Increasing thermal conductivity of the sediment layer requires a greater thickness in order to achieve melting. Lower surface heat flux also increases the thickness of the sediment package needed to achieve melting. At a critical point melting reaches a critical amount leading to the entire collapse of the overburden layer. When water reaches the surface an outflow channel will be carved where a topographic gradient is present. Otherwise the water will pool, freeze and sublimate in the current climate.

1.4.4 Clathrates

Clathrates are water-based compounds which have gas molecules trapped within them. Models using clathrate-induced chaotic terrain require high concentrations of volatiles to be present in the subsurface. Rodriguez et al. (2006) proposed that a frozen layer above liquid CO_2 fractured due to impact cratering, climatic warming, or changes in geothermal conditions, leading to a runaway degassing cycle. Rapid volatile exsolution caused by depressurization causes explosive expulsion of volatiles and clastic materials through fractures. Continued removal of subsurface volatiles would lead to regional subsidence, generating normal faults produced by extensional deformation of the crust. Faulting would cause liquefaction of poorly consolidated units, accelerating depressurization.

1.4.5 Excavation of Subsurface Volatiles

Formation mechanisms for secondary chaotic terrains require buried lenses of volatile-rich material (Rodríguez, et al., 2011), the simplest of these being lenses of pure water ice, other examples may include brines, CO_2 ice, or clathrates. Secondary chaotic terrain forms within outflow channels, suggesting the excavation of the channel by flooding is the cause of their formation (Rodríguez, et al., 2011). As flood waters remove the surface, exposed volatiles are more easily eroded then the surrounding terrain. Areas of relatively low concentrations of volatiles remain as mesas and knobs (Rodríguez, et al., 2011).

References

Andrews-Hanna, J. C., & Phillips, R. J. (2007). Hydrological modeling of outflow channels and chaos regions on Mars. *JGR, 112*(E08001). doi:10.1029/2006JE002881

Andrews-Hanna, J. C., Zuber, M. T., & Banerdt, W. B. (2008). The Borealis basin and the origin of the martian crustal dichotomy. *Nature, 453*(7199), 1212-1216.

Baker, V. R., Hamilton, C. W., Burr, D. M., Gulick, V. C., Komatsu, G., Luo, W., . . . Rodriguez, J. A. (2015). Fluvial geomorphology on Earth-like planetary surfaces: A review. *245*, 149-182. doi:10.1016/j.geomorph.2015.05.002

Bamberg, M., Jaumann, R., Asche, H., Kneissl, T., & Michael, G. G. (2014). Floor-Fractures Craters on Mars - Observations and Origin. *Planetary and Space Science, 98*, 146-162.

Carr, M. H., & Head, J. W. (2003). Oceans on Mars: An assessment of the observational evidence and possible fate. *Journal of Geophysical Research: Planets, 108*(E5).

Carr, M. H., Wu, S. S., Jordan, R., & Schafer, F. J. (1987). Volumes of Channels, Canyons and Chaos in the Circum-Chryse Region of Mars. *Lunar and Planetary Science Conference*, *XVIII*, p. 155.

Catling, D. C. (2009). Atmospheric evolution, Mars. *Encyclopedia of Paleoclimatology and Ancient Environments*, 66-75.

Chapman, M. G., & Tanaka, K. L. (2002). Related Magma–Ice Interactions: Possible Origins of Chasmata, Chaos, and Surface Materials in Xanthe, Margaritifer, and Meridiani Terrae, Mars. *Icarus, 155*, 324-339.

Citron, R. I., Manga, M., & Hemingway, D. J. (2018). Timing of oceans on Mars from shoreline deformation. *Nature, 555*. doi:10.1038/nature26144

Clifford, S. M., & Parker, T. J. (2001). The Evolution of the Martian Hydrosphere: Implications for the Fate of a Primordial Ocean and the Current State of the Northern Plains. *Icarus, 154*, 40-79. doi:10.1006/icar.2001.6671

Clifford, S. M., Lasue, J., Heggy, E., Boisson, J., McGovern, P., & Max, M. D. (2010). Depth of the martian cryosphere: revised estimates and implications for the existence and detection of subpermafrost groundwater. *J. Geophys. Res., 115*(E7). doi:10.1029/2009JE003462

Coleman, N. M. (2005). Martian megaflood triggered chaos formation, revealing groundwater depth, cryosphere thickness, and crustal heat flux. *JGR, 110*, E12S20. doi:10.1029/2005JE002419

Craddock, R. A., & Howard, A. D. (2002). The case for rainfall on a warm, wet early Mars. *JGR, 107*(E11), 5111. doi:10.1029/2001JE001505

Fanale, F. P., Postawko, S. E., Pollack, J. B., Carr, M. H., & Pepin, R. O. (1992). Mars: Epochal Climate Cahnge and Volatile History. In H. H. Kieffer, B. M. Jakosky, C. W. Snyder, & M. S. Matthews (Eds.), *Mars* (pp. 1135-1179). The University of Arizona Press.

Frey, H. V. (2006). Impact constraints on, and a chronology for, major events in early Mars history. *Journal of Geophysical Research: Planets, 111*(E8).

Greenberg, R., Hoppa, G., Tufts, B., Geissler, P., Riley, J., & Kadel, S. (1999). Chaos on Europa. *Icarus, 141*(2), 263-286.

Harrison, K. P., & Grimm, R. E. (2008). Multiple flooding events in Martian outflow channels. *JGR, 113*, E02002. doi:10.1029/2007JE002951

Harrison, K. P., & Grimm, R. E. (2009). Regionally compartmented groundwater flow on Mars. *Journal of Geophysical Research, 114*(E4). doi:10.1029/2008JE003300

Head, J. W., Hiesinger, H., Ivanov, M. A., Kreslavsky, M. A., Pratt, S., & Thomson, B. J. (1999). Possible ancient oceans on Mars: evidence from Mars Orbiter Laser Altimeter data. *Science, 286*(5447), 2134-2137.

Komatsu, G., Kargel, J. S., Baker, V. R., Strom, R. G., Ori, G. G., Mosangini, C., & Tanaka, K. L. (2000). A chaotic terrain formation hypothesis: Explosive outgas and outflow by dissociation of clathrate on Mars. *Lunar Planet. Sci. Conf. XXXI.* abstract 1434.

Leask, H. J., Wilson, L., & Mitchell, K. L. (2006). Formation of Aromatum Chaos, Mars: Morphological development as a result of volcano-ice interactions. *JGR, 111*(E08071). doi:10.1029/2005JE002549

Lucchitta, B. K., & Ferguson, H. M. (1983). Chryse Basin channels: Low-gradients and ponded flows. *Journal of Geophysical Research: Solid Earth, 88*(S02), A553-A568. doi:10.1029/JB088iS02p0A553

Manker, J. P., & Johnson, A. P. (1982). Simulation of Martian Chaotic Terrain and Outflow Channels. *Icarus, 51*, 121-132.

Marinova, M. M., Aharonson, O., & Asphaug, E. (2008). Mega-impact formation of the Mars hemispheric dichotomy. *Nature, 453*(7199), 1216-1219.

Melosh, H. J., & Vickery, A. M. (1989). Impact erosion of the primordial atmosphere of Mars. *Nature, 338*, 487-489.

Meresse, S., Costard, F., Mangold, N., Masson, P., & Neukum, G. (2008). Formation and evolution of the chaotic terrains by subsidence and magmatism: Hydraotes Chaos, Mars. *Icarus, 194*, 487-500. doi:10.1016/j.icarus.2007.10.023

Ori, G. G., & Mosangini, C. (1998). Complex depositional systems in Hydraotes Chaos, Mars' An example of sedimentary process interactions in the Martian hydrological cycle. *JGR, 103*(E10), 22,713-22,723.

Palumbo, A. M., Head, J. W., & Wordsworth, R. D. (2018). Late Noachian Icy Highlands climate model: Exploring the possibility of transient melting and fluvial/lacustrine activity through peak annual and seasonal temperatures. *Icarus, 300*, 261-286. doi:10.1016/j.icarus.2017.09.007

Parker, T. J., Gorsline, D. S., Saunders, R. S., Pieri, D. C., & Schneeberger, D. M. (1993). Coastal geomorphology of the Martian northern plains. *Journal of Geophysical Research: Planets, 98*(E6), 11061-11078.

Phillips, R. J., Zuber, M. T., Solomon, S. C., Golombek, M. P., Jakosky, B. M., Banerdt, W. B., . . . Hauck II, S. A. (2001). Ancient geodynamics and global-scale hydrology on Mars. *Science, 291*(5513), 2587-2591. doi:10.1126/science.1058701

Roberts, J. H., & Zhong, S. (2006). Degree-1 convection in the Martian mantle and the origin of the hemispheric dichotomy. *Journal of Geophysical Research, 111*. doi:10.1029/2005JE002668

Roda, M., Kleinhans, M. G., Zegers, T. E., & Govers, R. (2016). Origin of circular collapsed landforms in the Chryse region of Mars. *Icarus, 265*, 70-78. doi:http://dx.doi.org/10.1016/j.icarus.2015.10.020

Roda, M., Kleinhans, M. G., Zegers, T. E., & Oosthoek, J. H. (2014). Catastrophic ice lake collapse in Aram Chaos, Mars. *Icarus, 236*, 104-121. doi:http://dx.doi.org/10.1016/j.icarus.2014.03.023

Rodriguez, J. A., Kargel, J. S., Baker, V. R., Gulick, V. C., Berman, D. C., Fairén, A. G., . . . Glines, N. (2015). Martian outflow channels: How did their source aquifers form, and why did they drain so rapidly? *Scientific Reports, 5*, 13404.

Rodríguez, J. A., Kargel, J. S., Tanaka, K. L., Crown, D. A., Berman, D. C., Fairén, A. G., . . . Sasaki, S. (2011). Secondary chaotic terrain formation in the higher outflow channels of southern circum-Chryse, Mars. *Icarus, 213*, 150-194. doi:10.1016/j.icarus.2010.09.027

Rodriguez, J. A., Kargel, J., Crown, D. A., Bleamaster III, L. F., Tanaka, K. L., Baker, V., . . . Komatsu, G. (2006). Headward growth of chasmata by volatile outbursts, collapse, and drainage: Evidence from Ganges chaos, Mars. *Geophysical Research Letters, 33*(L18203). doi:10.1029/2006GL026275

Sato, H., Kurita, K., & Baratoux, D. (2010). The formation of floor-fractured craters in Xanthe Terra. *Icarus, 207*, 248-264. doi:10.1016/j.icarus.2009.10.023

Schultz, P. H., & Gault, D. E. (1975). Seismic effects from major basin formations on the Moon and Mercury. *The Moon, 12*(2), 159-177.

Sharp, R. P., & Malin, M. C. (1975). Channels on Mars. *Geological Society of America Bulletin, 86*(5), 593-609. doi:10.1130/0016-7606(1975)86<593:COM>2.0.CO;2

Sharp, R. P., Soderblom, L. A., Murray, B. C., & Cutts, J. A. (1971). The Surface of Mars: Uncratered Terrains. *JGR, 76*(2).

Tanaka, K. L., & Hartmann, W. K. (2012). The Planetary Time Scale. In F. M. Gradstein, J. G. Ogg, M. Schmitz, & G. Ogg, *The Geologic Time Scale* (pp. 275-298). Elsevier.

Tanaka, K. L., Isbell, N. K., Scott, D. H., Greeley, R., & Guest, J. E. (1988). The resurfacing history of Mars-A synthesis of digitized, viking-based geology. *Lunar and Planetary Science Conference Proceedings*, *18*, pp. 665-678.

Tanaka, K. L., Scott, D. H., & Greeley, R. (1992). Global Stratigraphy. In H. H. Kieffer, B. M. Jakosky, C. W. Snyder, & M. S. Matthews (Eds.), *Mars* (pp. 345-382). The University of Arizona Press.

Weiss, D. K., & Head, J. W. (2017). Evidence for stabilization of the ice-cemented cryosphere in earlier martian history: Implications for the current abundance of groundwater at depth on Mars. *Icarus*(288), 120-147. doi:10.1016/j.icarus.2017.01.018

Wordsworth, R. D., Kerber, L., Pierrehumbert, R. T., Forget, F., & Head, J. W. (2015). Comparison of “warm and wet” and “cold and icy” scenarios for early Mars in a 3-D climate model. *JGR: Planets, 120*, 1,201-1,219. doi:10.1002/2015JE004787

Wordsworth, R., Forget, F., Millour, E., Head, J. W., Madeleine, J. B., & Charnay, B. (2013). Global modelling of the early martian climate under a denser CO2 atmosphere: Water cycle and ice evolution. *Icarus, 222*, 1-19. doi:10.1016/j.icarus.2012.09.036

Zegers, T. E., & Roda, M. (2012). Chaotic Terrains on Mars: testing the subsurface lake hypothesis. *Rend. online Soc. Geol. It., 22*, 243-246.

Zegers, T. E., Oosthoek, J. H., Rossi, A. P., Blom, J. K., & Schumacher, S. (2010). Melt and collapse of buried water ice: An alternative hypothesis for the formation of chaotic terrains on Mars. *Earth and Planetary Science Letters, 297*, 496-504. doi:10.1016/j.epsl.2010.06.049

Chapter 2.0 : **Methodology**

2.1 Data Source

Imagery used for this study includes HRSC (50 – 75 m/pixel) and CTX (20 m/pixel) Digital Elevation Models (DEMs) adjusted to MOLA elevations. CTX DEMs were created using NASA's Ames Stereo Pipeline (Beyer, et al., 2018). HRSC DEMs were obtained through Freie Universität Berlin as level 4 processed FUB files. HRSC has a horizontal accuracy of ± 50 m and vertical accuracy of ± 10 m (Jaumann, et al., 2007). The global Mars MOLA MEGDR dataset, obtained from the PDS, was used as a base map to fill gaps in data coverage and has a spatial resolution of 463 m per pixel with a horizontal accuracy of ± 100 m and a vertical accuracy of ± 1 m (Smith, et al., 2001). All DEM elevations were corrected to the MOLA dataset as it has the highest accuracy of elevation datasets.

2.2 Data Display

HRSC, CTX, and MOLA data were loaded into Global Mapper 15.2 for visualization. This software served the function of overlaying different datasets of DEM and imagery, while also allowing traced slope measurements, elevation calculations, 3D visualization, and visual identification of features such as terraces, sapping channels, and cinder cones. Many of the base map images used were produced in Global Mapper.

2.3 Augmented Visualization of Attitude (AVA)

The AVA tool was created by Mikhail Minin (2015) which uses ArcGIS to create a colour-coded attitude visualization of a terrain surface. The AVA uses a hue-saturation-lightness colour wheel compensated for relative luminance and uses saturation as slope. This tool also calculates the strike and dip of each pixel within a DEM using a 3x3 moving window of pixels, calculating the central pixel using its elevation relative to the surrounding pixels as it moves left to right, top to bottom. Values are rounded to the nearest integer. For a full discussion of the AVA tool the reader is referred to Minin (2015).

2.4 Measurements

ArcGIS (ArcMap 10.5 & 10.7) was used to calculate strike and dip measurements based on the AVA tool using the combined DEM composites made up of HRSC, CTX, and MOLA data if needed. To calculate the dip and dip direction of mesas in ArcGIS hand-traced polygons were used. The polygons were traced by hand to conserve the highest number of pixels on the surface, while also avoiding crater impacts or large fracture which would give erroneous data. The trace was also close to but not on the edge of the mesas to avoid erroneous pixels. The average dip of all pixels within the traced polygons was then calculated to ensure individual pixels with spikes in dip values were smoothed out. The outlined polygons were also used to calculate total surface area of individual blocks (which are underestimated due to avoiding erroneous pixels) for use in relative comparison of block properties. Strike values were calculated using all pixels within individual polygons loaded into SpheriStat 3. This allowed processing of

directional data to find the true strike direction and, by association, the dip direction of mesas. Rose diagrams of the strikes of all mesas in a chaos zone was also produced in SpheriStat.

ArcGIS (ArcScene 10.5 & 10.7) was used to calculate total volume loss. The volume of missing material was calculated using a flat-top bounding surface at an average plateau elevation, for simplicity. Composite DEMs were first convert to Triangular Irregular Networks (TINs) in ArcGIS with an elevation tolerance of ± 10 m and a maximum of 1.5 million tie points. The volume between the bounding surface and TIN surface was then filled and this fill is the volume loss. This method also allowed the bounding surface to be changed to the elevation of terraces found within the chaos to find the volume of possible paleolakes, and also to calculate possible secondary collapses.

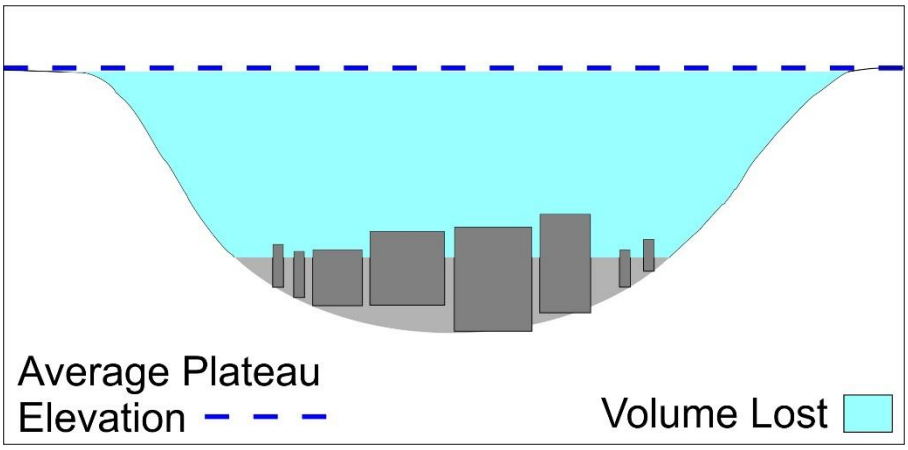

Figure 2-1 Schematic diagram of the total volume loss calculation completed using ArcGIS.

The larger the chaos area the more uncertainty there is in the results, with Hydraotes Chaos having an uncertainty of ± 550 km^3 over the 50,000 km^2. This was taken into account by simply rounding values to the nearest 1,000 km^3 for Hydraotes Chaos and rounding to the nearest 100 km^3 for the Hydraspis crater pair (± 85 km^3), Candor Chaos (± 40 km^3), and Baetis Chaos (± 33 km^3).

The distribution of mesas within chaos regions was done using an augmented version of Geovision 6.3 which fits ellipses to blocks. This then calculates inertia tensors, which also gave the aspect ratio and coordinates of the center of the ellipse. The center of the best fit ellipse was used to then calculate the distribution of blocks relative to a given point using trigonometry, in the case of Hydraotes Chaos that point being the center of the smooth basin area.

References

Beyer, R. A., Alexandrov, O., & McMichael, S. (2018). The Ames Stereo Pipeline: NASA's open source software for deriving and processing terrain data. *Earth and Space Science, 5*. doi:10.1029/2018EA000409

Jaumann, R., Neukum, G., Behnke, T., Duxbury, T., Eichentopf, K., Flohrer, J., . . . Hoffmann, H. (2007). The high-resolution stereo camera (HRSC) experiment on Mars Express: Instrument aspects and experiment conduct from interplanetary cruise through the nominal mission. *Planetary and Space Science, 55*(7-8), 928-952. doi:10.1016/j.pss.2006.12.003

Minin, M. (2015). Quantification and Extraction of Surface Features from Digital Terrain Models (Masters Thesis). Retrieved from http://dr.library.brocku.ca/handle/10464/7893

Smith, D., Zuber, M., Frey, H., Garvin, J., Head, J., Muhleman, D., . . . Banerdt, W. (2001). Mars Orbiter Laser Altimeter: Experiment summary after the first year of global mapping of Mars. *Journal of Geophysical Research: Planets, 106*(E10), 23689-23722. doi:10.1029/2000JE001364

Chapter 3.0 **: Hydraotes Chaos**

3.1 Introduction

Hydraotes Chaos (Figure 3-1) is located northeast of Valles Marineris in the large outflow channel between Xanthe Terra and Margaritifer Terra, which drains into Chryse Planitia. Hydraotes Chaos covers an area of approximately 50,000 km^2. The plateau surrounding Hydraotes is an average of 1,500 m below the global datum, and the lowest point of the basin is approximately 5,100 m below the global datum, a difference of 3,600 m.

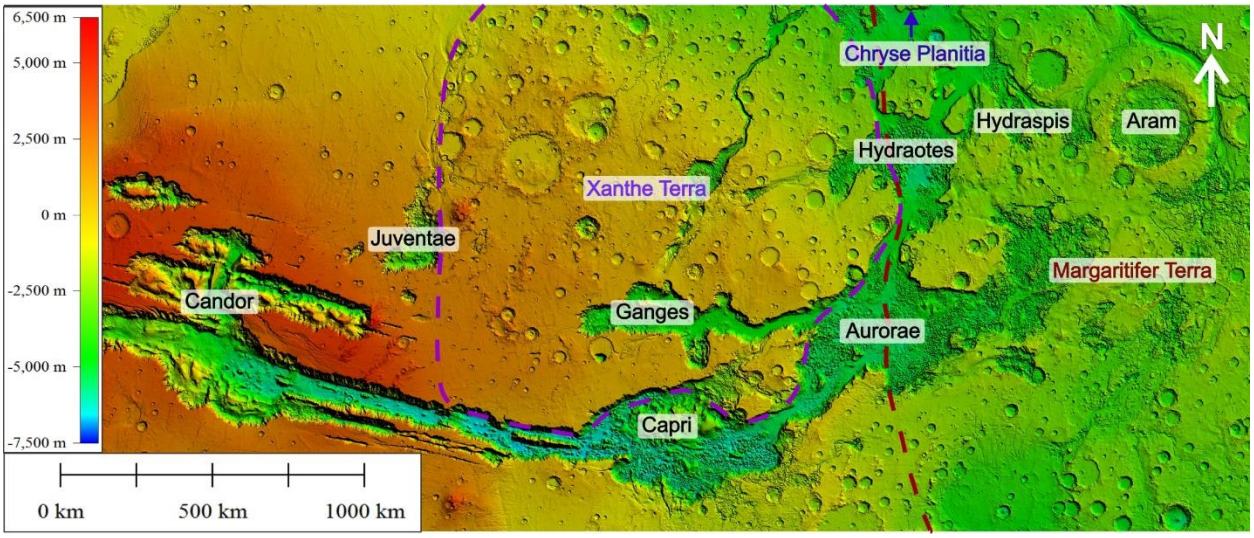

Figure 3-1 Overview of the area surrounding Hydraotes Chaos, the rough outline of Xanthe Terra (purple dashes) and Margaritifer Terra (red dashes) is shown.

Hydraotes Chaos possesses the basic morphological features of other chaos regions as shown in Figure 3-2: a central area of mesas (Fig 3-2:D), knobs, and ridges (Fig 3-2:B,C) separated by narrow channels within a large-scale depression. Knobs are generally triangular (Fig 3-2:B) and ridges are elongate/bladed (Fig 3-2:C) in shape, and usually display spur and gully textures along their walls. The mesas in Hydraotes Chaos have smooth tops and steep walls and have the highest density near the center of the chaos zone. Some mesas display sapping erosion and fissures (Figure 3-3:A). Many

show at least one prominent layer along their walls (Figure 3-3:A) which in some instances is faulted. The knobs in Hydraotes are dispersed throughout the area; however, the majority are found along the outskirts of the chaos zone. Mesa blocks can be seen breaking off the existing plateau, the best examples of which are on the eastern side of Hydraotes.

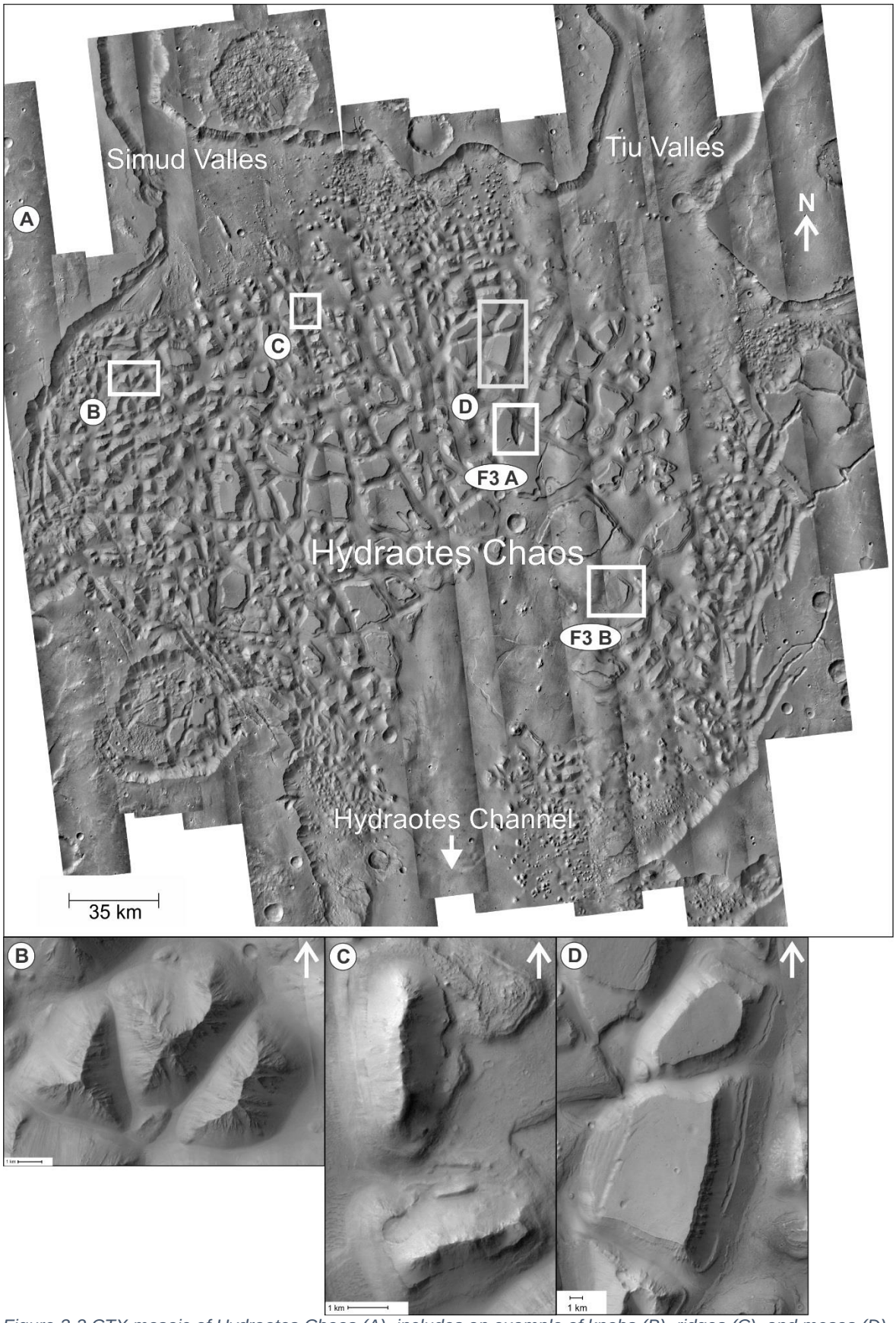

Figure 3-2 CTX mosaic of Hydraotes Chaos (A), includes an example of knobs (B), ridges (C), and mesas (D), also indicated is Figure 3 A & B.

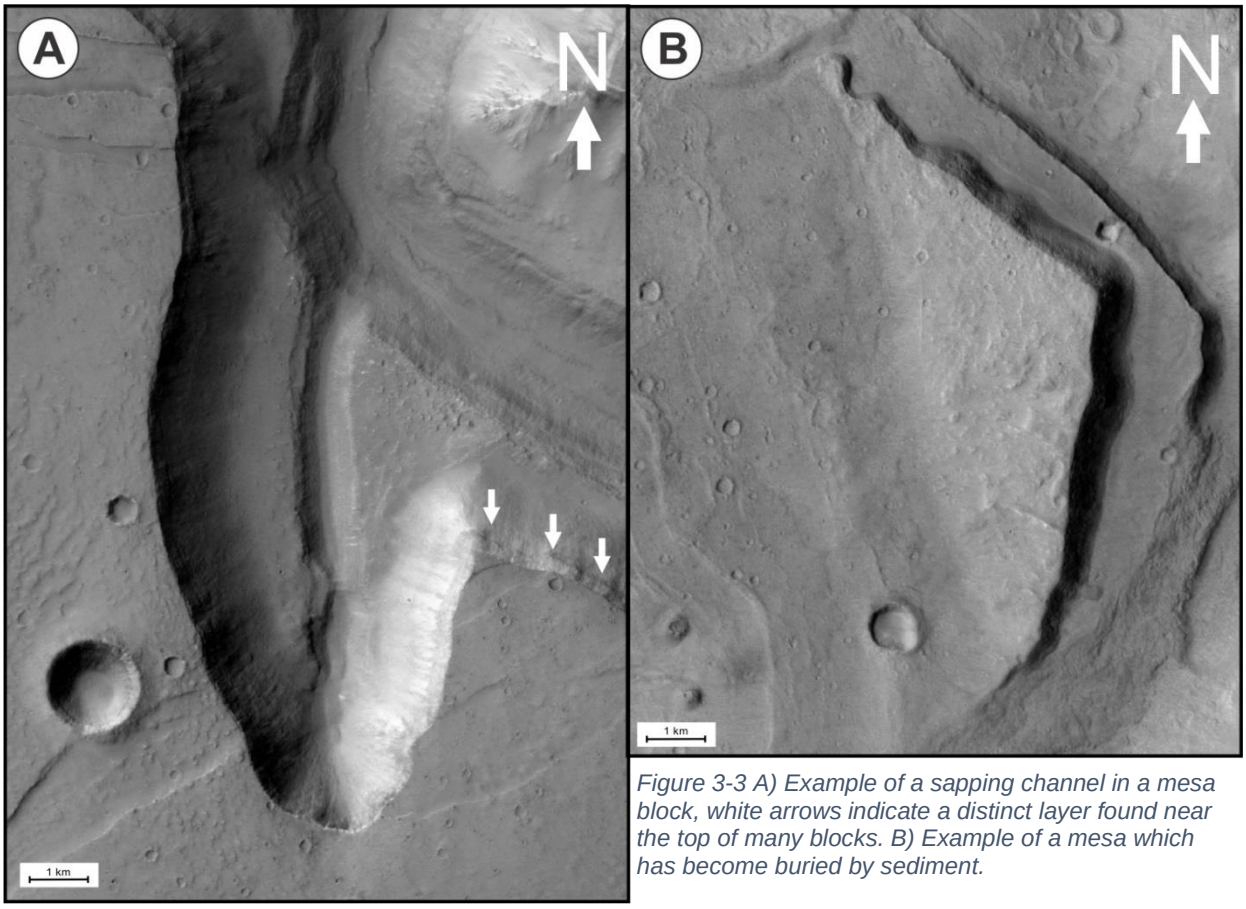

Figure 3-3 A) Example of a sapping channel in a mesa block, white arrows indicate a distinct layer found near the top of many blocks. B) Example of a mesa which has become buried by sediment.

Several features make Hydraotes unique among chaos regions. These include: large smooth topped mesas, a large open flat section of the basin floor, multiple channels, and mesa-surrounding terraces. Mesas in Hydraotes range in size from < 1 km to 40 km in width with several individual mesas exceeding 10 km in width. The smooth floor section of the basin is in the southern portion of the chasma and is filled with sediment that partly buries several blocks around the edge of the basin; an example is shown in Figure 3-3:B. The filling of the basin with sediments may be due to low energy subaqueous deposition in a lacustrine setting, with sediments being brought into the basin through the southern channel (Ori & Mosangini, 1998). The floor of the

basin is relatively devoid of craters but features small cone structures that have been identified as cinder cones (Brož, et al., 2015).

Sapping channels cut through several mesa blocks in Hydraotes (Figures 3-3:A and 3-4). These channels are created by slope undercutting though the release of groundwater onto the surface (Marra, et al., 2014). This erosive mechanism carries sediments from the subsurface resulting in the headward migration of channel systems (Marra, et al., 2014). Location of sapping channels in Hydraotes are shown in Figure 3-4 with a close-up example in Figure 3-3:A. Sapping produces steep sided U-shaped channels generally of a uniform width, with theater-shaped headwalls (Marra, et al., 2014). Sapping channels may also be formed through overland flow plunging into the valley (Marra, et al., 2014) or seasonal thawing (Petroff, et al., 2011).

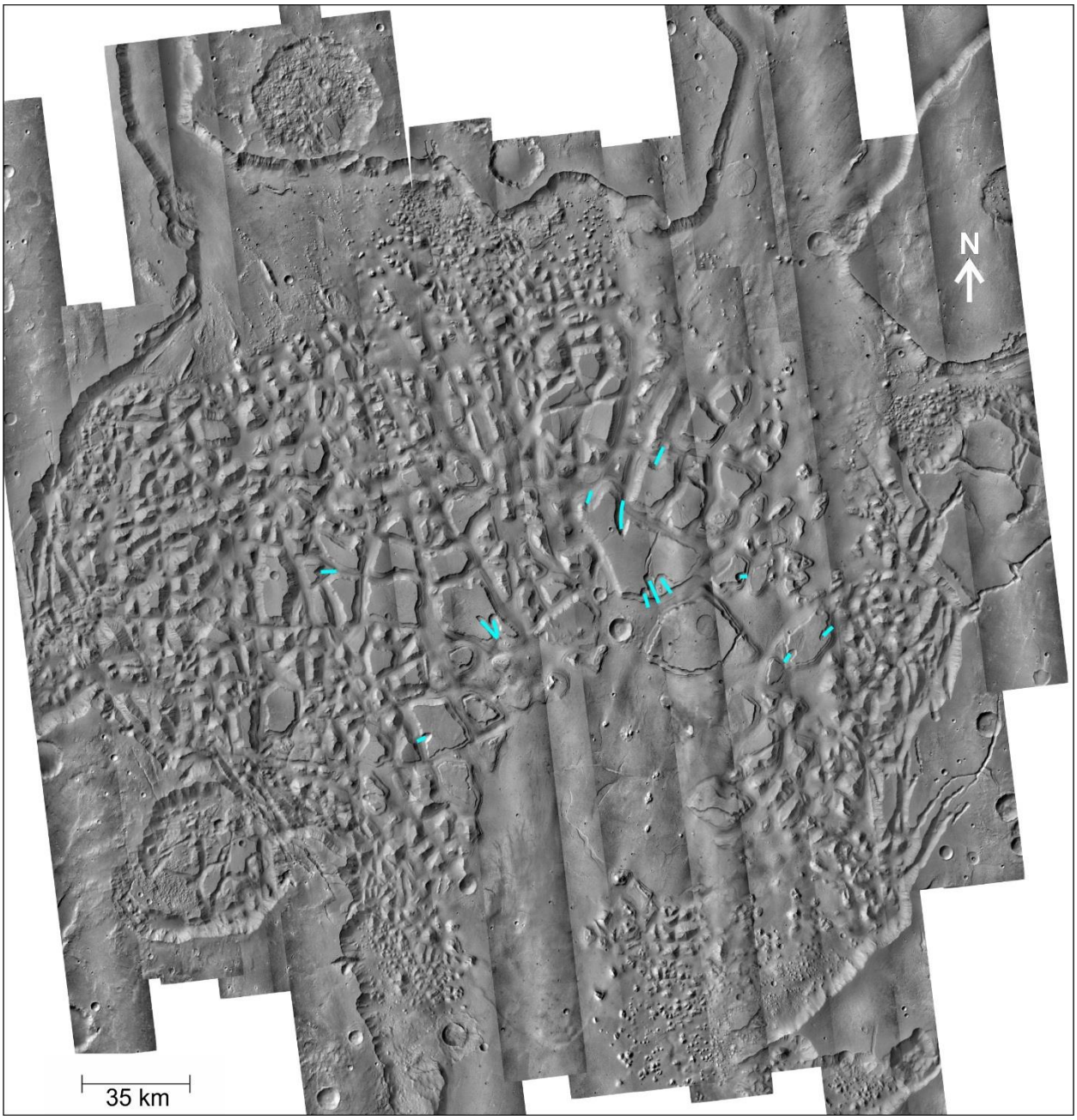

Figure 3-4 Locations of possible sapping channels within Hydraotes Chaos shown in blue.

Hydraotes has three main channels Simud Valles and Tiu Valles to the north and Hydraotes channel to the south (Figure 3-2 and 3-5). The channel flow directions may have changed over time (Pajola, et al., 2016), with water flowing into and out of the chaos region. Hydraotes channel and Tiu Valles both trend northeast in line with one another (Figure 3-5), while Simud Valles curves from its northwest entrance (Figure 3-5). Simud and Tiu Valles also display topographic highs where they meet Hydraotes chasma (Figure 3-5), which could indicate a debris fan or other resistant sediment package.

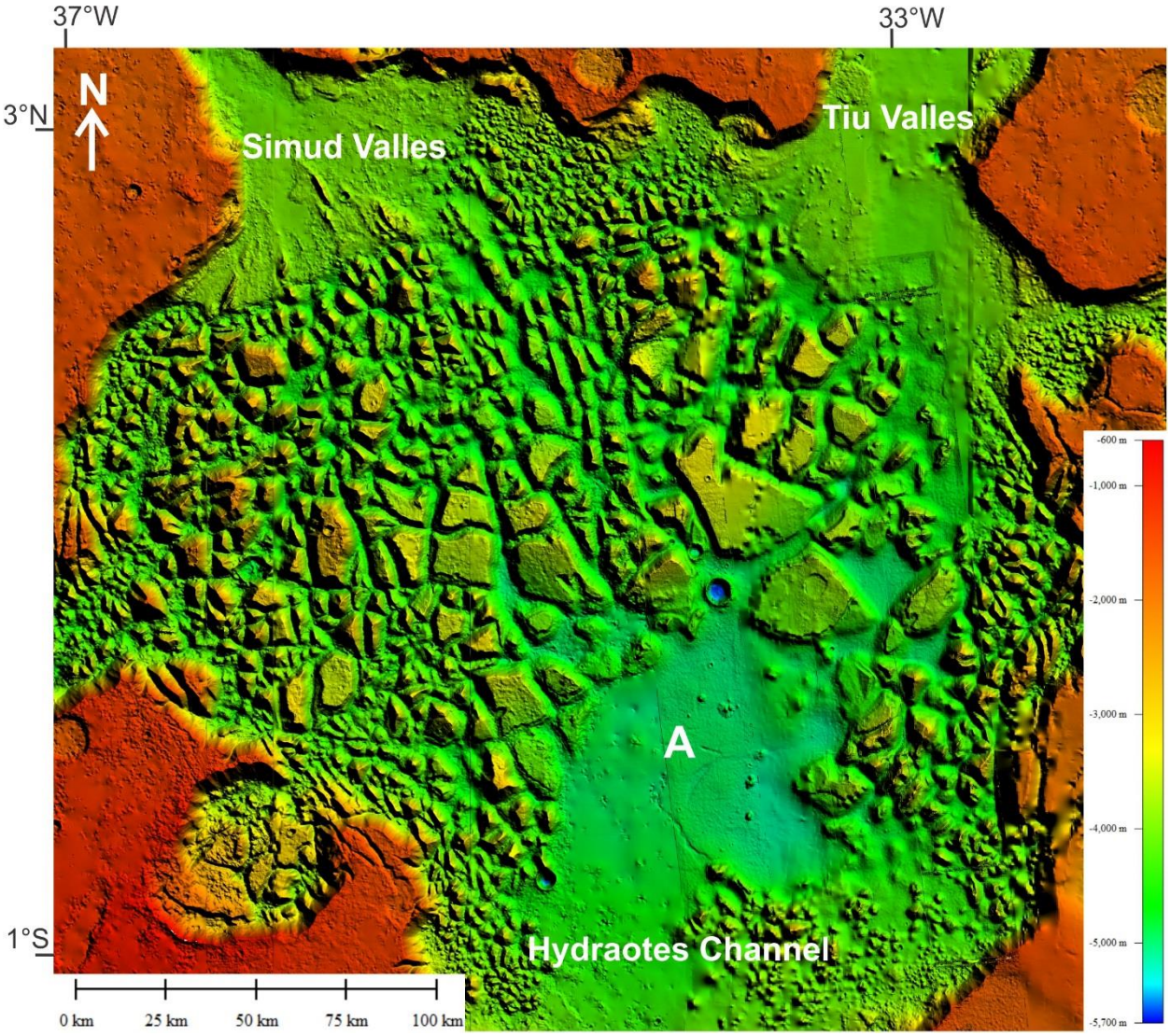

Figure 3-5 DEM overview of Hydraotes Chaos showing the major channels and the smooth floored southern basin (A).

No regional tectonic trends are apparent within Hydraotes or the surrounding uplands area according to the USGS Rotto & Tanaka (1995) or Tanaka et al. (2014) Geologic Map of Mars. Several N-S wrinkle ridges are located to the far west of Hydraotes.

3.2 Previous Work

Ori and Mosangini (1998) focused their study on sedimentary and hydrologic aspects of Hydraotes. They produced a geologic map of Hydraotes and mapped out three layers of terraces based on their width, which ranged from 100 m to 2 km, and vertical relation to each other. The highest terraces are approximately 550 m above the basin floor (Ori & Mosangini, 1998). The bottom two sets of terraces are localized, while the top set is the widest and highest in elevation and is found most extensively within Hydraotes (Ori & Mosangini, 1998). The terraces have been likened to terrestrial lacustrine terraces (Ori & Mosangini, 1998; Harrison & Chapman, 2008) and are thought to be caused by fluvial erosion during a period of ponding in a paleolake within the basin (Harrison & Chapman, 2008). Based on crater counts, the age of the surrounding plateau was dated to be middle Noachian, while the basin and channels are early to middle Amazonian (Ori & Mosangini, 1998). The central basin is thought to have contained mesas and knobs like the rest of the chaos region, but they have been subsequently eroded and/or buried by sediments brought in by the southern channel (Ori & Mosangini, 1998). Ori & Mosangini (1998) proposed that the most likely trigger for the creation of Hydraotes was liquefaction of the megaregolith caused by an ancient impact crater or an earthquake. They also suggested that the east side of the chaos tends to be more fault controlled, with SW-NE trending faults, while the west side is more impact controlled with more curved fractures. Hydraotes chasma is the only direct outflow path from the east side of Valles Marineris to Chryse Planitia; however, if catastrophic floods took place, they would have removed the mesas and knobs in Hydraotes (Ori & Mosangini, 1998). Ori and Mosangini (1998) suggest that water

ponded within the basin and filled to a level where it overflowed a topographic dam which repeated several times. The volume of water calculated by Ori & Mosangini (1998) suggests that water sourced from Hydraotes alone was not enough to produce the outflow channels, and that the volume of flood water coming from the south was too much. Therefore, the water must have lost velocity and ponded at some stage. The floor of Tiu Valles to the northeast and Simud Valles to the northwest (Fig. 3-2 and 3-5) were also studied, and it was determined that they display different sedimentation patterns, which may indicate a difference in how they formed (Ori & Mosangini, 1998). Tiu Valles is most likely to have been the main outflow channel for Hydraotes (Ori & Mosangini, 1998).

Meresse et al. (2008) produced topographic cross sections using a DEM generated from MOLA track data with HRSC imagery. They describe two types of mesas within the chaos, the smaller mesas along the outside which are at higher elevations, and the large central mesas which are at a much lower elevation. Meresse et al. (2008) found that the mesa tops are sloped, but with no preferred orientation along cross sections. They also note a significant drop in elevation from the outer small mesas to the larger interior mesas. They proposed that the central zone of Hydraotes, where the large mesa blocks are located, underwent a secondary collapse. The study also identified and classified three types of pitted cones within Hydraotes based on morphology (Meresse et al., 2008): basin cones which are larger (1,100 m -1,860 m basal diameter), valley cones which are smaller (350 m - 700 m basal diameter), and small cones which are potentially small eroded basin cones. A comparison with terrestrial analogs suggests that they may be cinder cones (Meresse et al., 2008). They

use this as evidence for volcanism being a major influence on the creation of the chaotic terrain, and suggest a magmatic intrusion causing destabilization of the cryosphere leading to progressive collapse. Initial subsidence would be caused by the discharge of pressurized water from an aquifer which in turn leads to successive collapses (Meresse et al., 2008).

3.3 Methodology

For methods used, refer to Chapter 2.0 – Methodology above. This standard is used for each case study except where otherwise indicated.

The 50 m/pixel DEM composite used for Hydraotes Chaos is composed of CTX, HRSC, and MOLA data. Orbits used are shown in Table 3-1. The majority of the DEM composite is 50 m HRSC data with CTX data filling in gaps. MOLA MEGDR-MEGR data fills in 5% of the total DEM of Hydraotes where no other data was available.

Table 3-1 Images used to create the composite DEM for Hydraotes Chaos.

HRSC Orbit	CTX DEM Pairs
h0018_0000_da4_53 (50 m/pixel)	B19_017212_1809_XN_00N033W- G19_025506_1809_XI_00N033W
h1991_0000_da4_51 (75 m/pixel)	F09_039128_1799_XI_00S032W- F10_039761_1798_XI_00S032W
h2013_0001_da4_51 (75 m/pixel)	F09_039484_1804_XN_00N033W- F10_039550_1804_XN_00N033W
h2024_0001_da4_51 (75 m/pixel)	G02_019124_1803_XN_00N034W- G03_019269_1803_XN_00N034W
h2035_0000_da4_51 (50 m/pixel)	
h3180_0000_da4_50 (50 m/pixel)	

3.4 Results

3.4.1 Orientations Obtained with AVA

The AVA (Figure 3-6) was used to calculate strike and dip statistics for mesas, terraces, and the surrounding plateau around Hydraotes Chaos. The dip of every pixel within the Hydraotes AVA is shown in Figure 3-7, with the averaged dips of mesas tops shown in Figure 3-8. The dips of the surrounding plateau and basin floor are 0-1°, the dips along the steep edges of the mesas and knobs vary between 17-40° based on visual assessment of these features.

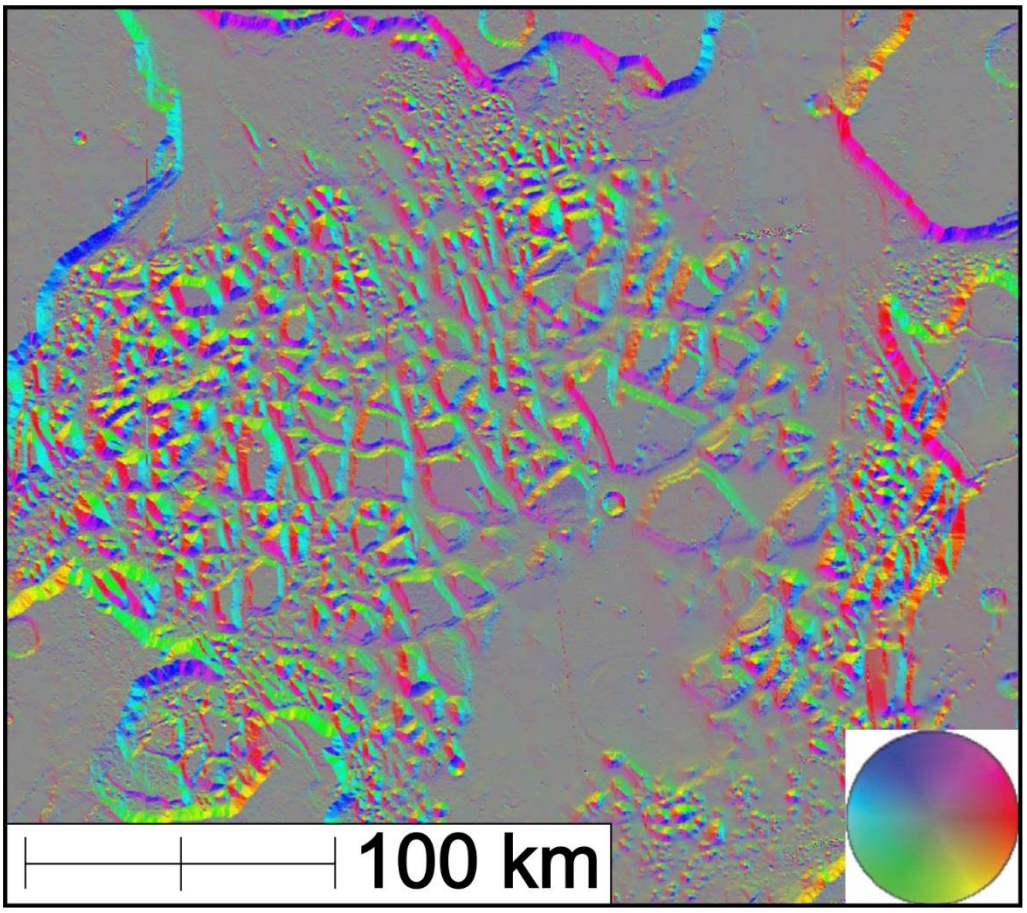

Figure 3-6 Colorized Augmented Visualization of Attitude (AVA) results using a color coded stereonet.

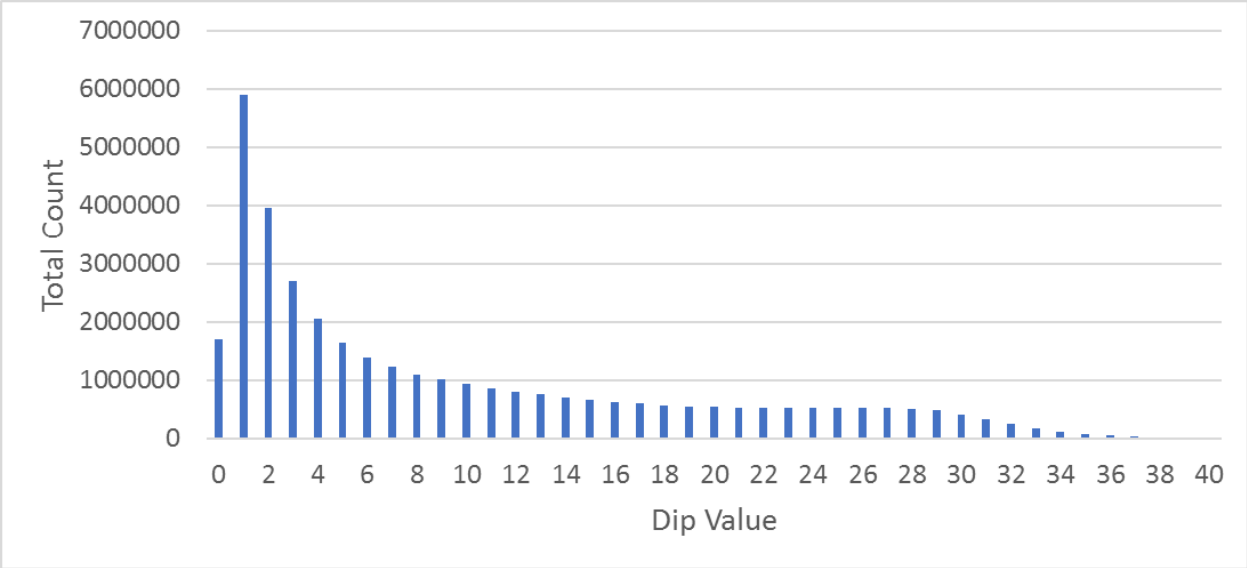

Figure 3-7 Dip value of all points calculated with the AVA of Hydraotes.

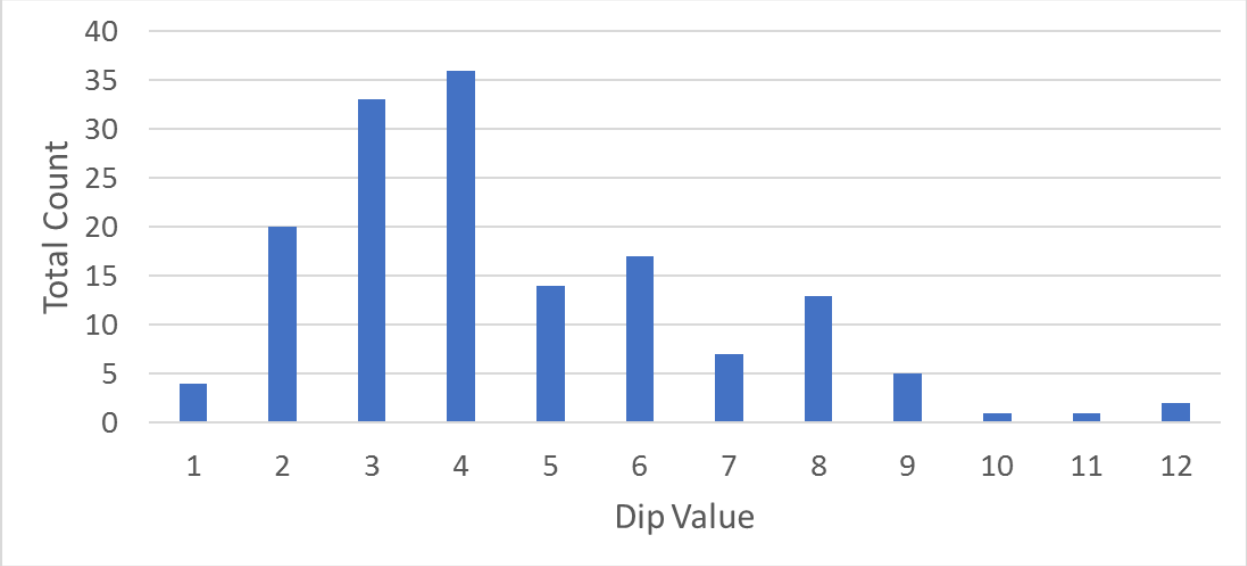

Figure 3-8 Average dip calculated for each mesa flat top within Hydraotes. A total of 132 mesa tops were calculated.

Figure 3-9 shows the strike values calculated within Hydraotes using the AVA. No preferred trend is found for the mesa tops (Figure 3-9:A), suggesting no preferred direction of collapse of these blocks. The steep sides of the mesas and knobs within Hydraotes (Dips between 17° – 40°) suggest a north-south trend is present (Figure 3-9:B), which coincides with the general trend of the channels connecting to Hydraotes.

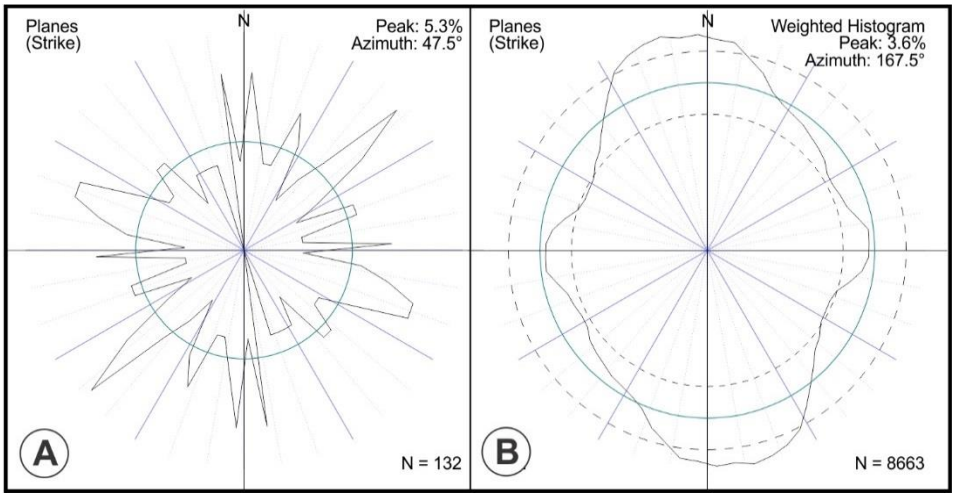

*Figure 3-9 A) Rose diagram of the strike for all mesa tops within Hydraotes. B) Rose diagram of strike for all points within Hydraotes that have dips from 17° - 40°. Due to computational limitations a histogram of all strike/dip value combinations with dips between 17-40 were used (360 strike values * 24 dip values= 8663 non-zero entries)*

3.4.2 Elevation and Distribution of Mesas

Figure 3-10 shows the main groups within Hydraotes which includes the southern smooth floor basin, chasma floor, large central blocks, and smaller peripheral blocks. These categories were grouped into contour ranges for better visualization. Note that the smooth basin floor dominates the southern area of Hydraotes. The largest mesas are located within the center of the chaos, with the majority of smaller mesas and knobs making up the periphery.

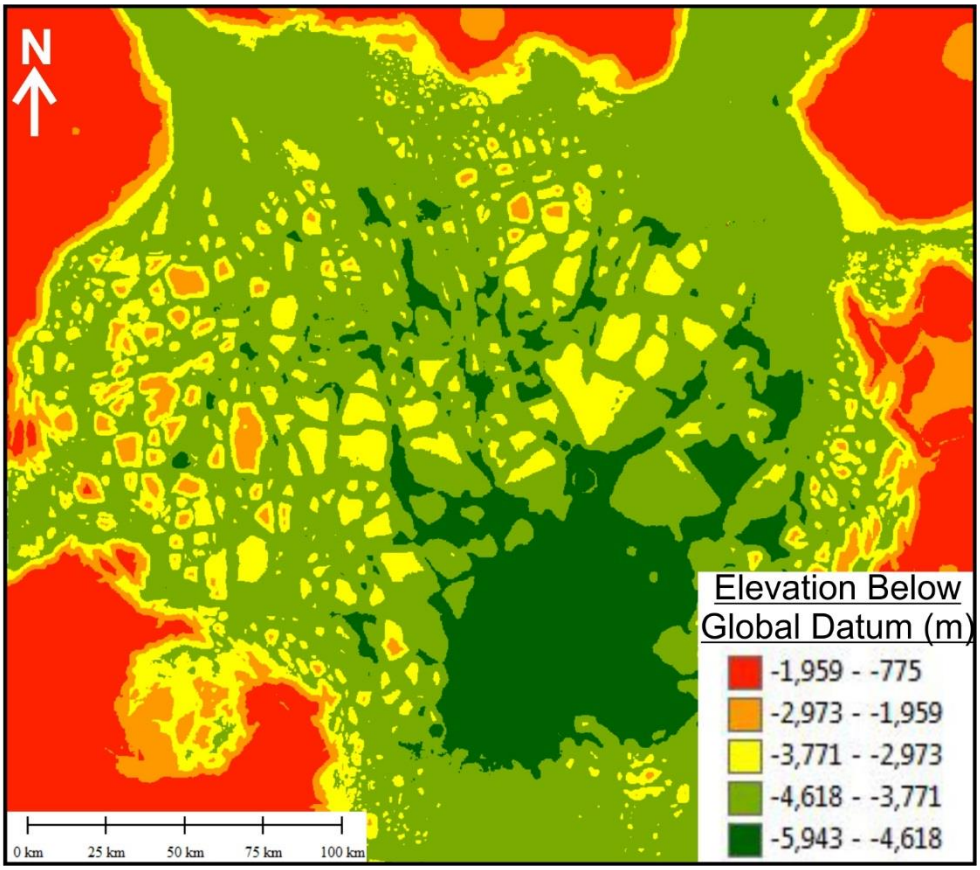

Figure 3-10 Manually set contours to allow for better visualization of sections of Hydraotes.

The distribution of 132 mesas within Hydraotes Chaos, which includes the largest mesas, is shown in Figure 3-11. The center zone is shown with a yellow dot in Figure 3-11 and represents the center of the smooth floor section of the basin, which has been proposed previously to be the zone which experienced first collapse (Ori & Mosangini, 1998). There are 5 large mesas, separated by an area difference of more than 100 km^2, and they are located < 90 km from the center of the basin. The majority of small mesas are located between 60 km and 120 km from the basin center, and the basin itself contains no visible mesas.

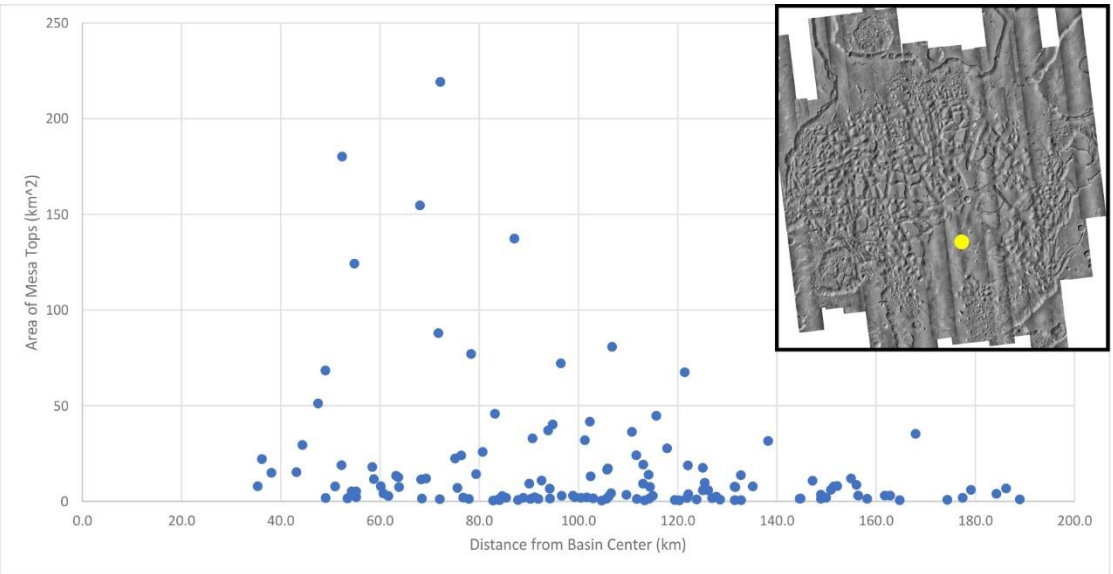

Figure 3-11 Plot of the distribution of mesas by size around the center of the basin shown in yellow in the subset image.

3.4.3 Orientation of Mesa Tops

The dips of the top surfaces of mesas calculated with the AVA tool are shown in Figure 3-12. The circular histogram of strikes (Figure 3-9:A) shows no preferred orientation of these mesa blocks. Generally low dip values are seen for the majority of mesa tops with an average dip of 4.6°.

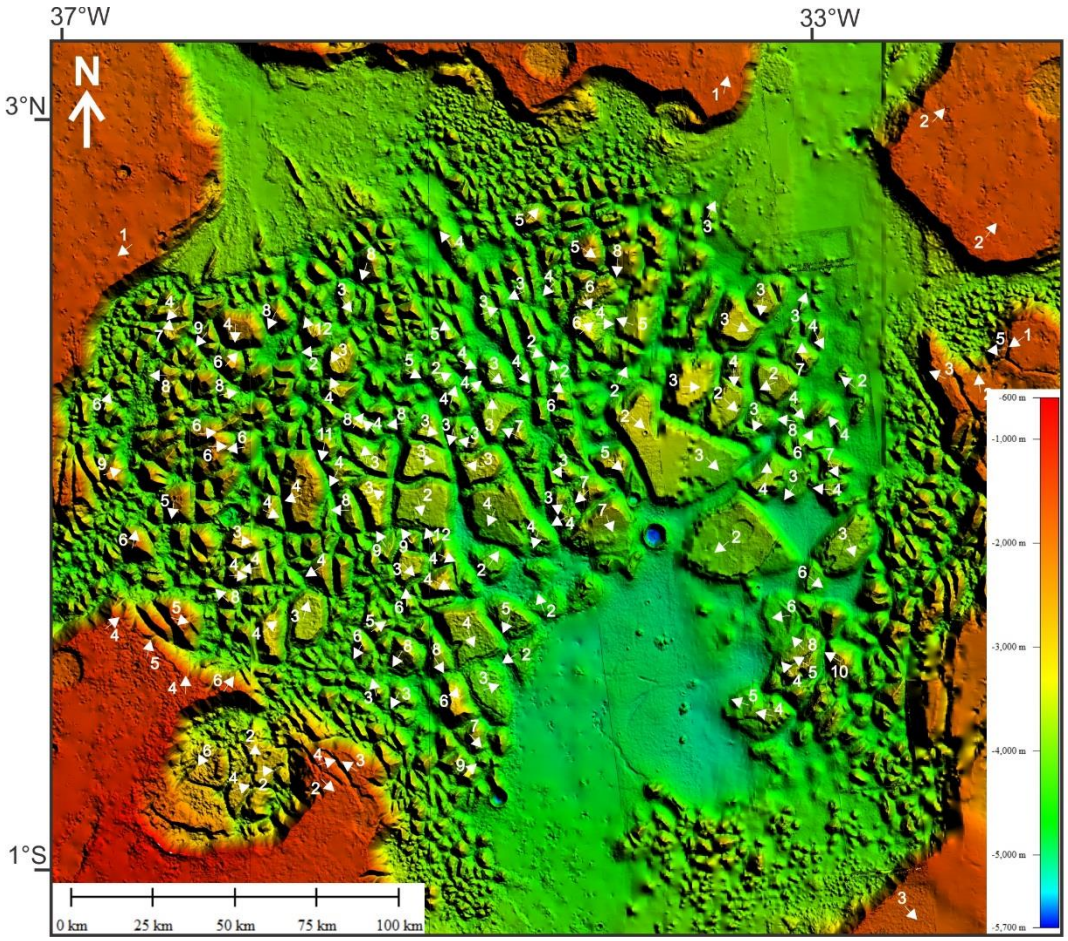

Figure 3-12 Composite DEM using CTX, HRSC, and MOLA DEMs, includes dip (numerical value) and dip direction (arrows) of mesas and the surrounding plateau.

3.4.4 Distribution and Orientations of Terraces

Terraces surround more than half of the mesa blocks within Hydraotes Chaos (Figure 3-13) and are preferentially located towards the center and northeast portion of the chaos. Three sets of terraces have been identified previously, based on width and vertical relation (Ori & Mosangini, 1998), with the most laterally extensive being the top-most terrace. Most blocks only show the largest terrace (Ori & Mosangini, 1998); the other terraces may have been heavily eroded/buried or may be localized features. The elevation of the terraces ranges from -4,532 m to -3,829 m below the datum, with an average elevation of -4,161 m, and they form 500 m – 1,000 m down from the mesa top.

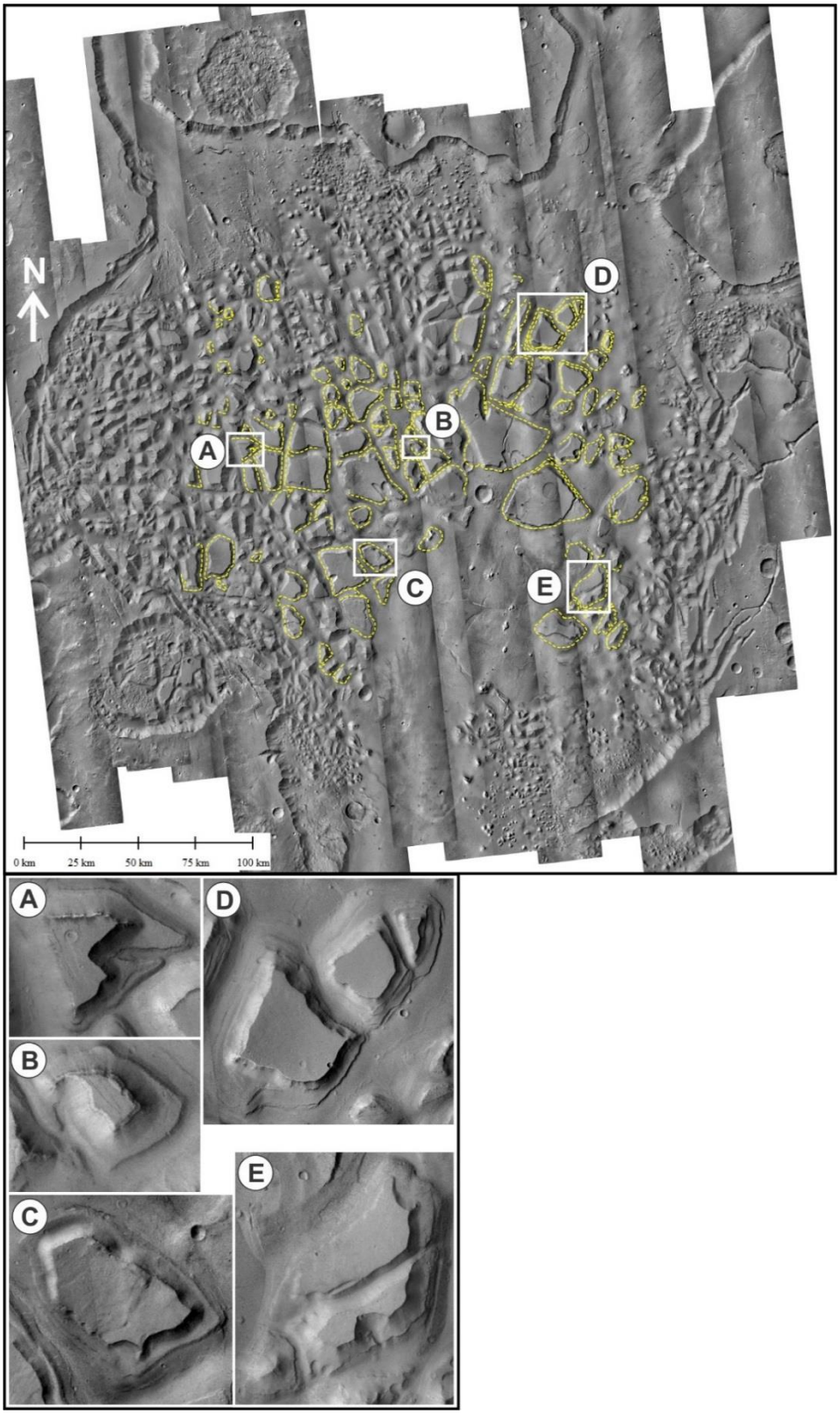

Figure 3-13 Outlined terraces found around mesas within Hydraotes, A-E are detailed examples.

3.4.5 Evidence of Volcanism in Hydraotes

Brož, et al. 2015 compared mud cones and cinder cones for three different sites include Hydraotes and determined them to be cinder cones based on their ballistic model. Figures 3-14 & 3-15 show locations of these cinder cones in Hydraotes. Nearly all are located within the eastern side of the chasma, with a large number within the basin. The cinder cones postdate the draining of the chaos area as they are weakly eroded; some have rubbly lava aprons deposited around them which have been preserved. In a previous study Meresse et al. (2008) identified 40 pitted cones; this study has identified a similar number of 46. Hauber et al. (2015) identified fields of cinder cones associated with chaotic terrain within Coprates Chasma in eastern Valles Marineris. Meresse et al. (2008) suggest that initial volcanism is the driving force of the destabilization of underground water ice and the cinder cones are an expression of later volcanism associated with magma displacement along faults.

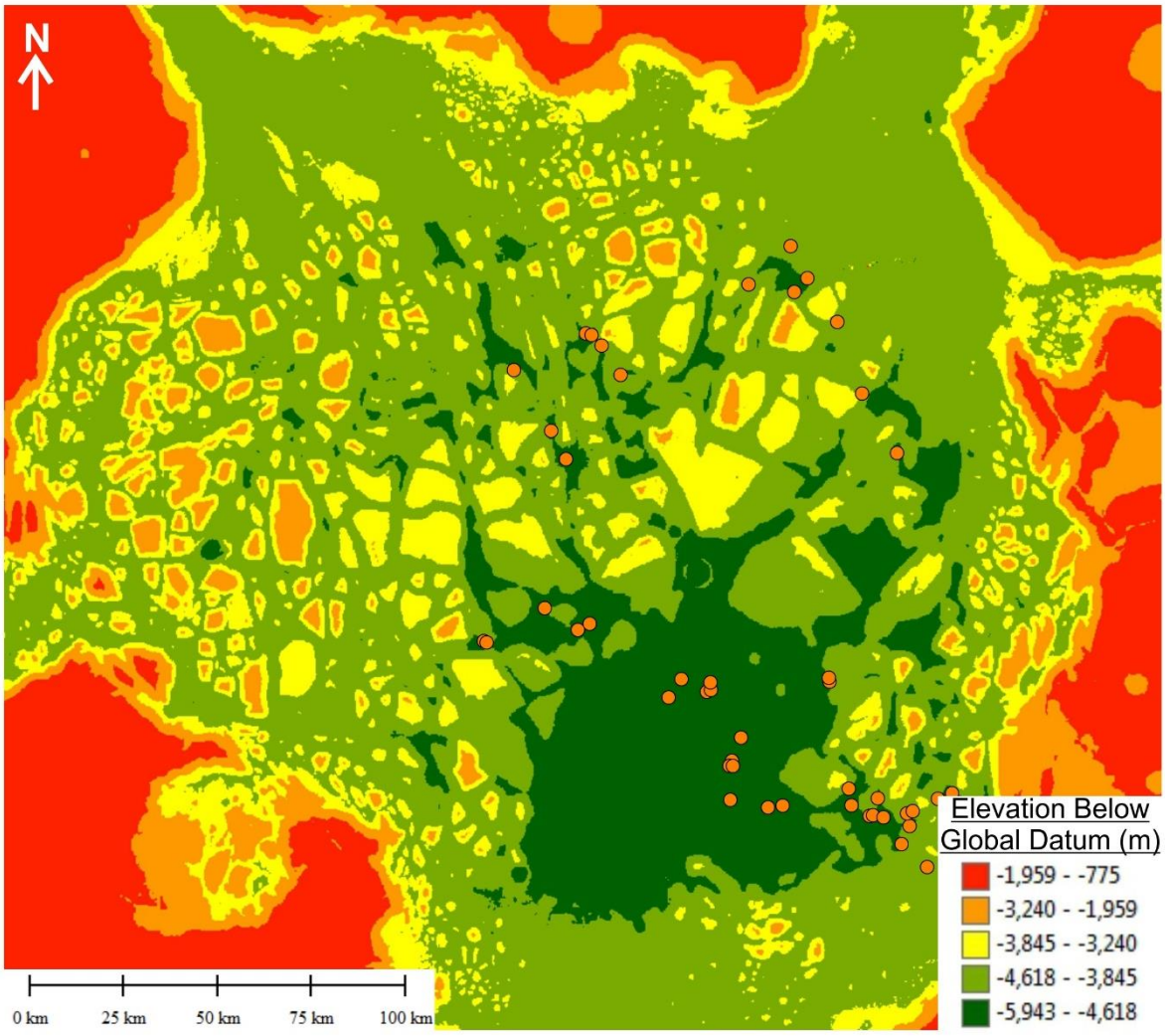

Figure 3-14 Cinder cone locations indicated by orange dots within Hydraotes chasma overlain on a contoured map of Hydraotes. Note that the bulk of the cinder cones are in the bottom basin layer.

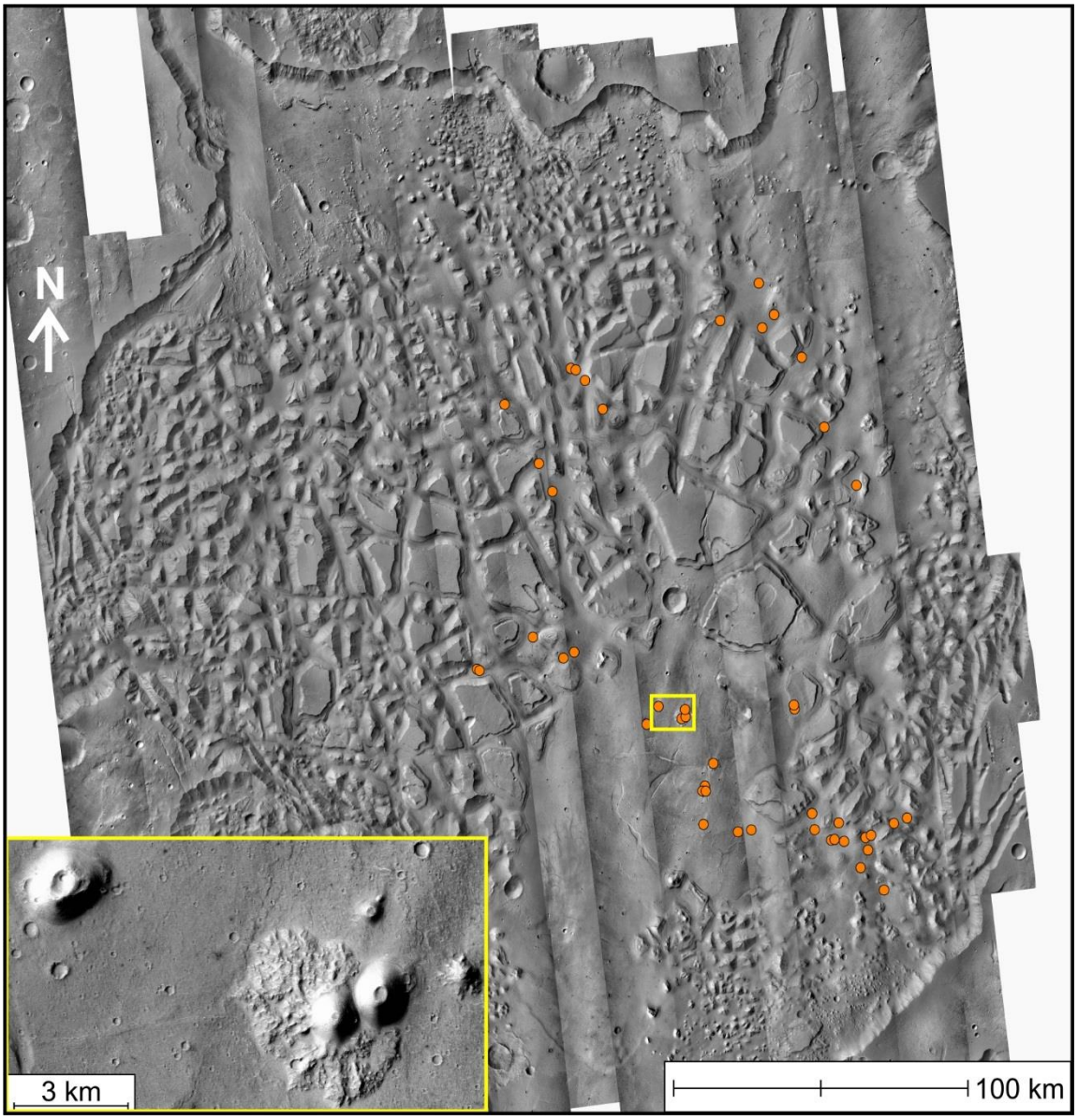

Figure 3-15 Location of cinder cones indicated by orange dots and a close up example of a cone (yellow box) within Hydraotes shown on a CTX composite mosaic.

3.4.6 Calculation of Volume Loss

In order to calculate the total volume loss due to the collapse of Hydraotes, a few assumptions and limitations had to be addressed. It is assumed that no significant changes in the elevation of the plateau have occurred. The current basin floor is used as the bottom for our calculations as there is no method to account for the sediment layer in the southern basin. It is accepted that the terraces were produced by lacustrine

action, as has been proposed, and assume that nearly all terraces in the chaos are from the same terrace group as described by Ori & Mosangini (1998) and were originally horizontal and that those at lower elevations have dropped. This drop must have occurred following the creation of the terraces and therefore it is assumed a minimum of two major periods of collapse, requiring a relatively stable environment in between giving the terraces a chance to form.

The total volume loss was calculated for Hydraotes chasma using a layer placed at the average surrounding plateau height of -1,500 m below the global datum. A schematic diagram of the total volume loss calculation is shown in Figure 2-1. The results are shown below in Table 3-2.

Table 3-2 Results of the main collapse volume loss calculation.

	Volume of Missing Material	Average Depth of Collapse
Plateau to Basin Collapse	157,000 km^3	1.65 km

Also calculated is the secondary collapse (Figure 3-16) which affected many of the terraces and therefore the mesas they surround, particularly in the southeast portion of Hydraotes. To calculate volume loss of the secondary collapse 69 terraces were chosen due to their being easily identified in DEM and their elevation was recorded and used to construct the TIN shown in Figure 3-17:B. To compare with the basin floor, 99 elevation points were selected from the floor around the terraces to create the TIN shown in Figure 3-17:C. Both TINs were then subtracted from each other to find the difference in elevation between the two shown in Figure 3-17:D. The secondary volume loss was calculated using the average of the most intact terraces at -3,854 m below the Mars datum as the top bounding surface and the current floor as the bottom surface.

The basin floor was chosen as the bottom bounding surface as several of the southeastern terraces are within 100 m of the basin floor, indicating some may also be buried. This also gives an estimate on the volume of the paleolake which created the terraces.

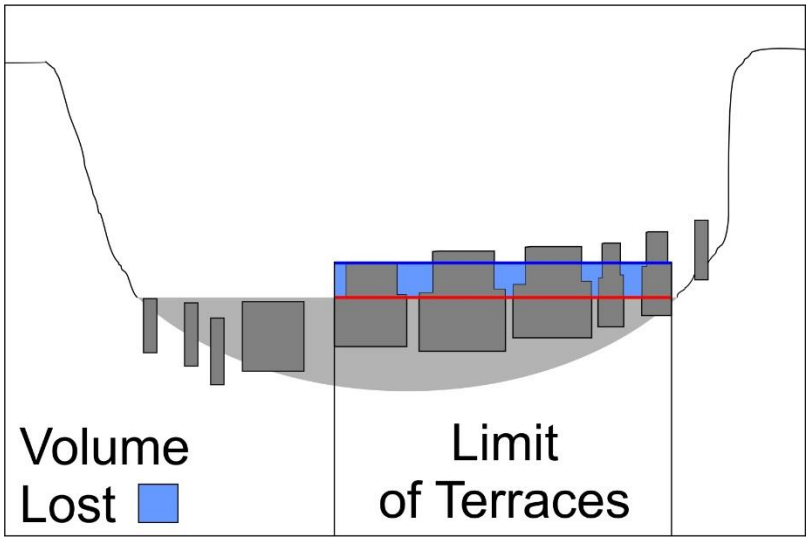

Figure 3-16 Schematic representation of the secondary collapse volume calculation. The highest terrace unit elevation (blue line) and the lowest terrace of the same unit (red line) are shown along with the calculated volume of missing material (blue shaded area).

The elevation of both datasets decreases towards the center of the basin. The elevation of the terraces should be approximately equal throughout the basin, assuming a horizontal surface to start; however, they instead mimic the current terrain. The results of this calculation and the sum of the main and secondary collapse are shown in Table 3-3.

Table 3-3 Results of the secondary collapse volume loss calculations, including the total volume loss within Hydraotes.

	Volume of Missing Material	Average Depth of Collapse
Post Terrace Collapse	22,000 km^3	0.45 km
Total Collapse	179,000 km^3	2.10 km

Using estimates of discharge rate by Ori & Mosangini (1998) of 40 X 10^6 m^3/s to 25 X 10^7 m^3/s and the volume loss shown in Table 3-3, an estimate of the time for complete drainage of Hydraotes chasma is between 8 and 50 days.

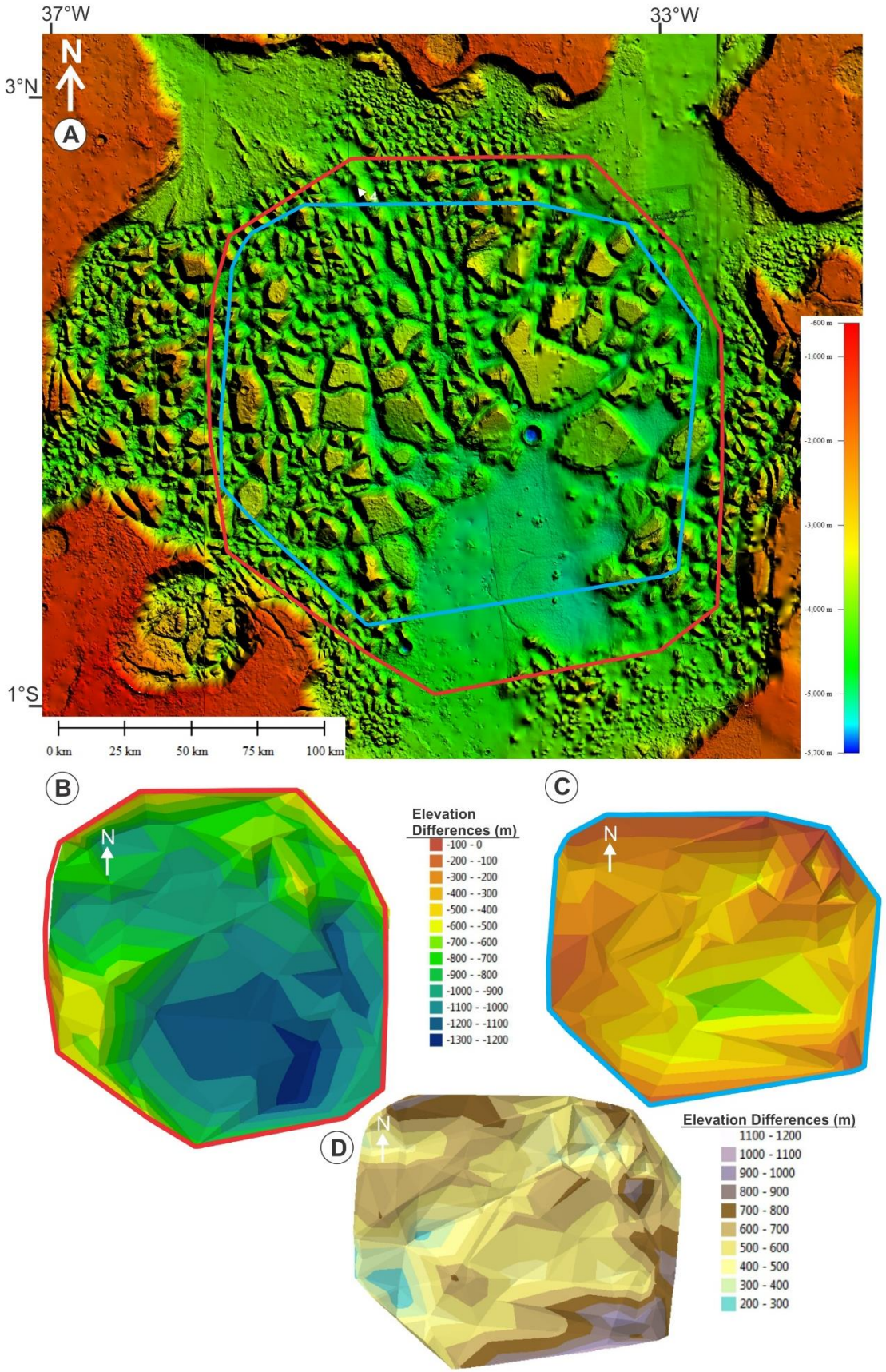

Figure 3-17 A) Composite DEM base map; B) Basin TIN created using 99 data points indicated by the red outline in A; C) Terrace TIN using 69 data points outlined in blue, using a simplified depth scale adjust to the highest elevation present; D) TIN comparison between B & C.

3.5.1 Orientation and Distribution of Mesas

The mesas within Hydraotes have been previously interpreted as the collapsed surface of the surrounding plateau (Ori & Mosangini, 1998; Meresse, et al., 2008). The mesas have shallow dips generally below 6°. The surrounding plateau is nearly horizontal at =/< 1°. This suggests that the mesas have undergone some rotation during collapse. The largest blocks are located near the center of the chaos zone, with the smooth floor section of the basin being the possible initial collapse location as suggested by Ori & Mosangini (1998). Several of the older blocks may also be remnants of past craters which have been heavily eroded.

The regional geology map by Rotto & Tanaka (1995) shows no regional structural trend, with only minor localized wrinkle ridges far to the west, and some fractures along the eastern wall of the chasma. No evidence of regional stresses is observed in the area surrounding Hydraotes. The distribution of the strikes of the tops of mesas within Hydraotes shows no strong preferred orientation, suggesting no underlying regional structural control on the collapse. There is a possibility that this lack of preferred orientation could indicate that the main chaos area was a crater or circular depression at one point; however, no elevated crater rim remnants can be identified within the chaos. The distribution of the strikes of the steep sides of the mesas does have a strong north-south preferred orientation, suggesting that they are oriented along the general north-south trend of the major channels adjacent to Hydraotes and have been subject to erosion during flooding.

The elongate ridges in the northwestern part of the chasma trend toward the northwest channel. These types of ridges are absent from the northeast portion of the

chasma. This suggests that the ridges were shaped by erosion and that greater erosion occurred within the northwestern channel. The current topography of the channel floors indicates that the northwest channel would be the last to cease flow, and most likely changed flow direction into the chasma, which is evident by the depositional fan on the basin floor.

3.5.2 Sedimentation of the Basin

The southern basin within Hydraotes is the lowest point in Hydraotes, smooth floored, and located at the entrance of the southern channel which leads into Hydraotes. The southern basin being flat suggests that sediment has been deposited through lacustrine deposition (Ori & Mosangini, 1998). Any water entering Hydraotes from Valles Marineris would have emptied into the basin. If the basin was the starting location for Hydraotes Chaos, then mesas or their eroded remnants should be present under the basin sediments.

3.5.3 Mesa Terraces

There is one main set of terraces and two minor sets, shown best in Figure 3-13:D. The sets are distinguished from each other based on their elevation difference with terrace sets being separated by 100 m – 200 m of elevation (Ori & Mosangini, 1998), with some blocks in the northeast corner showing all three sets of terraces. The highest set of terraces also shows the widest benches (Ori & Mosangini, 1998) and are found most often within the chaos. This would suggest that the largest set represents a more widespread lake in either water or ice form, while the minor sets are more

localized and represent localized ponding in depressions and may indicate the last areas where water was preserved at the surface.

Terraces can either be caused by erosion or deposition along a shoreline. Erosion suggests the presence of a cemented layer capable of producing a shelf as the layers above experience undercutting and subsequent failure as a wave cut platform. Deposition would indicate that sediments carried in the water either from within Hydraotes, produced during the collapse, or from the southern channel infill, would be deposited by lacustrine mechanisms, building out the platform. It is thought that the terraces are most likely erosional forms as there appears to be several resistant layers throughout the mesas.

The terraces mapped also mimic the terrain of the basin floor shown in Figure 3-17:B & C. This is evidence that the mesa blocks have collapsed following the formation of terraces, under the assumption that the terraces formed horizontal at the level of water within a paleolake. This secondary collapse has a calculated average depth of 0.45 km which would require material to be removed from underneath the exiting chaotic terrain. One of the possibilities is magma expulsion, which will be discussed in conjunction with the cinder cones below.

3.5.4 Presence of Cinder Cones Within Hydraotes

Cinder cones present within Hydraotes are less abundant (46) than in areas like Coprates (>100) (Hauber, et al., 2015). They are evidence of volcanism in the area that at the earliest, postdates the collapse and draining of Hydraotes, and therefore may have had no role in the initial collapse. Volcanic heating has long been considered a

trigger mechanism for producing the collapse and catastrophic flooding associated with chaotic terrains. The cinder cones present are relatively small with very small volumes of associated possible pyroclastic aprons. The low volume of pyroclastic material present around the cones suggests that the volume loss within the chaotic terrain was not caused by removal of magma. The cinder cones identified by Hauber et al. (2015) within Coprates are slightly smaller but far more numerous than those found in Hydraotes. The area with the highest density of cinder cones also coincides with the area of deepest secondary collapse; however, there is no oriented trend. By comparison the cinder cones in Coprates follow two main trends, one which follows Valles Marineris (~N 110°) and another at ~N 75° (Hauber, et al., 2015). Hauber et al. (2015) attributed the main trend following Valles Marineris to be following the underlying zone of weakness created during the formation of Valles Marineris. This may indicate that the area underlying the cinder cones in Hydraotes are also exploiting a weakness created through the process of chaos formation. The secondary collapse as evident by the terraces may have been triggered by late volcanic heating exploiting this underlying weakness.

3.5.5 Significance of Sapping Channels

Hydraotes Chaos is unique among chaotic terrain in that it had a standing body of water/ice which was fed from an incoming channel, as well as internally from subsurface water escape during the collapse process.

Models for the formation of sapping channels include non-pressurized or pressurized groundwater flow. Non-pressurized groundwater flow produces a channel

which then excavates headward, constantly moving the channel head forward (Marra, 2014). This is thought to be the process which occurs in a number of channels along Valles Marineris (Marra, et al., 2014). Pressurized groundwater produces a collapse, which becomes the valley head which remains stationary while incision occurs downslope (Marra, et al., 2014). Pressurized groundwater may have been the cause of Aromatum Chaos (Leask, et al., 2006).

This suggests that sapping occurs in the presence of large volumes of water. It is unlikely that the individual mesas on which sapping channels are located provided the water necessary for their formation. This suggests that the sapping channels predate the formation of the mesas. Marra et al. (2014) found that experiments with lower water levels produced more undercutting and resulted in steeper valley heads, which exist in Hydraotes. This may suggest that the sapping channels in Hydraotes occurred during a relatively dry period where much of the groundwater was still locked up in subsurface ice and could therefore represent periods of seasonal thawing. Figure 3-4 indicates however that there is a small number of possible sapping channels found within Hydraotes with no preferred orientation. This indicates that, although they are present within the chaos, they most likely are a secondary structure that do not influence the formation of chaotic terrain.

3.6 Origin of Hydraotes

The location of Hydraotes coincides with the approximate Arabia shoreline (Figure 3-18) (Citron, et al., 2018). This suggests that the initial deposit of water around Hydraotes may have been linked to a northern ocean. At that time Hydraotes may have

been a crater filled with water or a localized depression. The Arabia shoreline shown in purple in Figure 3-18 was most likely emplaced 4 Ga, immediately followed by Tharsis emplacement (Citron, et al., 2018). Whether this ocean was stable, or frozen with cyclic melting events, it would have provided large volumes of water in the Hydraotes region.

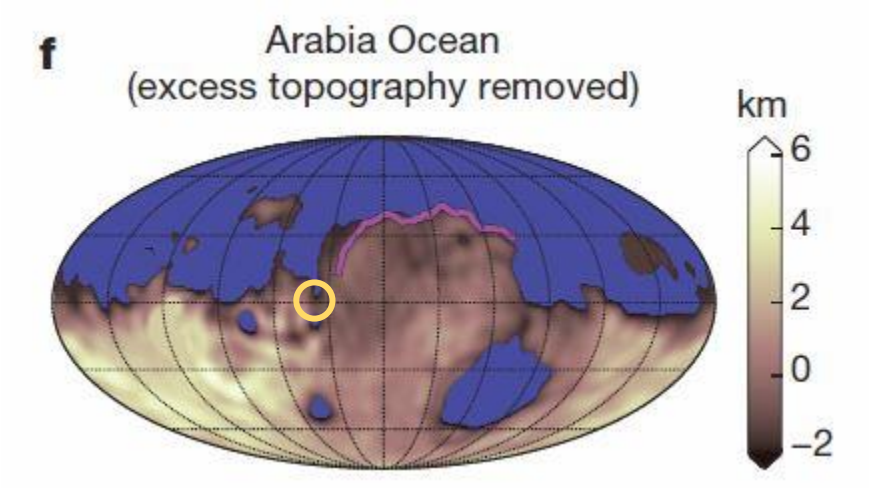

Figure 3-18 Part of Citron et al. (2018) Ocean model, edited to show the location of what would become Hydraotes (Yellow Circle).

3.7 Hydraotes Chaos Formation Model

A conceptual model (Figure 3-19) for the evolution of Hydraotes Chaos was created in order to better understand the possible stages of formation for Hydraotes. The model is simplified in that it only shows a cross section from Hydraotes channel to the Tiu Valles head therefore, it does not include Simud Valles to the northwest or the large collapse to the west of Hydraotes.

3.7.1 Model Assumptions

Assumptions also had to be made in order to create a model with the data available. The thickness of the mesa blocks was calculated to be ≥1.4 km using the average current mesa elevation and subtracting the current basin elevation, assuming a uniform thickness of the plateau in the area. The thickness of the proposed initial frozen lake is 2.1 km (Fig 3-19, inset 3) at the base of Hydraotes' center. This estimate is based directly on the average collapse depth. It is also assumed that the water flowed south initially (Fig 3-19, insets 5 & 6) due to the southern channel being at lower elevations than the center of collapse. Current climate models like the Late Noachian Icy Highlands model (Palumbo, et al., 2018) assume a cold and possibly wet climate for Mars. This assumption would mean that water on the surface would be frozen unless under turbulent flow, high salinity, or under pressure. In Hydraotes it is assumed to be a water lake (Fig 3-19, insets 1 & 2) which would only stay liquid during periods of high-volume flow, or during short periods of high temperature controlled by orbital characteristics. A single localized water source in Hydraotes similar to previous authors (Meresse, et al., 2008; Zegers, et al., 2010; Roda, et al., 2016) is assumed.

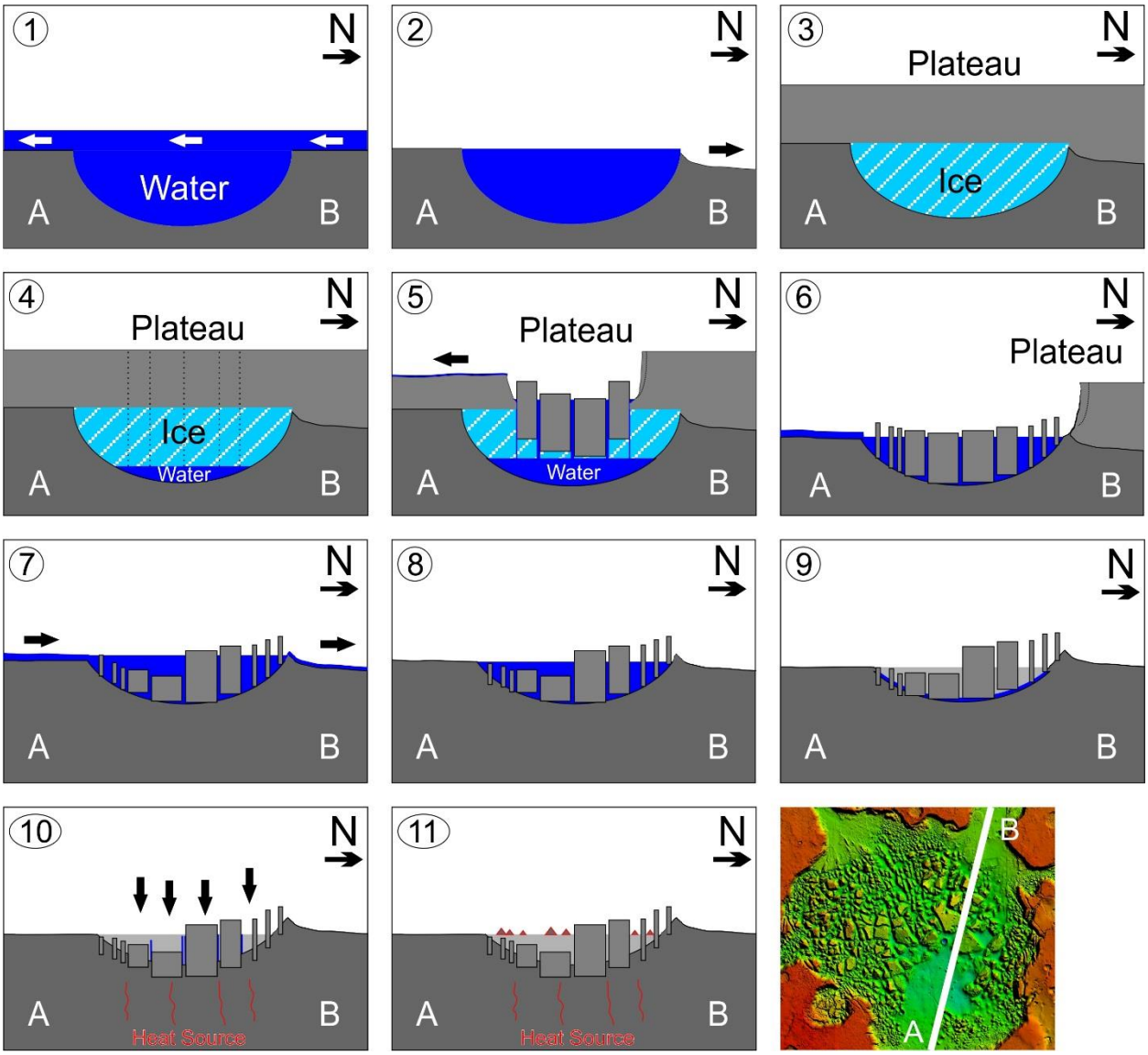

Figure 3-19 Cross sectional model of Hydraotes Chaos formation. The cross section starts at the mouth of Hydraotes channel in the south and ends at the head of Tiu Valles in the northeast.

3.7.2 Model Description

Initially the northern ocean which produced the Arabia shoreline would have extended to the current location of Hydraotes at its maximum (Fig 3-19, inset 1) (4 Ga, Citron, et al., 2018). This ocean would have provided a large volume of water to create a lake. It is assumed that water pooled in Hydraotes as the northern ocean receded (Fig 3-19, inset 2). The water would have filled a depression of unknown shape, which may have been an impact crater. The recession of the northern ocean may have been triggered by a change in climate coinciding with the emplacement of Tharsis (Citron, et al., 2018).

Tharsis emplacement occurs over an unknown period of time, but the bulk of Tharsis is thought to have been in place by 3.6 Ga (Citron, et al., 2018, Tanaka & Hartmann, 2012, Anderson, et al., 2001). During active volcanism, material would be deposited on top of a frozen lake within Hydraotes (Fig 3-19, inset 3). Further sedimentation would fill Hydraotes to the current plateau elevation. During this period water in the subsurface would leach downslope following the topography (Fig 3-19, inset 4 & 5) creating sapping channels. The insulating effect of the overburden would increase as the thickness of the sediment package increases, with enough insulation melting can begin to occur where the ice is in contact with the surrounding basement which has a higher thermal conductivity than the overburden (Fig 3-19, inset 4) (Zegers & Roda, 2012).

Relatively small amounts of subsidence would occur as basal ice melts, centralized within the basin. Gradual subsidence may cause fractures to form (Fig 3-19, inset 4) or they may form through other means including Mars quakes or impacts.

Fractures in the subsurface would propagate upwards through hydrofracturing, and on reaching the surface would release the water at high pressure (30 MPa, Zegers et al., 2010). Water escaping to the surface would drain southward following the topography away from the basin (Fig 3-19, inset 5). Collapse of the central plateau would follow, produced by a combination of liquefaction and subsurface faulting (Fig 3-19, inset 5). Collapse would start in the current southern smooth floor basin of Hydraotes spreading outwards. The collapsing mesas cause flexure in the surrounding wall rock which forces smaller blocks to collapse from the plateau, producing knobs along the edges of the basin with a small degree of rotation (Fig 3-19, inset 6). This explains why the central mesas within Hydraotes are larger than the surrounding blocks with some of them exceeding 50 km^2 and having dips less than 6°. Water would continue to reach the surface and carve out the channel southward, draining much of Hydraotes (Fig 3-19, inset 6).

The opening of Valles Marineris (late Noachian/Early Hesperian, Tanaka & Hartmann, 2012; Anderson, et al., 2001) and subsequent flooding events would have caused the flow out of the southern channel to reverse, as water would start pouring into Hydraotes basin from the southern channel (Fig 3-19, inset 7). No large channels exist within Hydraotes Chaos which could have transported water directly from the southern channel to the northern channels, so the incoming water must have pooled in the southern basin initially. Eventually the incoming water would have filled Hydraotes and overflowed the topographic restriction situated at the head of what is now Tiu Valles (Fig 3-19, inset 7). During this time the southern basin blocks either collapsed further and/or are heavily eroded by the incoming water (Fig 3-19, inset 7,8,9).

As flow events subsided periods of relatively stable water/ice levels formed the multiple levels of terraces within Hydraotes (Fig 3-19, inset 8). A frozen top layer is plausible due to Mars' surface temperatures, and water/ice interactions can produce prominent erosional surface on Earth seen in Antarctic beaches on Earth (Ori & Mosangini, 1998). Multiple levels of terraces exist which indicate at least 3 time periods when water levels were stable for extended periods. The terraces would have formed a horizontal surface, parallel to the water level. Freezing and sublimation is a probable mechanism for removing the remaining surface water from Hydraotes following the creation of the terraces.

The initial collapse is assumed to have not fully drain the subsurface water in Hydraotes as the velocity and volume of water would naturally decrease over time, this accompanied by the loss of the thermal insulation of the overburden causes freezing to set in. The remaining ice would be trapped under the plateau blocks. At some time following the removal of surface waters some type of magmatic activity occurred in which the subsurface is heated externally from below (Fig 3-19, inset 10). The heating would melt any remaining ice leading to removal of a subsurface volume of ice, calculated to be approximately 22,000 km^3 (Fig 3-19, inset 10). This removal triggers a secondary collapse of a large area of the chaotic terrain, collapsing an average of 450 m. The majority of the water would most likely make it to the surface where it would freeze and sublimate, leaving the floor between mesas sediment covered. Cinder cone development on the surface of the basin floor occurs following this secondary collapse (Fig 3-19, inset 11), and may be evidence of that magmatic activity with the creation of at least 46 individual cones primarily formed within the basin unit.

References

Anderson, R. C., Dohm, J. M., Golombek, M. P., Haldemann, A. F., Franklin, B. J., Tanaka, K. L., . . . Peer, B. (2001). Primary centers and secondary concentrations of tectonic activity through time in the western hemisphere of Mars. *JGR, 106*(E9), 20,563-20,585.

Brož, P., Čadek, O., Hauber, E., & Rossi, A. P. (2015). Scoria cones on Mars: Detailed investigation of morphometry based on high-resolution digital elevation models. *JGR: Planets, 120*, 1,512-1,527. doi:10.1002/2015JE004873

Citron, R. I., Manga, M., & Hemingway, D. J. (2018). Timing of oceans on Mars from shoreline deformation. *Nature, 555*. doi:10.1038/nature26144

Harrison, K. P., & Chapman, M. G. (2008). Evidence for ponding and catastrophic floods in central Valles Marineris, Mars. *Icarus, 198*, 351-364. doi:10.1016/j.icarus.2008.08.003

Hauber, E., Brož, P., Rossi, A. P., & Michael, G. (2015). A Field of Small Pitted Cones on the Floor of Coprates Chasma Mars: Volcanism Inside Valles Marineris? *46th Lunar and Planetary Science Conference.*

Leask, H. J., Wilson, L., & Mitchell, K. L. (2006). Formation of Aromatum Chaos, Mars: Morphological development as a result of volcano-ice interactions. *JGR, 111*(E08071). doi:10.1029/2005JE002549

Marra, W. A., Braat, L., Baar, A. W., & Kleinhans, M. G. (2014). Valley formation by groundwater seepage, pressurized groundwater outbursts and crater-lake overflow in flume experiments with implications for Mars. *Icarus, 232*, 97-117. doi:10.1016/j.icarus.2013.12.026

Meresse, S., Costard, F., Mangold, N., Masson, P., & Neukum, G. (2008). Formation and evolution of the chaotic terrains by subsidence and magmatism: Hydraotes Chaos, Mars. *Icarus, 194*, 487-500. doi:10.1016/j.icarus.2007.10.023

Ori, G. G., & Mosangini, C. (1998). Complex depositional systems in Hydraotes Chaos, Mars' An example of sedimentary process interactions in the Martian hydrological cycle. *JGR, 103*(E10), 22,713-22,723.

Pajola, M., Rossato, S., Baratti, E., Mangili, C., Mancarella, F., McBride, K., & Coradini, M. (2016). The Simud–Tiu Valles hydrologic system: A multidisciplinary study of a possible site for future Mars on-site exploration. *Icarus, 268*, 355-381. doi:10.1016/j.icarus.2015.12.049

Palumbo, A. M., Head, J. W., & Wordsworth, R. D. (2018). Late Noachian Icy Highlands climate model: Exploring the possibility of transient melting and fluvial/lacustrine activity through peak annual and seasonal temperatures. *Icarus, 300*, 261-286. doi:10.1016/j.icarus.2017.09.007

Petroff, A. P., Devauchelle, O., Abrams, D. M., Lobkovsky, A. E., Kudrolli, A., & Rothman, D. H. (2011). Geometry of valley growth. *Journal of Fluid Mechanics, 673*, 245-254. doi:10.1017/S002211201100053X

Roda, M., Kleinhans, M. G., Zegers, T. E., & Govers, R. (2016). Origin of circular collapsed landforms in the Chryse region of Mars. *Icarus, 265*, 70-78. doi:http://dx.doi.org/10.1016/j.icarus.2015.10.020

Rotto, S., & Tanaka, K. L. (1995). *Geologic/geomorphic map of the Chryse Planitia region of Mars.* USGS. doi:10.3133/i2441

Tanaka, K. L., & Hartmann, W. K. (2012). The Planetary Time Scale. In F. M. Gradstein, J. G. Ogg, M. Schmitz, & G. Ogg, *The Geologic Time Scale* (pp. 275-298). Elsevier.

Tanaka, K., Skinner, J. A., Dohm, J., Irwin, R. I., Kolb, E., Fortezzo, C., . . . Hare, T. (2014). Geologic map of Mars: U.S. Geological Survey Scientific Investigations Map 3292. *scale 1:20,000,000, pamphlet 43 p.* doi:https://dx.doi.org/10.3133/sim3292

Zegers, T. E., & Roda, M. (2012). Chaotic Terrains on Mars: testing the subsurface lake hypothesis. *Rend. online Soc. Geol. It., 22*, 243-246.

Zegers, T. E., Oosthoek, J. H., Rossi, A. P., Blom, J. K., & Schumacher, S. (2010). Melt and collapse of buried water ice: An alternative hypothesis for the formation of chaotic terrains on Mars. *Earth and Planetary Science Letters, 297*, 496-504. doi:10.1016/j.epsl.2010.06.049

Chapter 4.0 **: Hydraspis Chaos**

4.1 Introduction

Hydraspis Chaos is a large region of chaotic terrain located directly east of Hydraotes Chaos (Figure 4-1). This chapter will focus on the Fractured-Floor Crater (FFC) (Bamberg, et al., 2014) which is most likely a crater pair (Korteniemi, et al., 2006) at the western edge of the Hydraspis region. The chaotic terrain present within the Hydraspis crater pair shares several morphological features with other chaotic terrains, namely large mesas and knobs separated by narrow channels.

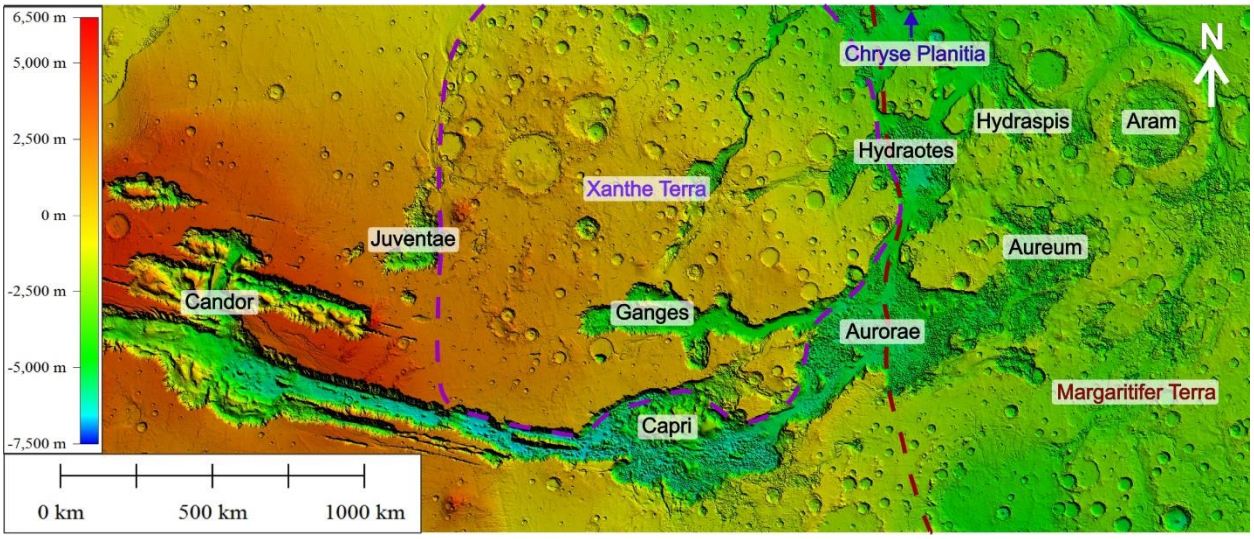

Figure 4-1 Overview of the area surrounding Hydraspis, the rough outline of Xanthe Terra (purple dashes) and Margaritifer Terra (red dashes) is shown.

The morphology of the mesas and knobs are similar to those found in Hydraotes; the main difference is that the chaos is completely contained within a crater pair. The crater pair covers an area ~7,700 km^2 (Figure 4-2) with the surrounding plateau having an average height of -1,400 m. The eastern side is higher than the western side by ~200 to 600 m, unlike the plateau surrounding Hydraotes which is fairly uniform in elevation. The eastern rim of the crater is the highest point in the area and may indicate the direction of impact. The highest point of the surviving rim is -800 m below the global

datum, with the lowest point of the floor of the crater pair at -4,300 m; however this is in areas which were most likely scoured by water. The rest of the crater floor is at an elevation closer to -4,000 m. The larger of the two craters has a central peak with a current elevation of -2,100 m while the deepest portion of the floor surrounding the peak is -3,800 m. No rim can be seen dividing the two craters (Figure 4-2 & 4-3); therefore the pair most likely formed from a single large bolide which broke into two pieces prior to impact.

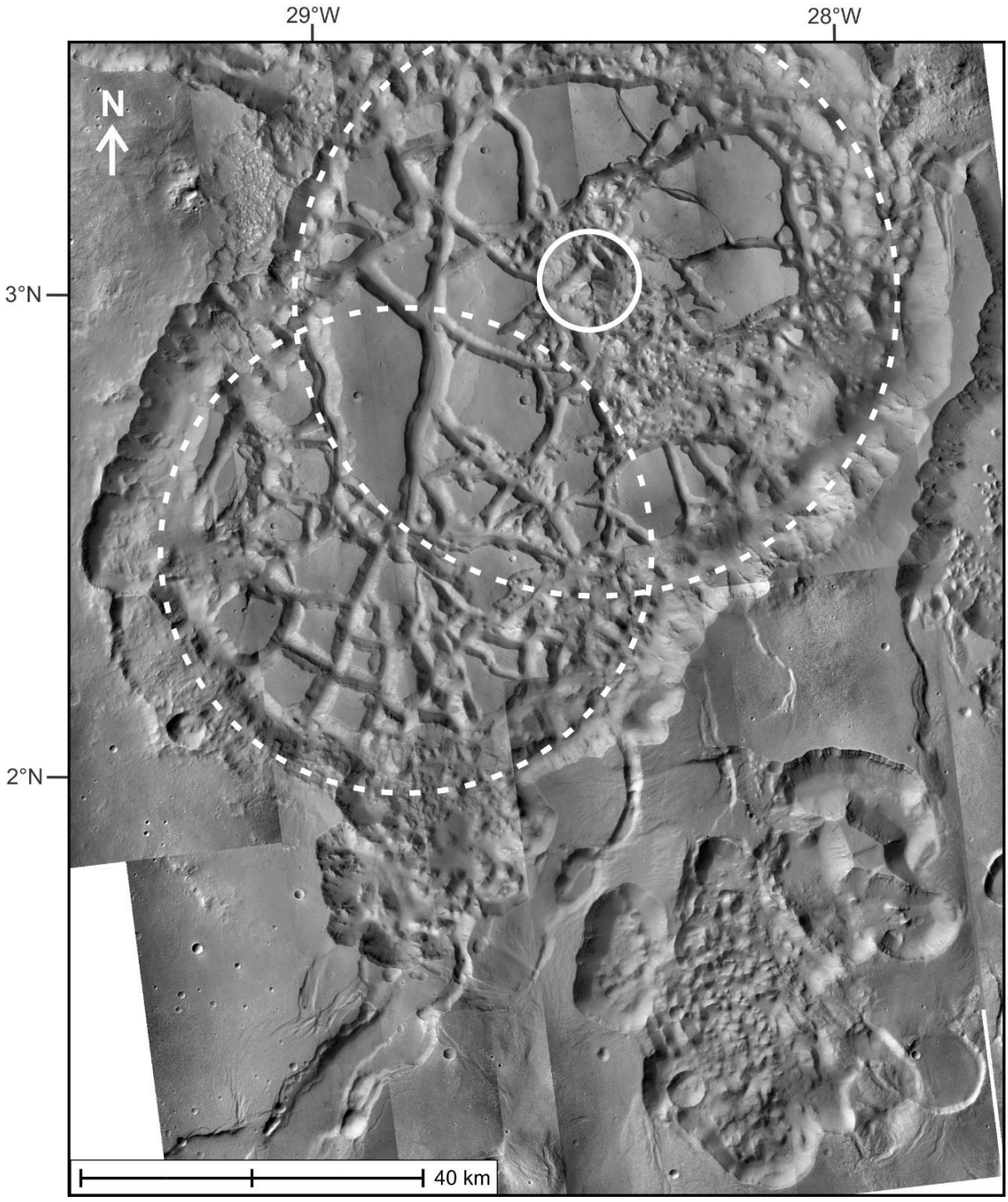

Figure 4-2 CTX mosaic of the Hydraspis crater pair including southern plateau, with the central peak circled in white, approximate crater outlines are shown with dashed lines.

Figure 4-3 shows a DEM composite of the crater pair. The northern rim is absent, likely allowing water to flow out of the crater northward to outwash channels.

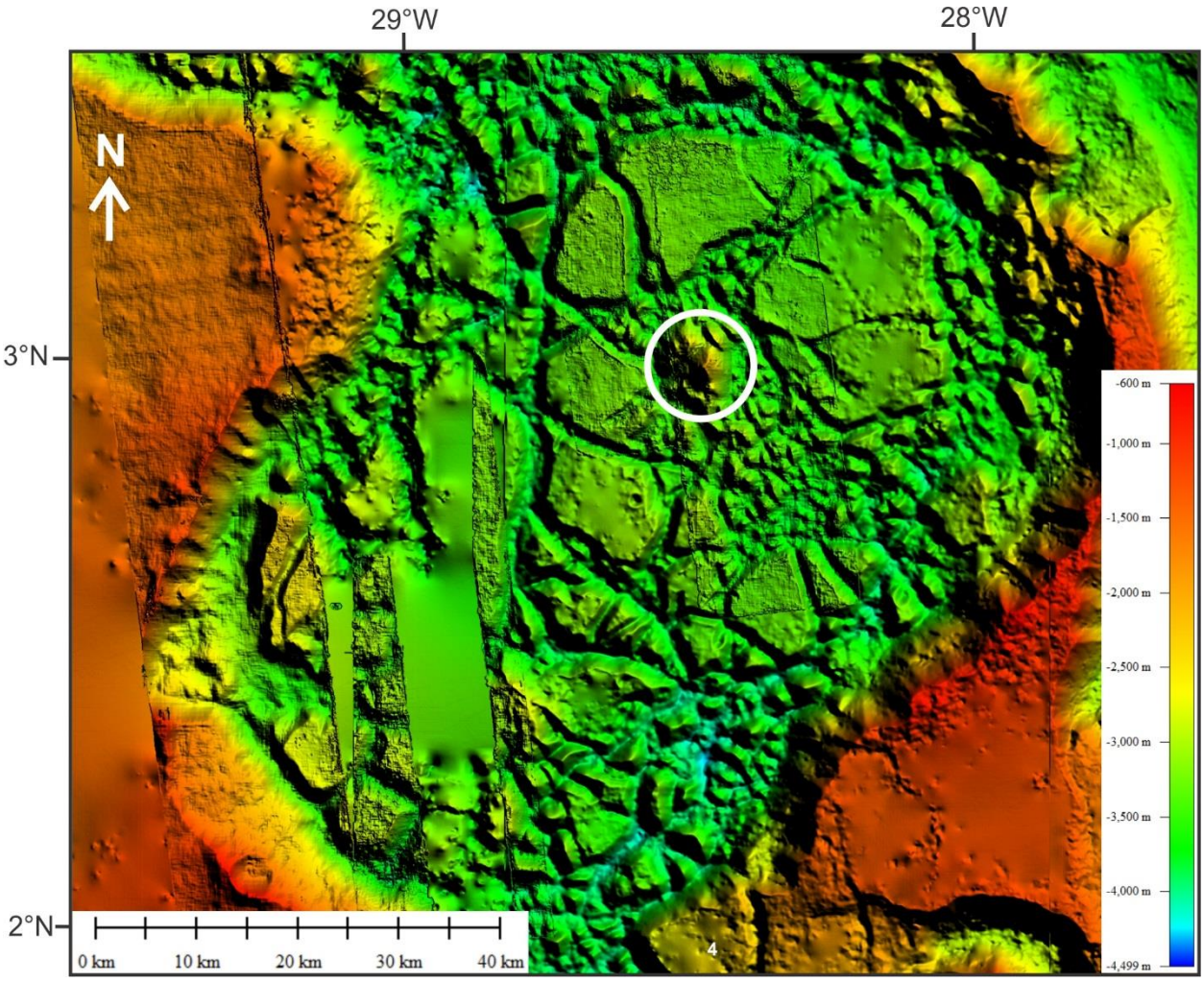

Figure 4-3 DEM mosaic of the Hydraspis crater pair with the central peak circled in white.

No regional tectonic trends are apparent within or surrounding the Hydraspis crater pair according to the USGS Rotto & Tanaka (1995) or Tanaka et al. (2014) Geologic Map of Mars. There is one N-S wrinkle ridge nearby, which has the same strike as those near Hydraotes. There is also significant fracturing in the plateau south of the craters near Aureum Chaos (Figure 4-1), that dominantly strikes NW-SE.

Sapping channels are also present within the Hydraspis crater pair (Figure 4-4). These channels cut through several of the mesa blocks and can be created by slope undercutting via groundwater release (Marra, et al., 2014). Sapping channels follow a headward migration resulting from erosive mechanisms carrying sediments from the subsurface (Marra, et al., 2014). The location of the sapping channels is confined to the northeastern crater with no channels located in the southwestern portion. The larger channels are also eroding away from the central peak.

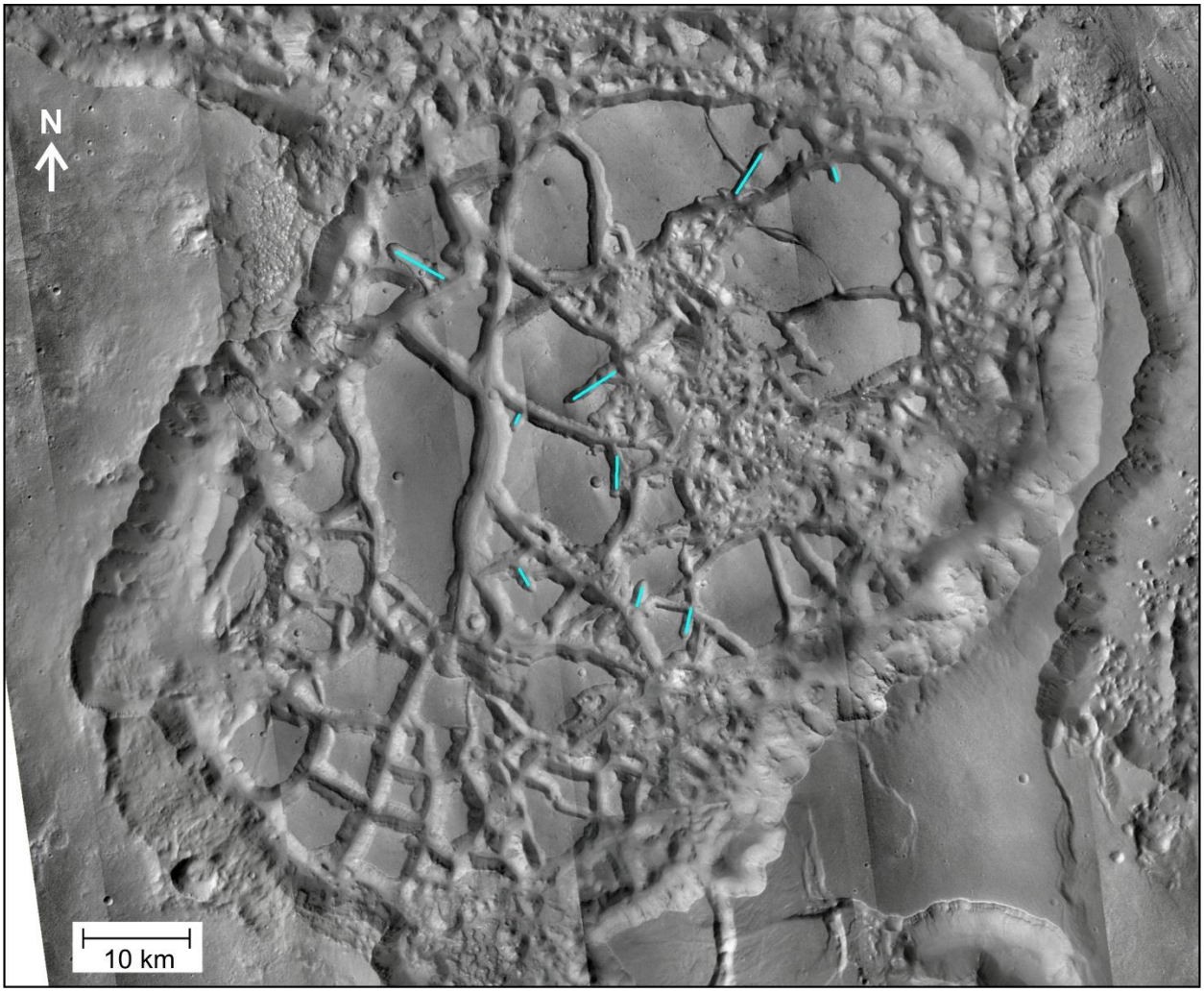

Figure 4-4 Locations of possible sapping channels within the Hydraspis crater pair.

4.2 Previous Work

This pair of craters on the western edge of Hydraspis Chaos has not been the subject of previous studies. There has however, been several studies on FFCs that have investigated their formation, morphology, and occurrence.

Bamberg et al. (2014) found a high spatial density correlation of FFCs along the dichotomy boundary. In their study area east of Arabia Terra (Figure 1-1), the majority of FFCs have fractures and channels that extend outside craters and into the surrounding terrain, some of which connect to other FFCs (Bamberg, et al., 2014). The FFCs analyzed show layering and terraces to be common characteristics of FFCs (Bamberg, et al., 2014). The most likely models proposed for the creation of FFCs include an intrusive volcanism model and a groundwater migration model (Bamberg, et al., 2014).

Sato et al. (2010) suggest that the larger craters have more developed chaotic terrains which led them to propose a sequence of morphologies for FFCs. The morphology ranges from a few fractures, to many fractures and mesas, to the erosion of mesas into many knobs as intensity increases (Sato, et al., 2010). These fractures often extend deeper than the original crater floor and most likely occurred long after impact crater formation (Sato, et al., 2010). Sato et al. (2010) determined that there is a strong link between FFCs and chaotic terrains suggesting water drainage in the late Hesperian played a major role in both formations. The thickness of infilling of the craters was not found to correlate with the FFC type. However, an onset depth of 1,000 – 2,000 m is required for chaos formation in FFCs (Sato, et al., 2010).

4.3 Methodology

For methods used, refer to Chapter 2.0 – Methodology above. This standard is used for each case study, except where otherwise indicated.

The 50 m/pixel DEM composite used for Hydraspis Chaos is composed of CTX and HRSC. Orbits used are shown in Table 4-1. Approximately 20% of the DEM composite is 20 m CTX data with HRSC data filling the rest.

Table 4-1 Images used to create the composite DEM for the Hydraspis crater pair.

HRSC Orbit	CTX DEM Pairs
h0155_0001_da4_53 (50 m/pixel)	P17_007573_1837_XN_03N029W- P17_007718_1825_XI_02N029W
h1055_0000_da4_53 (75 m/pixel)	D10_031242_1830_XN_03N028W- F02_036767_1832_XN_03N028W
h1066_0000_da4_53 (75 m/pixel)	B16_015880_1845_XN_04N028W- D10_031242_1830_XN_03N028W
	B11_014113_1836_XN_03N029W- P06_003314_1836_XI_03N028W
	B11_014113_1836_XN_03N029W- P17_007718_1825_XI_02N029W

4.4 Results

4.4.1 Orientations Obtained with AVA

Strike and dip measurements for the mesas and surrounding plateau region around the Hydraspis crater pair were calculated using a 3x3 AVA kernel (Figure 4-5). The dip of every pixel within the crater pair was also calculated with the AVA (Figure 4-6), with the average dip of the mesa top surfaces shown in Figure 4-7. The surrounding plateau has an average dip of < 3°. The dip of the steep sides (dips of 17-40°) of the mesa blocks was calculated using a value range consistent with previous analyses.

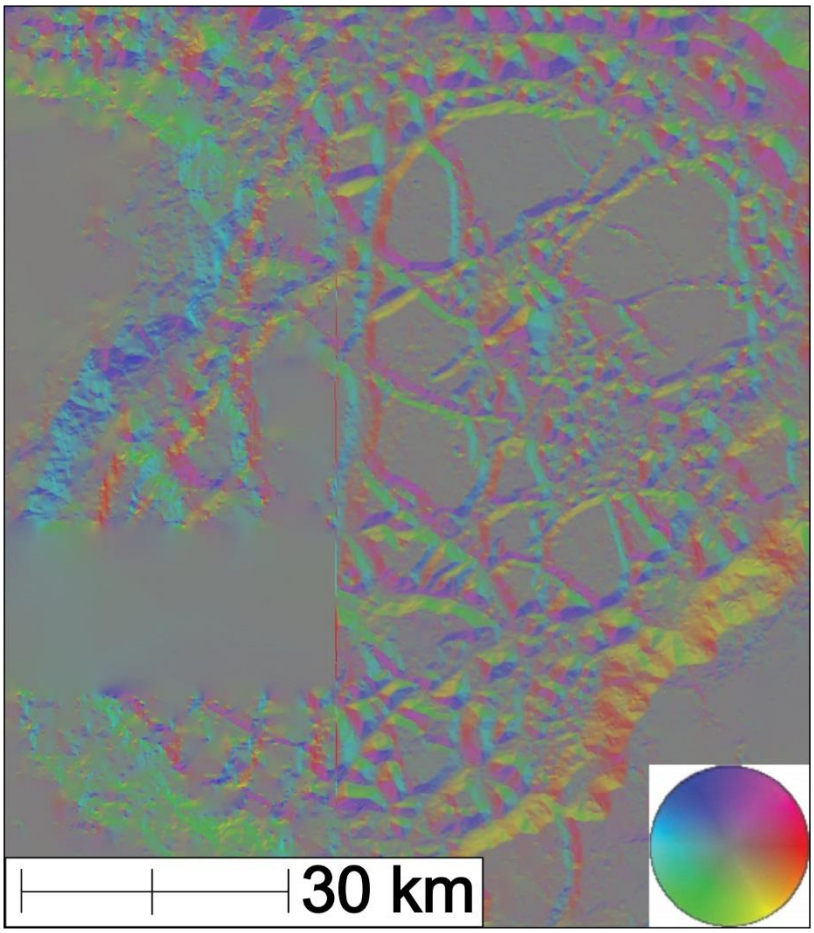

Figure 4-5 Colourized Augmented Visualization of Attitude (AVA) results using a colour-coded stereonet.

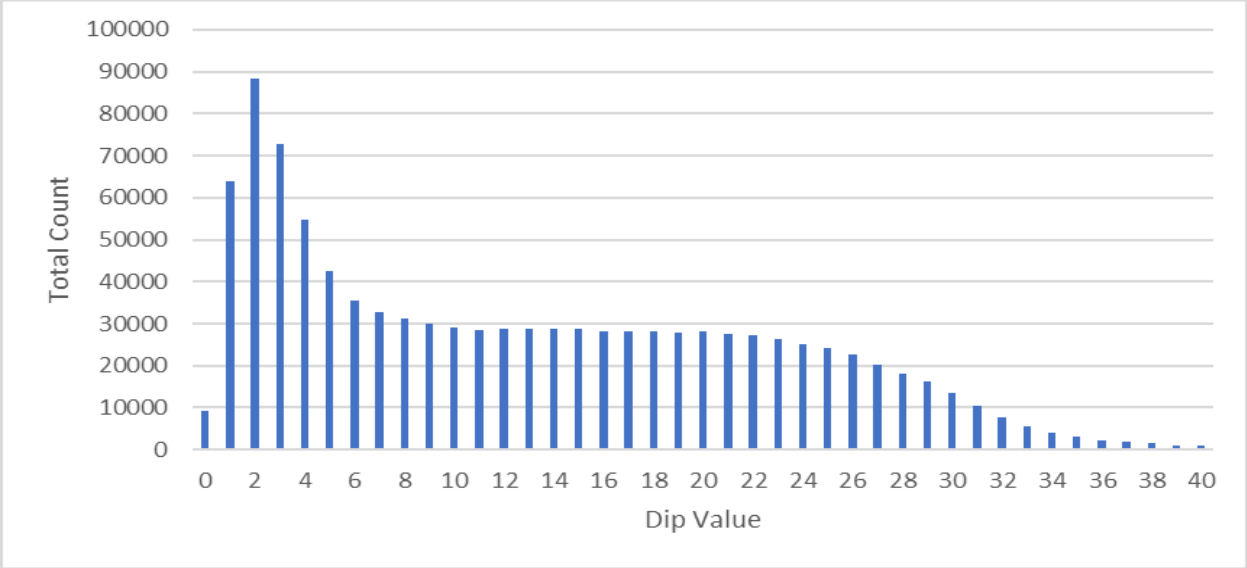

Figure 4-6 Dip value of all points calculated with the AVA of the Hydraspis crater pair.

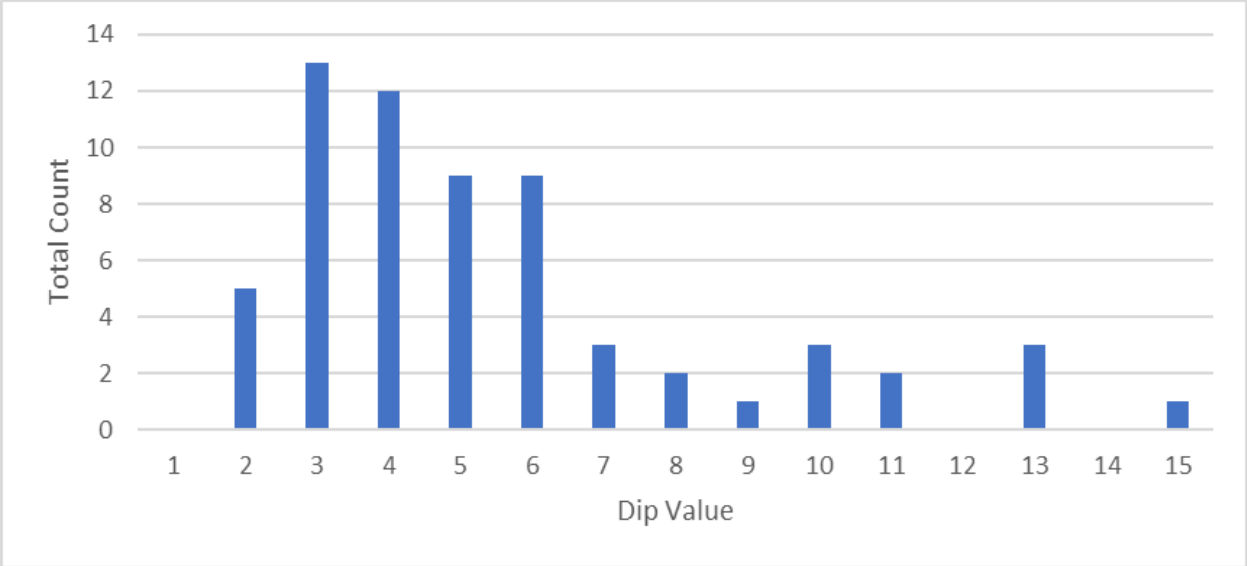

Figure 4-7 Average dip calculated for each mesa flat top within the Hydraspis crater pair. A total of 63 mesa tops were calculated.

Figure 4-8 shows the strike values calculated using the AVA within the Hydraspis crater pair. The mesa blocks show no preferred orientation of collapse. The steep sides of the blocks show a weak north-south trend, which coincides with the northward movement of water out of the crater.

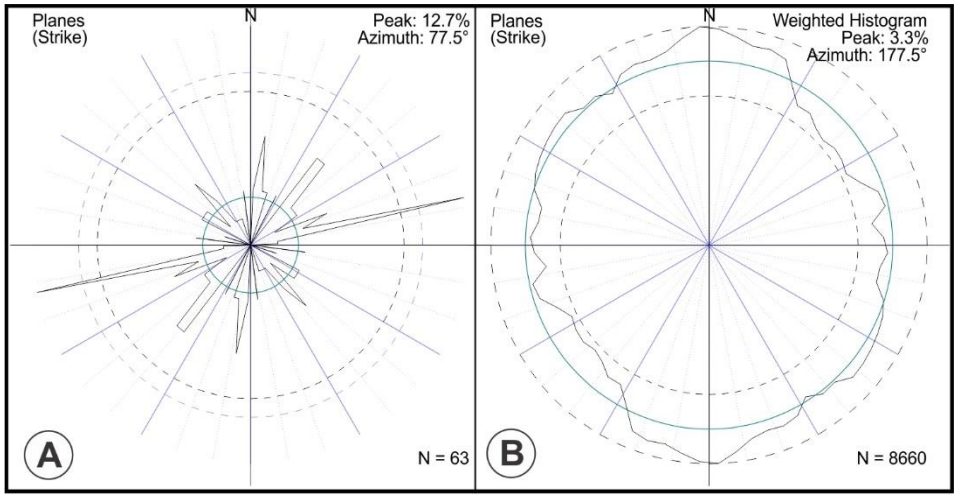

*Figure 4-8 A) Rose diagram of the strike for all mesa tops within the Hydraspis crater pair. B) Rose diagram of strike for all points within the Hydraspis crater pair that have dips from 17° - 40°. Due to computational limitations a histogram of all strike/dip value combinations with dips between 17-40 were used (360 strike values * 24 dip values= 8660 non-zero entries)*

4.4.2 Elevation and Distribution of Mesas

Figure 4-9 shows a contoured image of the Hydraspis crater pair showing the major morphologic groups: the surrounding plateau (red), mesa blocks (yellow), transition from rim to blocks (orange), and the crater floors (greens). The southwestern portion of the crater pair shows a higher elevation of collapsed mesas. The smaller knobs have a higher concentration along the southern and southeastern edge of the crater basin, as well as immediately adjacent to the central peak, which coincides with the deepest portions of the basin.

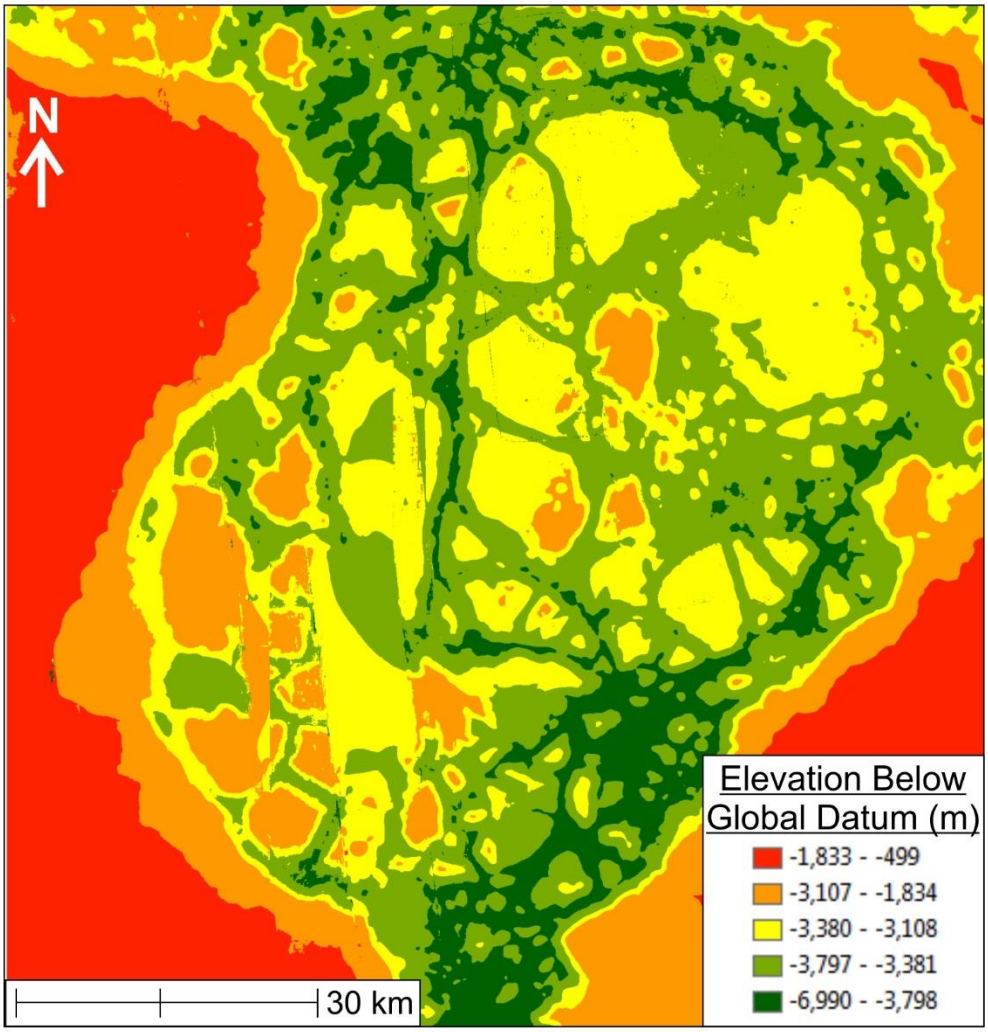

Figure 4-9 Manually set contours to allow for better visualization of sections of the Hydraspis crater pair.

4.4.3 Orientation of Mesa Tops

The dips of the top surfaces of the mesa blocks were calculated using the AVA (Figure 4-10). The rose diagram (Figure 4-8:A) shows no preferred orientation of these blocks. Generally low dip values are observed within the crater mesas and surrounding plateau. Some higher values (>10°) are observed in the southwest sections, which is where more wall collapse has occurred. There is also no apparent trend surrounding the central peak of the northern crater.

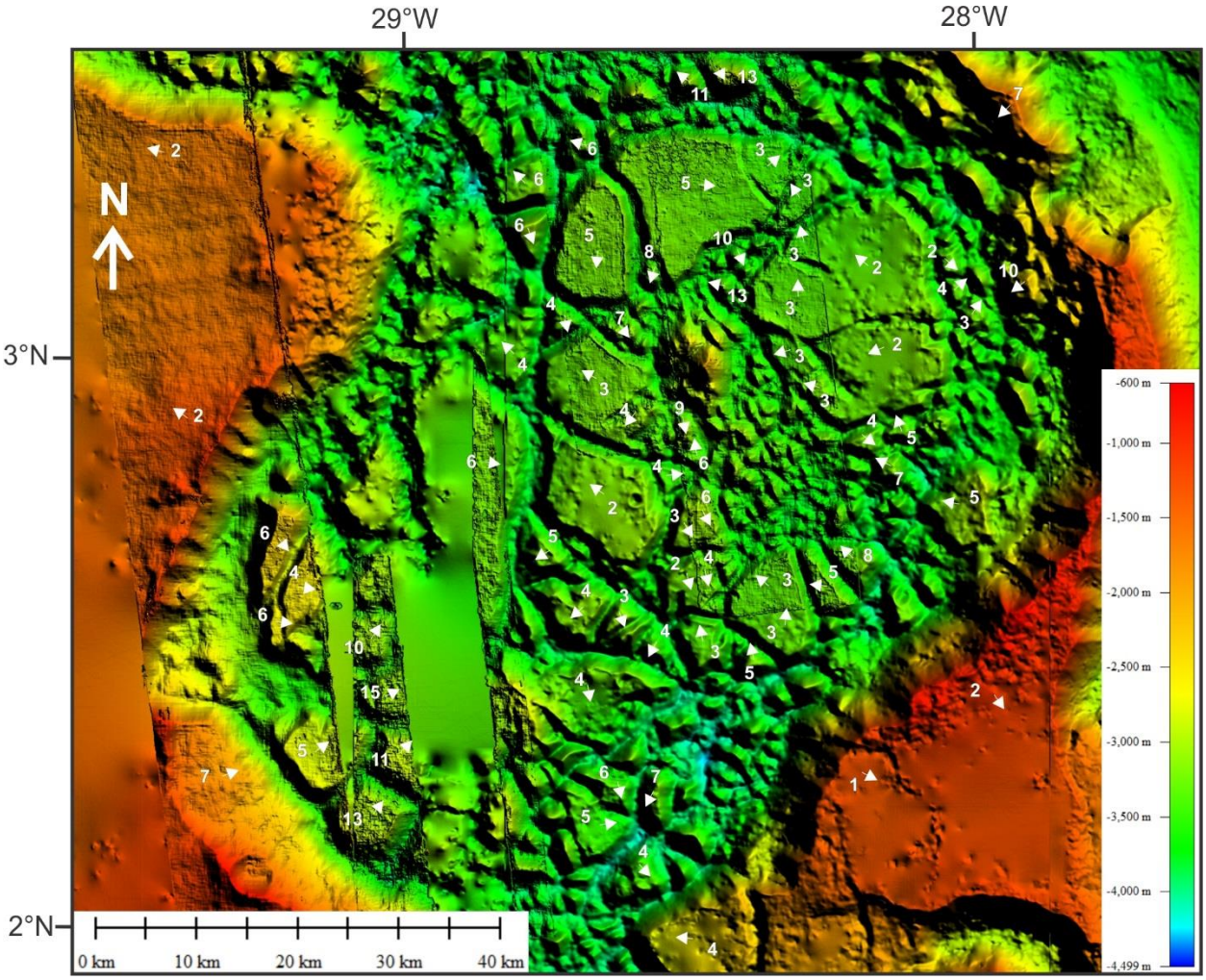

Figure 4-10 Composite DEM using CTX and HRSC DEMs, includes dip (numerical value) and dip direction (arrows) of mesa tops and the surrounding plateau.

4.4.4 Presence of Terraces and Light-toned Deposit

Unlike Hydraotes Chaos, there is little evidence for terraces within the Hydraspis crater pair. It is possible that a few of the mesa blocks have terrace units (Figure 4-11:A); some terraces completely surround the mesas and are most likely a more competent layer unit being exposed by erosion. A small deposit of light-toned material is in the eastern section of the Hydraspis crater pair Figure 4-11:B. There are several areas nearby which also show light-toned deposits, including Aram, Aureum, Iani, and Arsinoes (Glotch & Rogers, 2007). The material may have been eroded from one of

these sources and deposited in the Hydraspis crater pair; however, it is more likely that it formed in situ, as the closest light-toned deposits are those found within Aram Crater, ~400 km to the east.

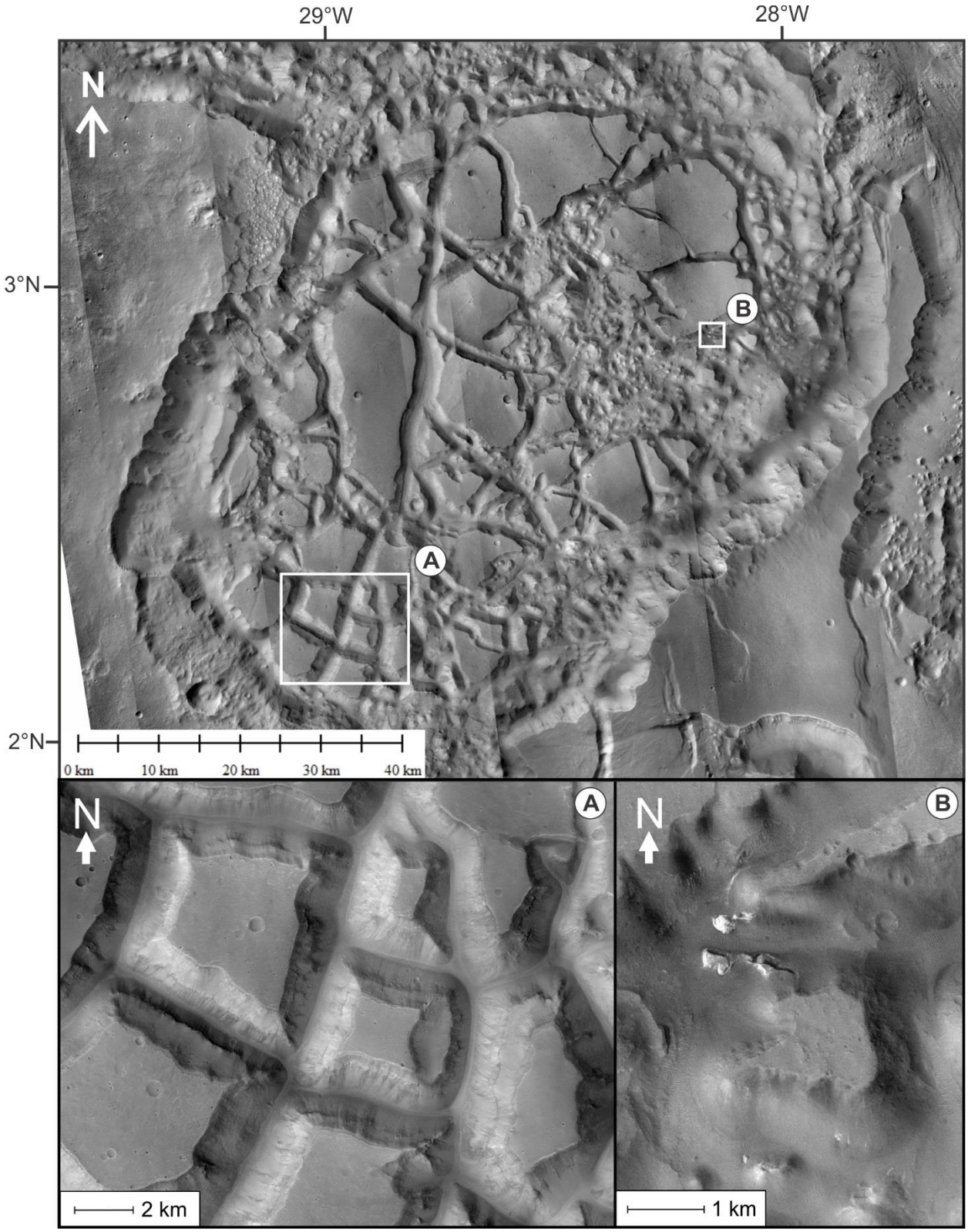

Figure 4-11 – CTX of the Hydraspis crater pair with examples of terraces (A), and the Light-toned deposit (B).

4.4.5 Calculation of Volume Loss

Volume loss during chaotic terrain formation was calculated using a similar method to that of Hydraotes Chaos (Figure 2-1). A bounding surface at -1,700 m was used instead of the average plateau elevation of -1,400 m because the rim of the crater artificially increases the average elevation of the surrounding area. The elevation of -1,700 m is the average plateau elevation west of the crater where the surface is flat and assumed to have been unaffected by the formation of the crater. The current basin floor is used as the bottom surface and it is therefore assumed that the crater was filled prior to collapse and subsequent expulsion of water. As there is a lack of evidence to support standing water for long periods, it is assumed to have been a single collapse event. The results of this calculation are shown in Table 4-2.

Table 4-2 Results of the collapse volume loss calculation.

	Volume of Missing Material	Average Depth of Collapse
Plateau to Basin Collapse	10,900 km^3	1.45 km

4.5 Discussion

4.5.1 Orientation and Distribution of Mesas

The mesa blocks in chaotic terrains have been previously interpreted as collapsed plateau surfaces in several areas including: Hydraotes (Ori & Mosangini, 1998; Meresse, et al., 2008), Hydraspis region (Rodriguez, et al., 2005), Ganges (Rodriguez, et al., 2006), and Eos (Greeley, et al., 2003) . The majority of mesas within the Hydraspis crater pair have low dips <6° suggesting little rotation has occurred from the surrounding plateau. There are, however, several blocks with much higher dips >10°

which might indicate rotation has occurred during or following collapse of those blocks. Two blocks located near the central rise of the northern crater may have been broken off from the larger mesas near them and have rotated following those secondary breaks. They may also have been affected by the proximity to the uplift of the central rise following impact excavation of the site, giving a sloped ground for sediment to accumulate on. It is likely that the northern crater mesas are emplaced on sloped ground surrounding the central peak; however this prior slope does not appear to control the dip of the mesas. The rest of the mesas with higher dips (>10°) are located along the rim of the craters and dip inwards toward the center.

4.5.2 Central Peak

Robbins & Hynek (2012) found a lack of central peaks in older craters which represent a global average of ~6.3% of craters ≥ 15 km diameter, while >90% of fresh craters of the same size range have central peaks. This demonstrates that the central peaks have been buried or eroded over geologic time (Robbins & Hynek, 2012). It is suggested that the central peak was buried prior to collapse for it to remain preserved. It is not clear why only one of these craters has a central peak. There is a lack of mesas immediately adjacent to the central peak. Sediment would cover the peak last as it fills up the crater over time. The sediment package immediately above the peak may not have been thick enough to consolidate prior to collapse, which would have made it more susceptible to erosion during collapse. As the floor collapsed, these small pieces were deposited around the base of the peak with the rest being removed in the outflow event.

4.5.3 Crater Rim

The majority of the raised crater rims are intact around both craters. The northern section of rim of the northernmost crater is missing however, and may have been destabilized by the collapse of plateau and then removed by catastrophic flooding, contributing to outflow channels north of the craters. The eastern portion of crater rim is the highest, possibly indicating that the northern section was topographically lower and therefore a path of less resistance during catastrophic flooding.

The southern portion of the southernmost crater includes a collapsed area (Figure 4-2) which continues into the plateau. There is also a region directly southeast of the crater pair (Figure 4-2) which shows a large area of collapse of the surrounding plateau region. A channel is present on the plateau surface which would drain into the Hydraspis crater pair.

4.5.4 Mesa Terraces & Light-toned Deposit

There are several mesas within the craters that have a prominent layer which looks similar to the units that form the terraces seen in Hydraotes (Figure 4-12). The highest terraces in Hydraotes form approximately 500 m below the top of the mesas while the layers in Hydraspis form 200 m below the tops. They both form at a similar elevation from their respective basin floors (≤ 500 m), however there is only one level in Hydraspis where as Hydraotes has three levels of terraces. The major differences between the two is the width of the layers (2-4 km in Hydraotes and ≤ 1 km in Hydraspis) and presence of spur and gully textures on the layer in Hydraspis that are

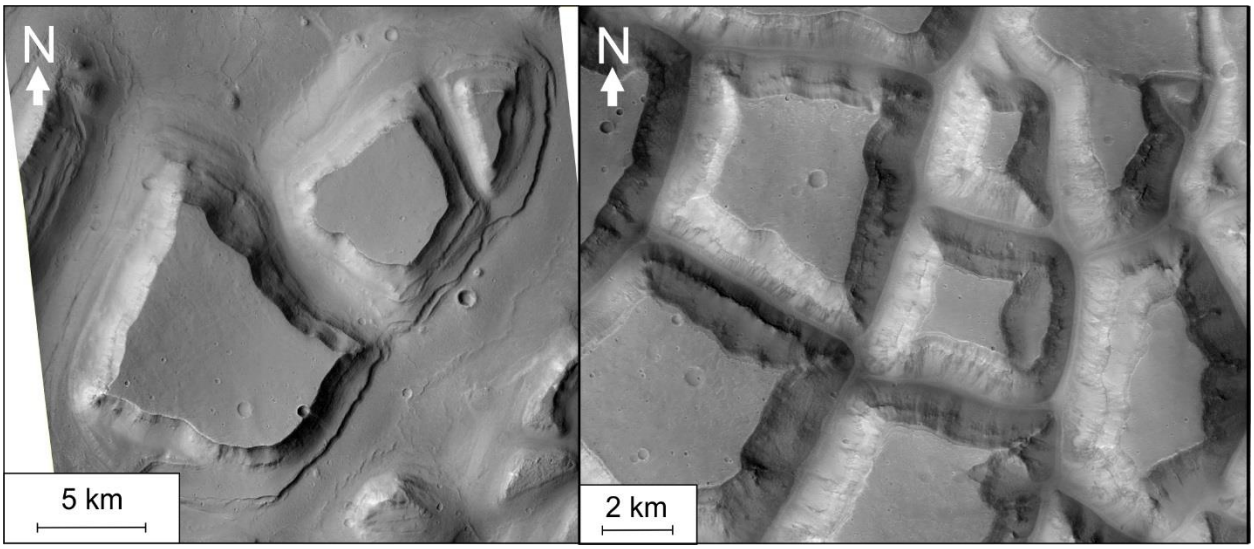

Figure 4-12 Comparison of terrace units in Hydraotes (Left) with resistant layer in the Hydraspis crater pair (Right).

not present on the layers in Hydraotes. It is suggested that the layers in Hydraspis are produced by top down erosion which intersects a more competent layer.

Juxtaposed to the resistant layer is the light-toned deposit. These deposits have been interpreted to form in standing water (Schmidt, et al., 2018). When compared to other deposits present throughout Valles Marineris (Hebes, Juventae, Candor, Ganges, etc.) (Fueten, et al., 2014; Hore, 2015; Schmidt, 2015; Fueten, et al., 2017;), it is extremely small and may therefore be a secondary deposit that formed after chaos formation in small localized ponds, requiring a change in the environment that produced the chaos terrain.

4.6 Origin of the Hydraspis Crater Pair

This area of Hydraspis has been interpreted as a crater pair by previous authors (Korteniemi, et al., 2006). Several possibilities for how chaotic terrain forms inside craters include volcanic expulsion causing collapse (Bamberg, et al., 2014); volcanic-assisted melting of subsurface ice (Leask, et al., 2006; Meresse, et al., 2008); or

subsurface lake destabilization (Zegers, et al., 2010). No evidence of volcanism has been identified within or surrounding the Hydraspis crater pair; therefore, the most likely mechanism for collapse is that of subsurface lake destabilization proposed by Zegers et al. (2010). This method of collapse proposed is nearly identical to the main collapse of Hydraotes Chaos.

4.7 Hydraspis Crater Pair Chaos Formation Model

A conceptual model is proposed for the evolution of the Hydraspis crater pair as shown in Figure 4-13; this model is similar to the model put forth by Roda et al. (2016). The model is illustrated by a north/south cross section of the craters.

4.7.1 Model Assumptions

The thickness of the initial water/ice lake is proposed to be 1.45 km. This is less than the ice thickness used in the Zegers & Roda (2012) model (2 km), but the total thickness of material is close to the extreme end of the model of 2.5 km (≥ 700 m of mesas + 1.45 km of ice = 2.15 km total). This estimate is based on the average collapse depth calculated during volume loss and may not have enough thermal insulation from the overburden to produce melting. A closed system is assumed, with the missing section of the northern rim intact prior to collapse. There is no widespread evidence of terrace formations as there is in Hydraotes, it is therefore assumed that no long-standing lake existed following collapse. The assumption of a cold and possibly wet climate on Mars following the Late Noachian Icy Highlands model (Palumbo, et al.,

2018) is continued. This assumption means that any surface water would most likely be frozen unless under turbulent flow, high salinity, or under pressure.

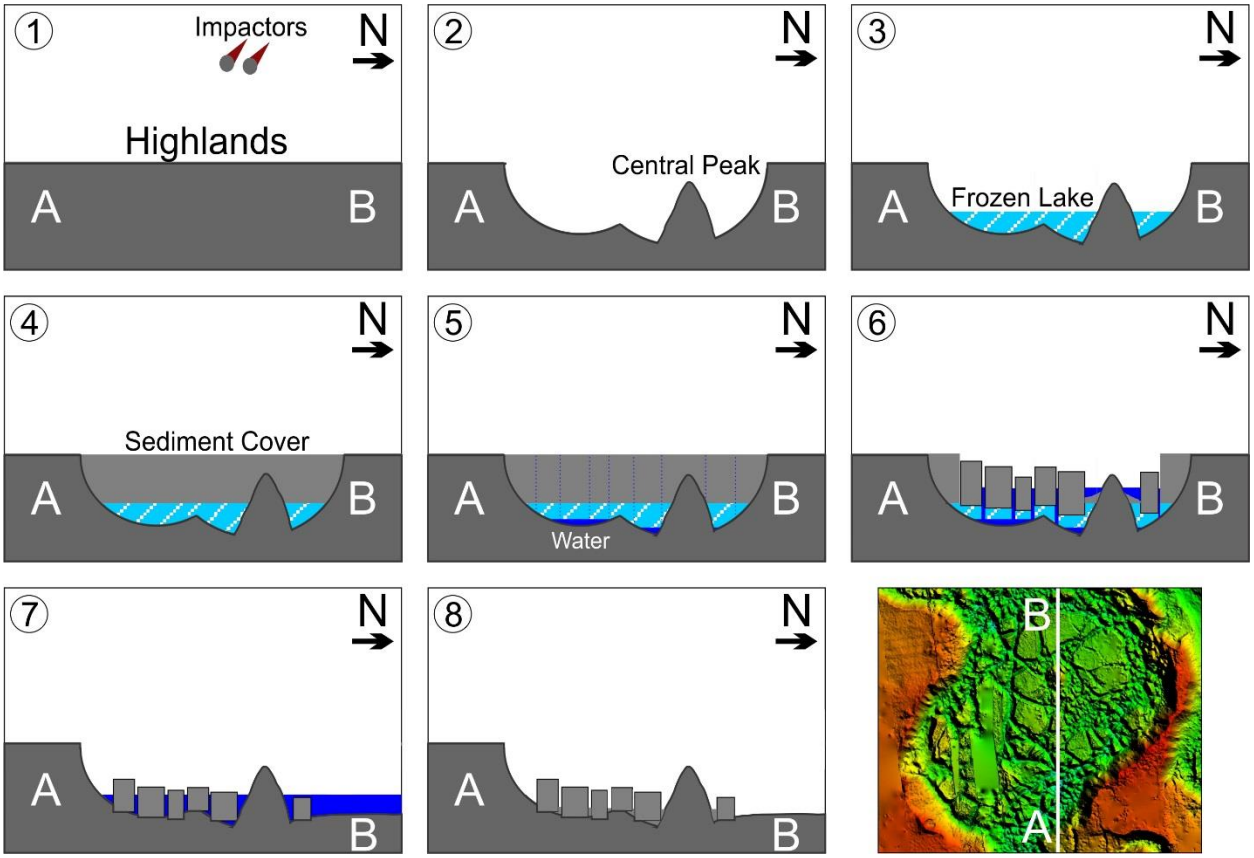

Figure 4-13 Cross-sectional model along a north/south transect of the Hydraspis crater pair, A-B covers a length of 90 km.

4.7.2 Model Description

Initially the plateau was impacted by two projectiles which would have been a single mass that likely separated as it approached the surface (Figure 4-13 inset 1). These two projectiles impact the surface producing a double impact crater with the larger of the two craters producing a central peak (Figure 4-13 inset 2). A lake filled the basin following crater excavation (Figure 4-13 inset 3). Due to the close proximity to Hydraotes Chaos and therefore the possible extent of the Arabia shoreline (Citron, et

al., 2018), this lake could have been part of or close to the northern ocean. The lake water froze over time, producing an ice unit.

Subsequent burial of the ice unit occurred over geologic time. Previous studies estimate the opening of the outflow channels Tiu and Simud to the north at Hesperian – Early Amazonian (3.34 – 3.14 Ga) (Pajola, et al., 2016) with peak modification of the channels by flooding events in the Middle Amazonian (Rodriguez, et al., 2015) therefore burial most likely occured following the emplacement of Tharsis (3.6 Ga) (Citron, et al., 2018) (Figure 4-13 inset 4). Ash filled the crater to an elevation of the surrounding plateau region, which is lower than the average elevation of the crater rim. The sediment package became thicker and lithified. Sedimentation eventually reached a critical depth of 500 – 1,500 m (Zegers & Roda, 2012) when the insulating effect of the overburden is enough to allow for melting of the ice unit where it is in contact with the basement which has a higher thermal conductivity than the overburden (Figure 4-13 inset 5). In the case of the Hydraspis crater pair there would be ≥ 700 m of sediment as this is the measured thickness of the mesas. Basal melting of the ice caused minor subsidence leading to the formation of fractures in the overlying units. Fractures propagated upwards through hydrofracturing, eventually reaching the surface and releasing water at high pressures (up to 30 MPa) (Zegers, et al., 2010).

The deepest areas which had the highest insulation would have been the first to produce melting and therefore would have collapsed first (Figure 4-13 inset 6). This area of highest insulation, which may have formed a ring surrounding the central peak, is where the largest blocks are located. The cover on top of and immediately adjacent to the central peak did not have as thick a sediment package and collapsed around the

central peak causing mechanical erosion (Figure 4-13 inset 6). This could explain why there are no large mesa blocks on the central peak. Drainage was directed away from the central peak, eroding mesa blocks to the southeast of the peak leaving the current knobs and mesa remnants that are currently see.

Destabilization of the northern rim occurred following the collapse of the mesa blocks (Figure 4-13 inset 7). There is another collapse region on the north side of this section of rim leaving it more vulnerable to erosion. This could be why no remnant of the northern rim can be seen. Water flowed north out of the craters (Figure 4-13 inset 7 & 8). As water levels dropped it pooled in isolated lows where it froze and sublimated into the Martian atmosphere, the light-toned deposit may have formed as an evaporite during this time in an isolated pool (Figure 4-13 inset 8).

References

Bamberg, M., Jaumann, R., Asche, H., Kneissl, T., & Michael, G. G. (2014). Floor-Fractures Craters on Mars - Observations and Origin. *Planetary and Space Science, 98*, 146-162.

Citron, R. I., Manga, M., & Hemingway, D. J. (2018). Timing of oceans on Mars from shoreline deformation. *Nature, 555*. doi:10.1038/nature26144

Fueten, F., Flahaut, J., Stesky, R., Hauber, E., & Rossi, A. P. (2014). Stratigraphy and mineralogy of Candor Mensa, West Candor Chasma, Mars: Insights into the geologic history of Valles Marineris. *J. Geophys. Res. Planets*(119), 331-354. doi:10.1002/2013JE004557

Fueten, F., Novakovic, N., Stesky, R., Flahaut, J., Hauber, E., & Rossi, A. P. (2017). The Evolution of Juventae Chasma, Valles Marineris, Mars: Progressive Collapse and Sedimentation. *Journal of Geophysical Research: Planets*(122), 2223-2249. doi:10.1002/2017JE005334

Glotch, T. D., & Rogers, A. D. (2007). Evidence for aqueous deposition of hematite- and sulfate-rich light-toned layered deposits in Aureum and Iani Chaos, Mars. *Journal of Geophysical Research, 112*. doi:10.1029/2006JE002863

Greeley, R., Kuzmin, R. O., Nelson, D. M., & Farmer, J. D. (2003). Eos Chasma, Mars: Regional setting for a potential landing site for astrobiology. *J. Geophys. Res., 108*(E12), 8083. doi:10.1029/2002JE002014

Korteniemi, J., Aittola, M., Öhman, T., & Raitala, J. (2006). Floor-Fractured Craters on the Terrestrial Planets – The Martian Perspective. *Proceedings of the First International Conference on Impact Cratering in the Solar System, Eur. Space Agency Spec. Publ., SP-612*.

Leask, H. J., Wilson, L., & Mitchell, K. L. (2006). Formation of Aromatum Chaos, Mars: Morphological development as a result of volcano-ice interactions. *JGR, 111*(E08071). doi:10.1029/2005JE002549

Marra, W. A., Braat, L., Baar, A. W., & Kleinhans, M. G. (2014). Valley formation by groundwater seepage, pressurized groundwater outbursts and crater-lake overflow in flume experiments with implications for Mars. *Icarus, 232*, 97-117. doi:10.1016/j.icarus.2013.12.026

Meresse, S., Costard, F., Mangold, N., Masson, P., & Neukum, G. (2008). Formation and evolution of the chaotic terrains by subsidence and magmatism: Hydraotes Chaos, Mars. *Icarus, 194*, 487-500. doi:10.1016/j.icarus.2007.10.023

Pajola, M., Rossato, S., Baratti, E., Mangili, C., Mancarella, F., McBride, K., & Coradini, M. (2016). The Simud–Tiu Valles hydrologic system: A multidisciplinary study of a possible site for future Mars on-site exploration. *Icarus, 268*, 355-381. doi:10.1016/j.icarus.2015.12.049

Palumbo, A. M., Head, J. W., & Wordsworth, R. D. (2018). Late Noachian Icy Highlands climate model: Exploring the possibility of transient melting and fluvial/lacustrine activity through

peak annual and seasonal temperatures. *Icarus, 300*, 261-286. doi:10.1016/j.icarus.2017.09.007

Robbins, S. J., & Hynek, B. M. (2012). A new global database of Mars impact craters ≥1 km: 2. Global crater properties and regional variations of the simple-to-complex transition diameter. *Journal of Geophysical Research, 117*. doi:10.1029/2011JE003967

Roda, M., Kleinhans, M. G., Zegers, T. E., & Govers, R. (2016). Origin of circular collapsed landforms in the Chryse region of Mars. *Icarus, 265*, 70-78. doi:http://dx.doi.org/10.1016/j.icarus.2015.10.020

Rodriguez, J. A., Kargel, J., Crown, D. A., Bleamaster III, L. F., Tanaka, K. L., Baker, V., . . . Komatsu, G. (2006). Headward growth of chasmata by volatile outbursts, collapse, and drainage: Evidence from Ganges chaos, Mars. *Geophysical Research Letters, 33*(L18203). doi:10.1029/2006GL026275

Rodriguez, J. A., Platz, T., Gulick, V., Baker, V. R., Fairén, A. G., J., K., . . . Glines, N. (2015). Did the martian outflow channels mostly form during the Amazonian Period? *Icarus, 257*, 387-395. doi:10.1016/j.icarus.2015.04.024

Rodriguez, J. A., Sasaki, S., Kuzmin, R. O., Dohm, J. M., Tanaka, K. L., Miyamoto, H., . . . Ferris, J. C. (2005). Outflow channel sources, reactivation, and chaos formation, Xanthe Terra, Mars. *Icarus, 175*, 36-57. doi:10.1016/j.icarus.2004.10.025

Rotto, S., & Tanaka, K. L. (1995). *Geologic/geomorphic map of the Chryse Planitia region of Mars.* USGS. doi:10.3133/i2441

Sato, H., Kurita, K., & Baratoux, D. (2010). The formation of floor-fractured craters in Xanthe Terra. *Icarus, 207*, 248-264. doi:10.1016/j.icarus.2009.10.023

Schmidt, G. (2015). Geology of Hebes Chasma, Valles Marineris, Mars (Masters Thesis). Retrieved from http://dr.library.brocku.ca/handle/10464/7326

Schmidt, G., Fueten, F., Stesky, R., Flahaut, J., & Hauber, E. (2018). Geology of Hebes Chasma, Mars: 1. Structure, Stratigraphy, and Mineralogy of the Interior Layered Deposits. *Journal of Geophysical Research: Planets, 123*, 2893-2919. doi:10.1029/2018JE005658

Tanaka, K., Skinner, J. A., Dohm, J., Irwin, R. I., Kolb, E., Fortezzo, C., . . . Hare, T. (2014). Geologic map of Mars: U.S. Geological Survey Scientific Investigations Map 3292. *scale 1:20,000,000, pamphlet 43 p.* doi:https://dx.doi.org/10.3133/sim3292

Zegers, T. E., & Roda, M. (2012). Chaotic Terrains on Mars: testing the subsurface lake hypothesis. *Rend. online Soc. Geol. It., 22*, 243-246.

Zegers, T. E., Oosthoek, J. H., Rossi, A. P., Blom, J. K., & Schumacher, S. (2010). Melt and collapse of buried water ice: An alternative hypothesis for the formation of chaotic terrains on Mars. *Earth and Planetary Science Letters, 297*, 496-504. doi:10.1016/j.epsl.2010.06.049

Chapter 5.0 **: Candor Chaos**

5.1 Introduction

Candor Chasma (Figure 5-1) is part of Valles Marineris which has been hypothesized to have opened in the Early Hesperian (Tanaka & Hartmann, 2012). Like the other chasmata in Valles Marineris, it most likely started as an isolated basin (Komatsu, et al., 1993; Warner, et al., 2013; Fueten, et al., 2014) that filled with sediment over geologic time. Currently Candor Chasma is open to two other chasmata, Ophir to the north and Melas to the south. Candor Chasma is approximately 800 km long and 170 km at its widest. The surrounding plateau is at an elevation of 5,000 m above the global datum with some sections of eastern Candor reaching depths of -5,200 m, giving it high variability in the terrain.

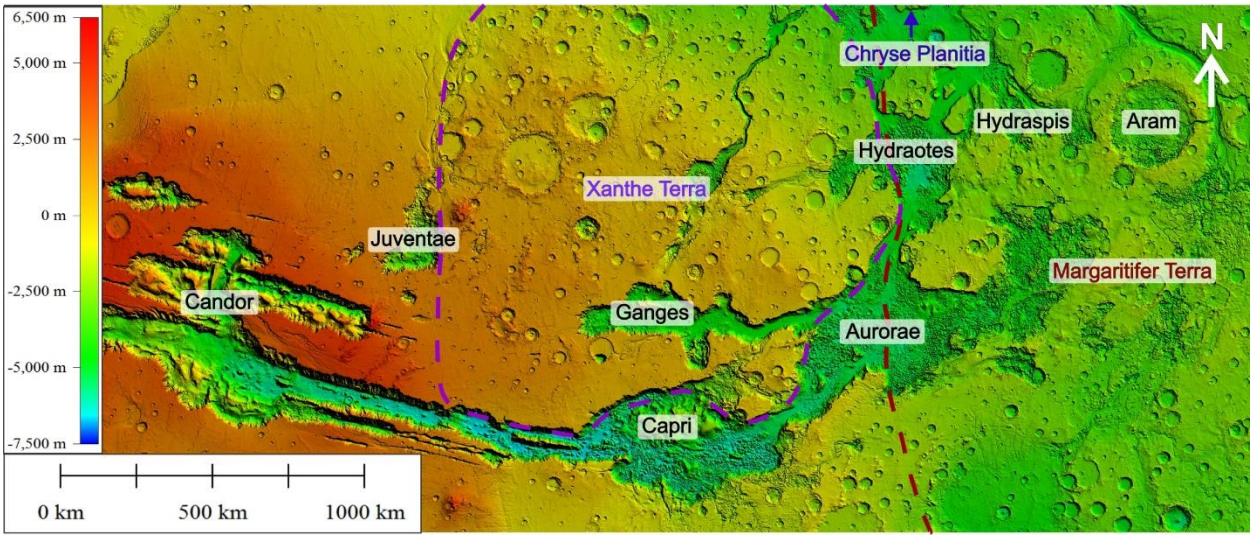

Figure 5-1 Overview of the area east of Valles Marineris, the rough outline of Xanthe Terra (purple dashes) and Margaritifer Terra (red dashes) is shown. Candor is located on the left side of the image.

The central basin of Candor has mesas and knobs similar to Hydraotes and Hydraspis at first glance (Figure 5-2), with some mesas being 10's of km across, however the elevation change from mesa top to basin floor is 100's of meters (Figure 5-3) which is an order of magnitude less than Hydraotes and Hydraspis chaotic terrains.

The chaos region (Figure 5-2) of central Candor covers an area approximately 3,600 km^2. The elevation within the chaos area, including mesa tops, ranges from -4,100 m down to -4,800 m, where as areas like Hydraotes have several kilometers of difference.

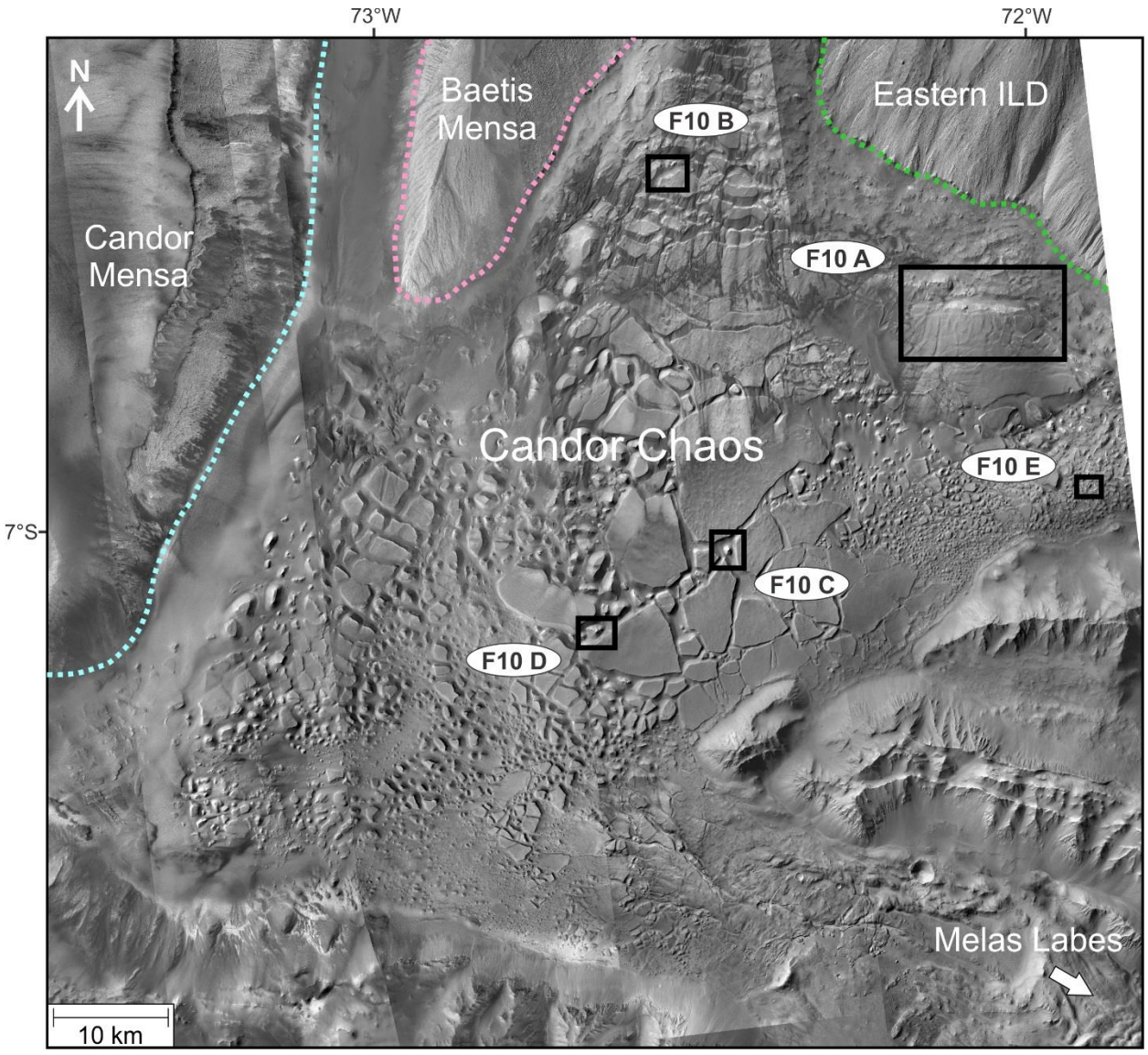

Figure 5-2 CTX Mosaic of Candor Chaos and the surrounding ILDs; Candor Mensa, Baetis Mensa, and the unnamed Eastern ILD.

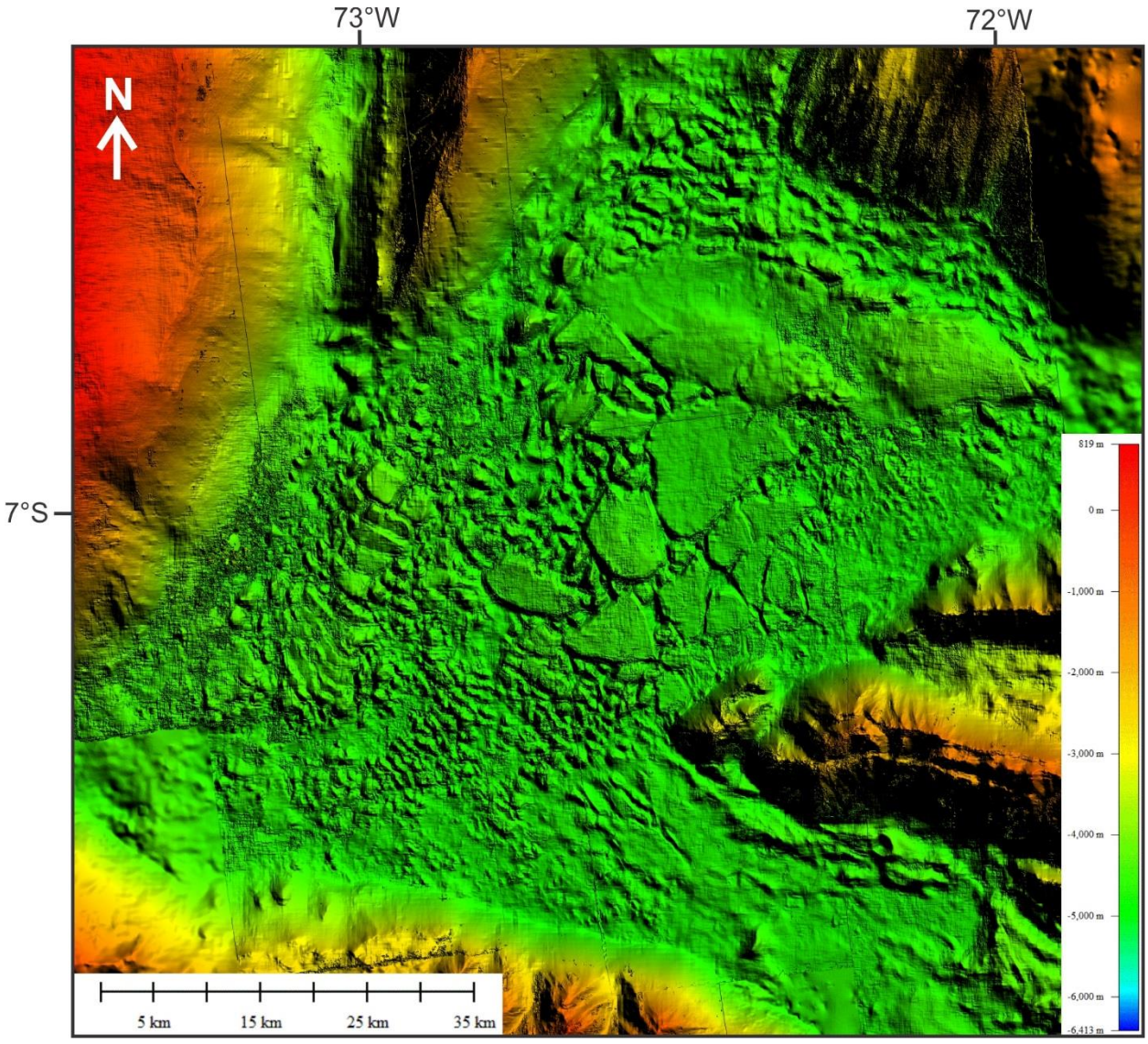

Figure 5-3 DEM mosaic of central Candor.

The plateau region surrounding Candor contains approximately north/south-trending wrinkle ridges and east/west-trending grabens (Lucchittas, 1999; Tanaka, et al., 2014) which are part of Valles Marineris. It is therefore more likely that regional tectonics influenced chaotic terrain development than in Hydraotes and Hydraspis.

The most prominent feature which makes Candor Chaos unique when compared with the other study sites thus far is the presence of large Interior Layered Deposits

(ILDs) which are along the north, east, and western edges of the chaos (Figure 5-2). These large mounds are thought to have been a single mound (Komatsu, et al., 1993; Fueten, et al., 2014) at one time which has been subsequently eroded into three distinct mounds by outbursts of water when the chasma opened (Warner, et al., 2013) and continued aeolian erosion since then. This single mound would have formed in an isolated water-filled basin (Komatsu, et al., 1993; Fueten, et al., 2014; Schmidt, et al., 2018). The original mound likely formed in an isolated basin and covered a much larger area than it does now, including the area which is now Candor Chaos.

5.2 Previous Work

The ILDs within Candor have been studied (Fueten, et al., 2014) as well as the regional tectonics (Tanaka, et al., 2014) of the chasma, however the chaos region has only been examined by Lucchitta & Ferguson (1983) and more recently by Gourronc et al. (2014).

Fueten et al. (2014) investigated Candor Mensa, which is the western ILD in the central basin. They identified two distinct packages within the ILD, a dominant base approximately 5 km thick that is unconformably overlain by a thin upper layer. The change in layering is postulated to be caused by a change in depositional environment, with the bottom package being deposited in an enclosed water-filled basin with possible freeze/thaw cycles. This bottom package would have taken up the bulk of the basin as a single ILD (Komatsu, et al., 1993; Fueten, et al., 2014). The second package was deposited after the draining and erosion of a large portion of ILD by water/ice which was triggered by the linking of Candor to the rest of Valles Marineris (Komatsu, et al., 1993;

Fueten, et al., 2014). This environment allows for large volumes of water/ice localized within Candor giving a possible trigger for chaotic terrain formation.

Gourronc et al. (2014) suggest that the mesa blocks in Candor Chaos are relict ice left over from the Late Noachian to Early Hesperian following the formation of Valles Marineris. This relict ice would be the sediment capped ice leftover following sublimation. They explain that the morphologies of the surfaces found within the basin are similar to terrestrial wet-based glacial valleys which have been eroded. They also identified what they call a glacial trimline at which there is a change in morphologies along the chasma walls from spur and gully textures to a smooth basal escarpment. They found this trimline to vary from -4,000 m to -4,300 m in the basin area. They suggest a minimum thickness of ice of 700 m in the central basin of Candor with the possibility of thicknesses greater than 1,000 m.

5.3 Methodology

For methods used, refer to Chapter 2.0 – Methodology above. This standard is used for each case study except where otherwise indicated. The 20 m/pixel DEM composite used for Candor Chaos is composed of CTX and HRSC. Orbits used are shown in Table 5-1. Approximately 90% of the DEM composite is 20 m CTX data with HRSC data filling the rest.

Table 5-1 Images used to create the composite DEM for Hydraspis Crater.

HRSC Orbit	CTX DEM Pairs
h0334_0001_da4_54 (100 m/pixel)	B09_013007_1726_XI_07S072W-
h2083_0000_da4_51 (50 m/pixel)	B01_010027_1735_XN_06S073W-
	B18_016686_1738_XI_06S072W-
	G02_019020_1743_XI_05S073W-
	F20_043705_1722_XI_07S072W-
	J22_053410_1728_XN_07S072W-

5.4 Results

5.4.1 Orientations Obtained with AVA

The AVA (Figure 5-4) was used to calculate strike and dip measurements for the mesas and surrounding basin area of Candor Chaos. The dip of every pixel within the basin was calculated using the AVA (Figure 5-5), with the average dip of the mesa top surfaces shown in Figure 5-6.

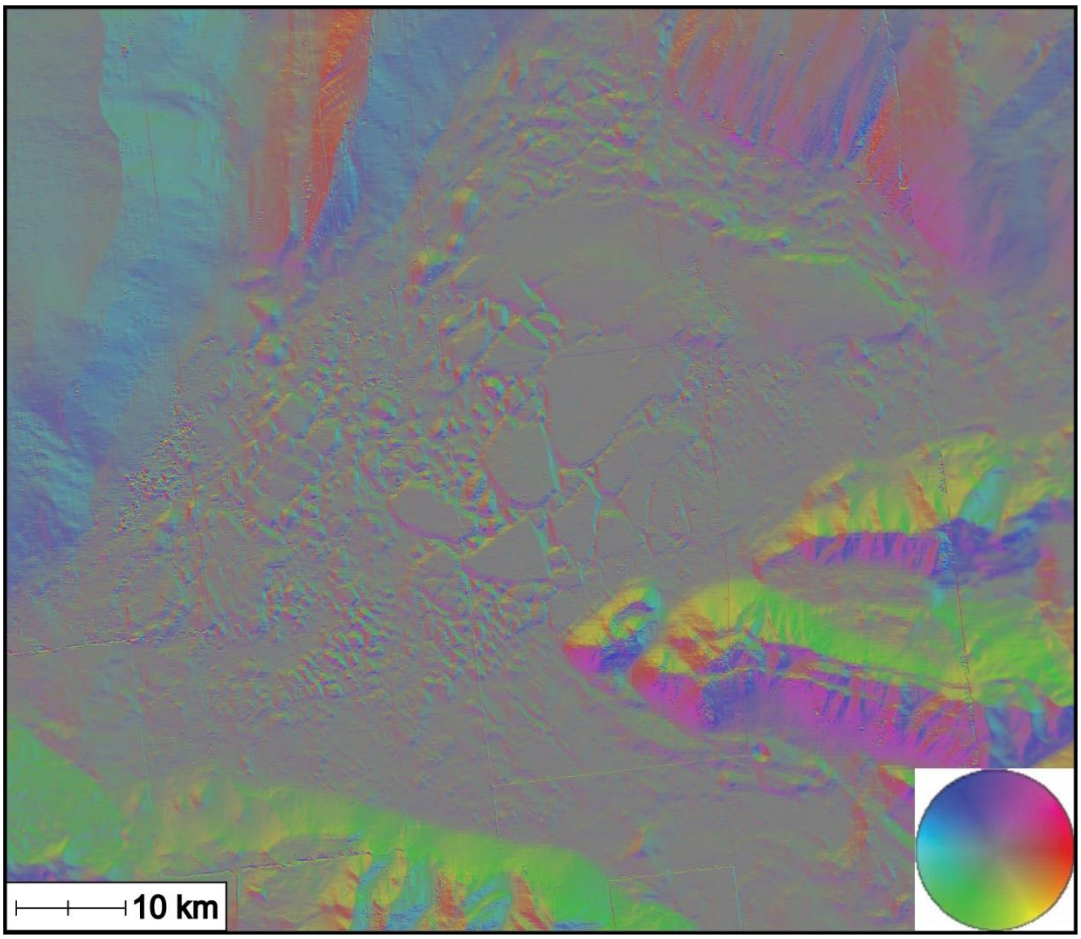

Figure 5-4 Colourized Augmented Visualization of Attitude (AVA) results using a colour coded stereonet.

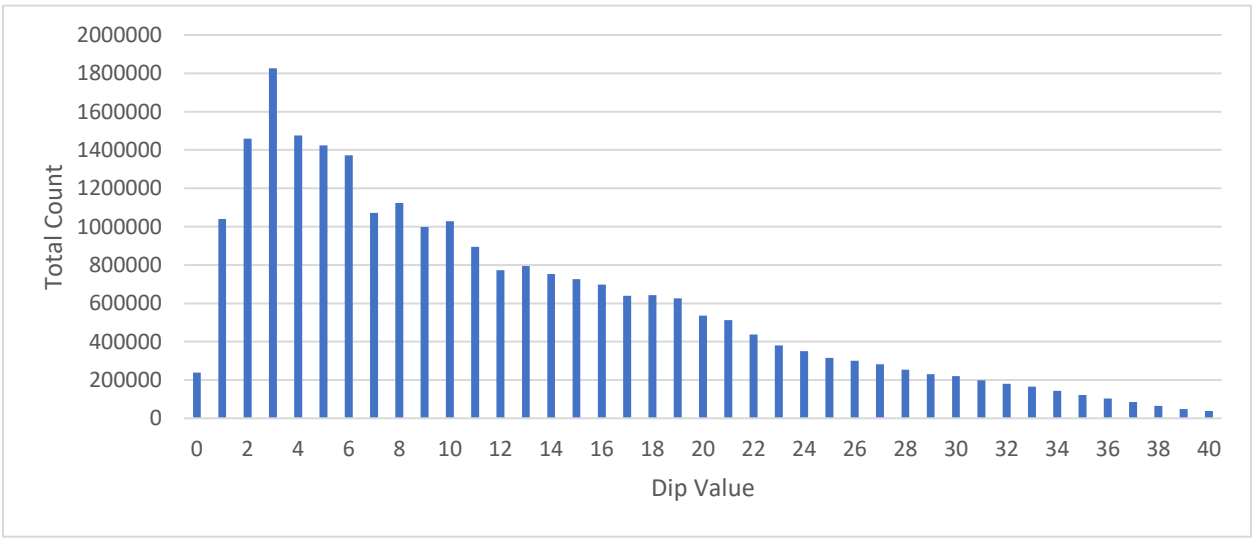

Figure 5-5 Dip value of all points calculated with the AVA of the central Candor basin.

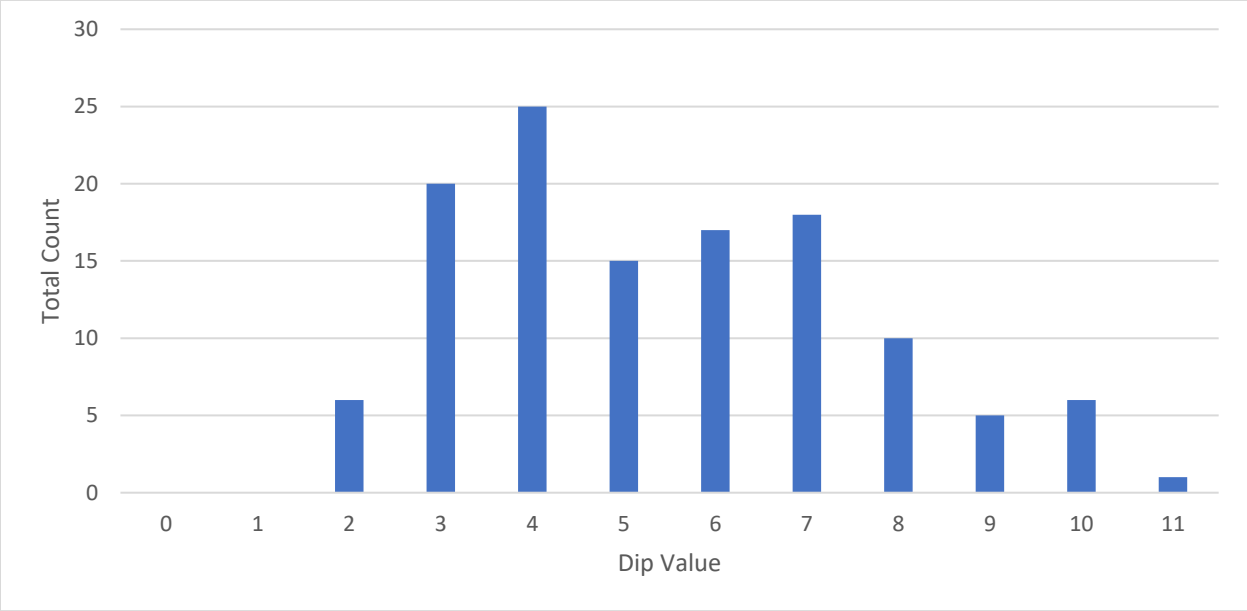

Figure 5-6 Average dip calculated for each mesa flat top within Candor Chaos. A total of 123 mesa tops were calculated.

The strike of the mesa block tops is shown in Figure 5-7:A, while the strike of the steep sides of the mesa blocks was calculated (Figure 5-7:B) using only pixels with dip values of 17°- 40° for consistency with previous analyses. The mesa blocks show a preferred south/south-east orientation of collapse, which corresponds with the direction of the southern outlet channel to Melas Labes (Figure 5-2). The steep sides of the blocks show a weak north-south trend similar to the other chaotic terrains.

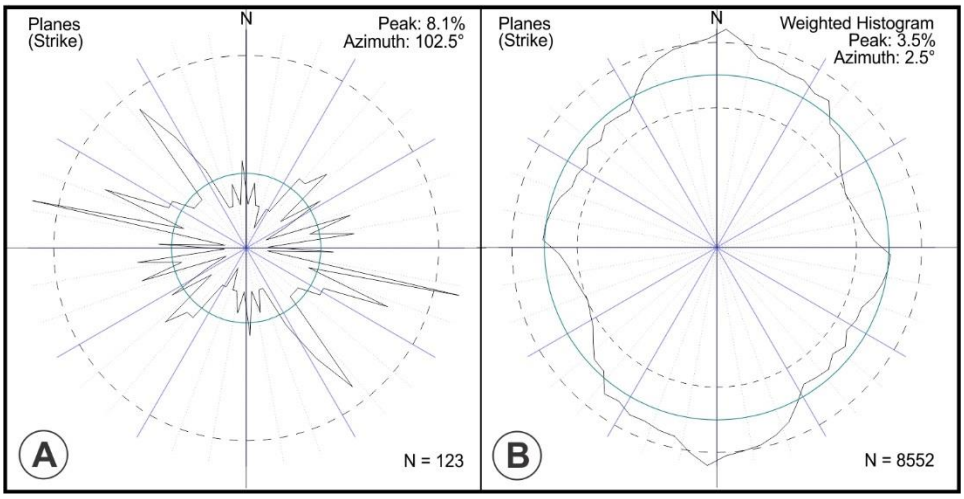

*Figure 5-7 A) Rose diagram of the strike for all mesa tops calculated within Candor Chaos. B) Rose diagram of strike for all points within the central Candor basin that have dips from 17° - 40°. Due to computational limitations a histogram of all strike/dip value combinations with dips between 17°- 40° were used (360 strike values * 24 dip values = 8552 non-zero entries).*

5.4.2 Elevation and Distribution of Mesas

Figure 5-8 shows a contoured image of Candor Chaos showing the extreme variation in elevation in the area of the basin. The surrounding plateau and ILD mounds are shown in yellow, orange and red, while the majority of the basin floor is dark green with some of the larger mesas in light green. This image highlights that the western side of the basin is the highest, along with a large section in the northeast.

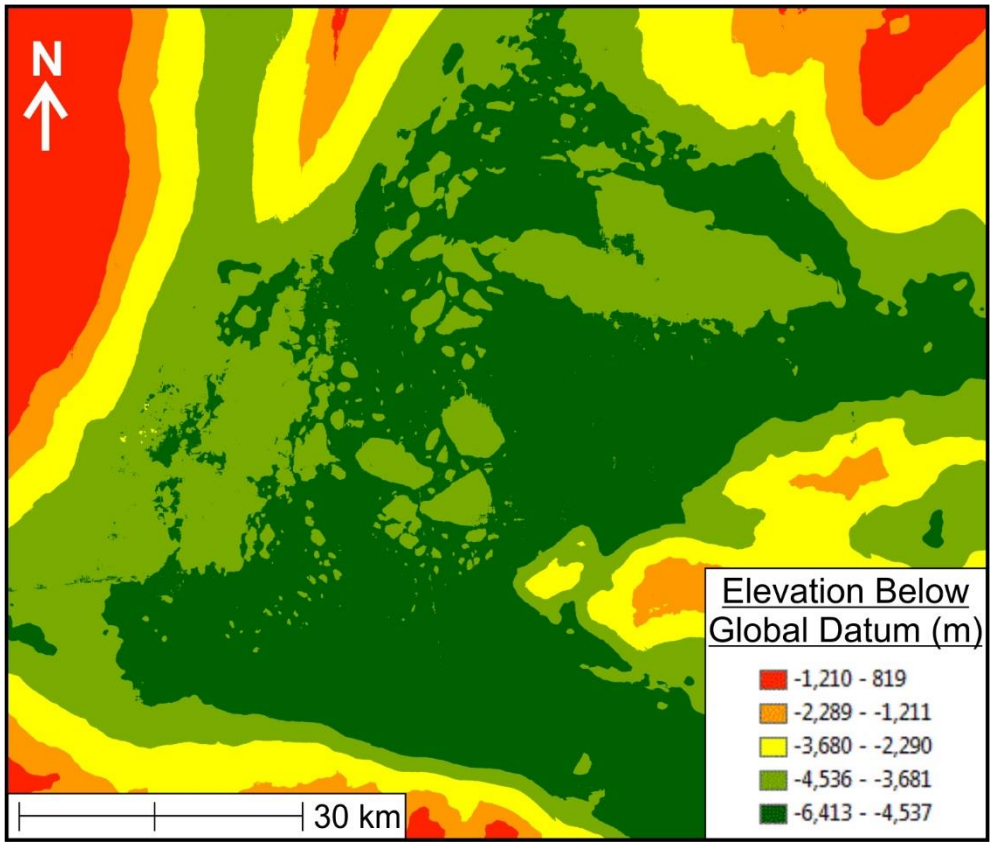

Figure 5-8 Manually set contours to allow for better visualization of sections of Candor Chaos.

5.4.3 Orientation of Mesa Tops

The dips of the top surfaces of the mesa blocks were calculated using the AVA (Figure 5-9). The rose diagram (Figure 5-7:A) shows a south/southeast preferred strike orientation of these blocks. Generally low dip values are observed on the mesa tops with the majority being between 2° to 8° (Figure 5-6). The highest values (≥10°) are only identified on three small (<1 km across) mesa blocks.

5.4.4 Interior Layered Deposits

There are three ILD mounds which border the chaos zone along the north, east, and western sides. These ILDs fill a large portion of the chasma that they are present in

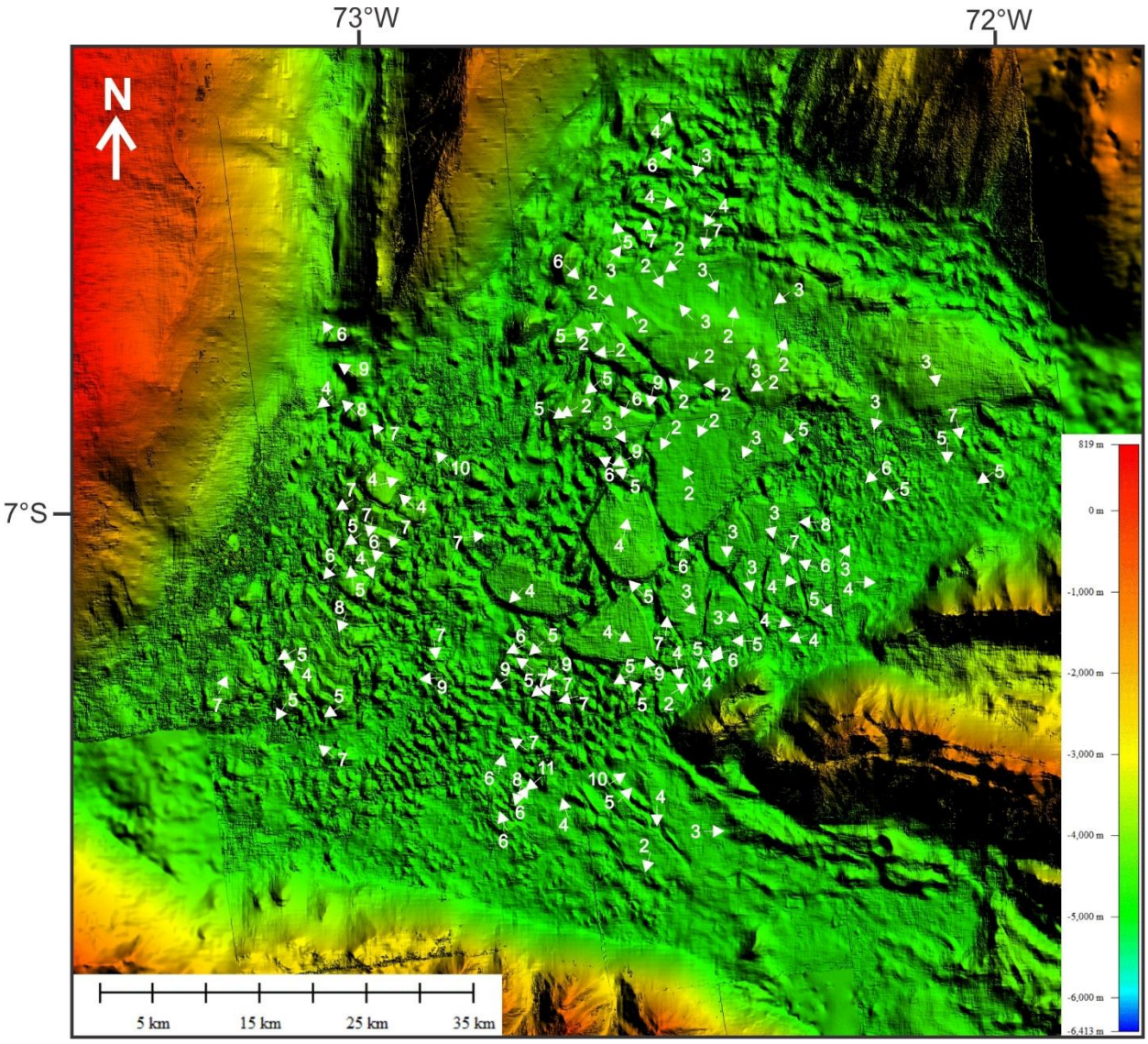

Figure 5-9 Composite DEM using CTX and HRSC DEMs, includes dip (numerical value) and dip direction (arrows) of mesa tops calculated for Candor Chaos.

and distinguish Candor from Hydraotes which has no light-toned deposits or Hydraspis which only has a very small isolated deposit (Figure 4-11:B). Candor Mensa on the west side is the largest of the three ILD mounds at 70 km east to west and 115 km north to south and is approximately 8 km in height (Fueten, et al., 2014).The three mounds are thought to have once been a single large deposit before the development of large erosion channels now separating them (Komatsu, et al., 1993; Fueten, et al., 2014). Outcrops of light-toned material that resembles ILD are located within Candor Chaos

(Figure 5-10) and range in size from <500 m (Figure 5-10:B,C) to several kilometers across (Figure 5-10:A).

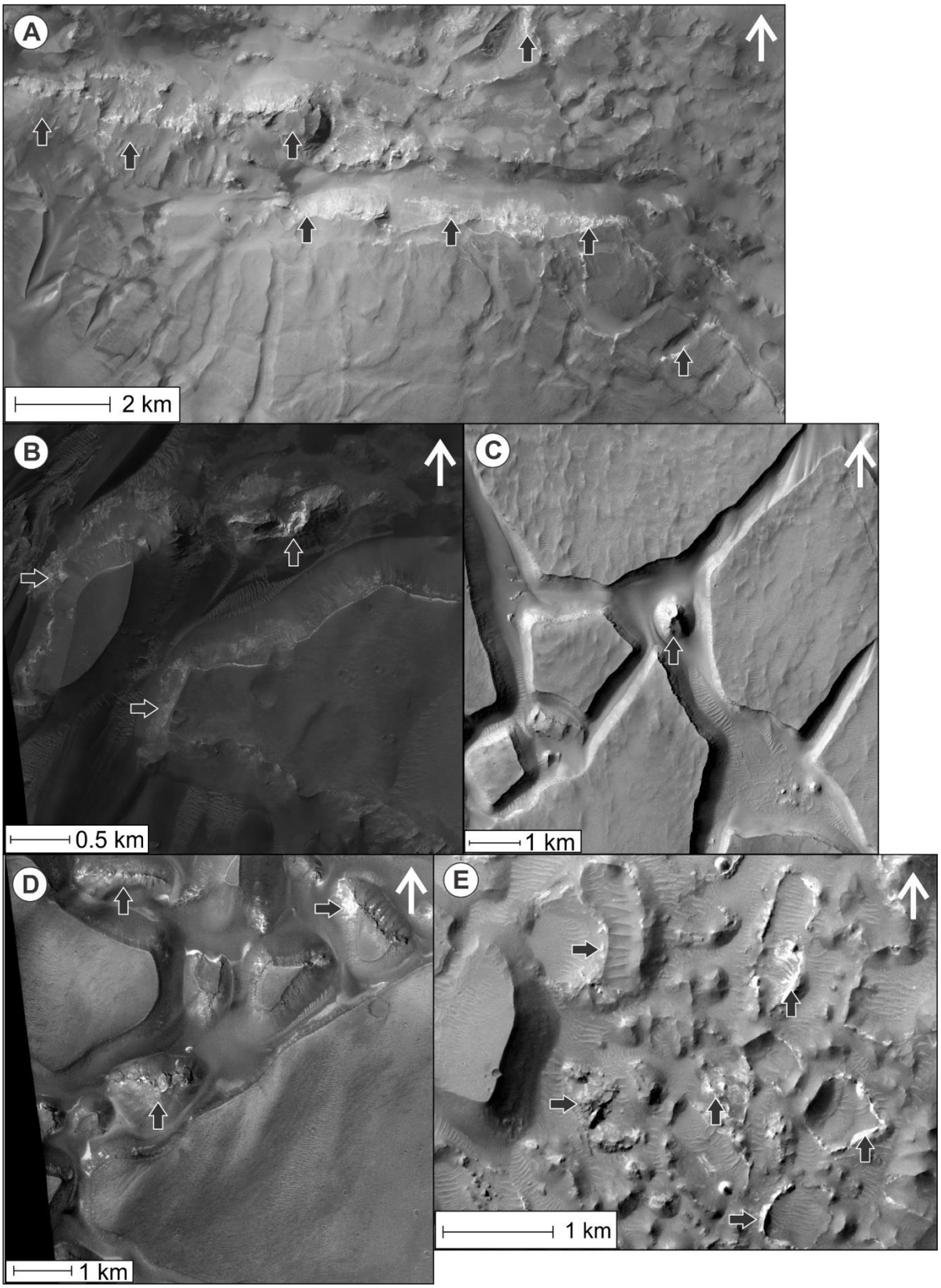

Figure 5-10 Examples of ILD within Candor Chaos, black arrows indicate possible ILD deposits.

5.4.5 Calculation of Volume Loss

Volume loss within Candor Chaos was calculated differently than for Hydraotes and Hydraspis because the terrain is not surrounded by plateau. It is unreasonable to assume that the basin was filled with material to the plateau level. There has not been a level found in the surrounding area which could suggest a maximum level of fill either. A series of volume loss calculation was therefore performed altering the thickness of ice as a proxy for collapse depth (Figure 5-11). The values for ice thickness used (200 m, 300 m, 500 m, 1 km, and 1.2 km) are from measurements by Rodriguez et al. (2011), that represent the total collapse depth of secondary chaotic terrains with similarly sized mesas around southern Circum-Chryse. There is an estimated volume loss ranging from 400 km^3 (with no buried ice) to 4,300 km^3 (with 1.2 km of ice).

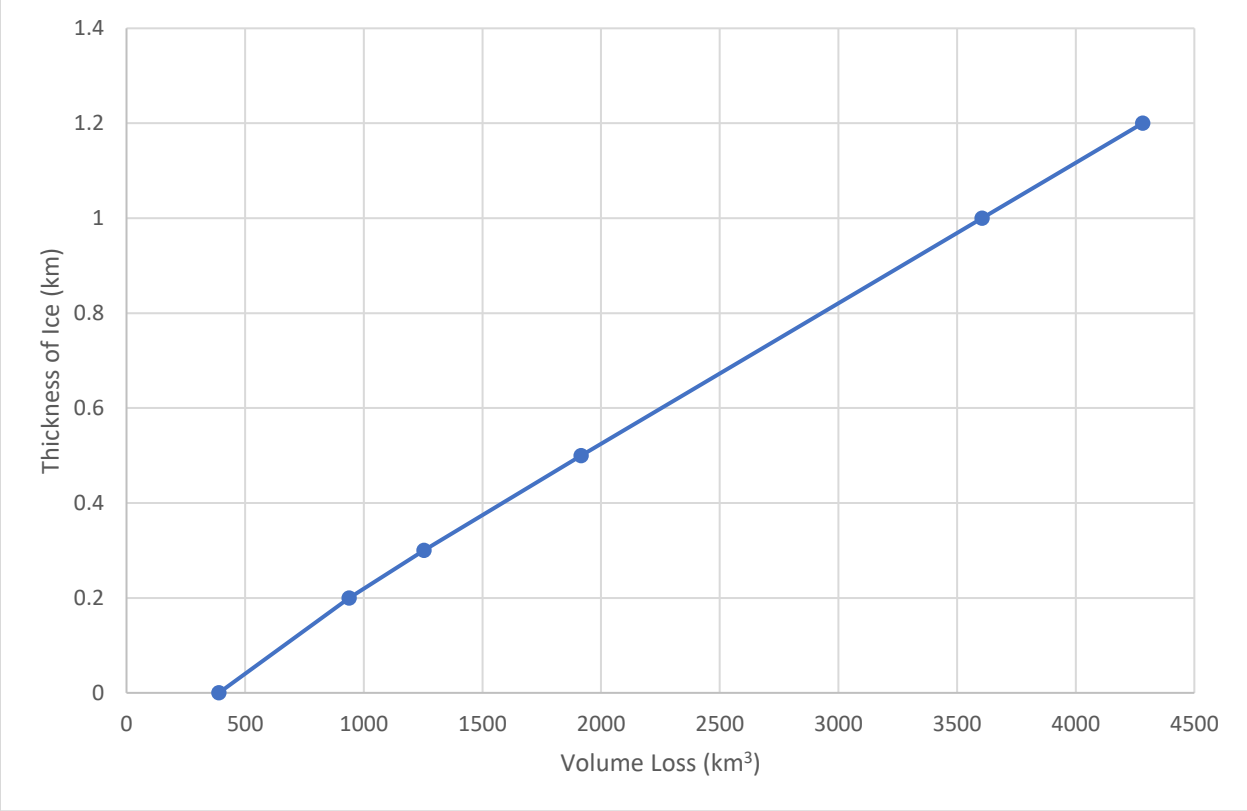

Figure 5-11 Results of volume loss calculation within Candor Chaos.

5.5 Discussion

5.5.1 Lack of Sapping Channels

The previously investigated chaotic terrains had large sapping channels (Marra, et al., 2014) (Figure 5-12:A & B) in a number of the larger mesa blocks. The pattern of fractures in the chaotic terrain in Candor appears to be different (Figure 5-12:C) than those seen in Hydraotes and Hydraspis. The sapping channels in those chaotic terrains have uniform widths with theatre heads. The fractures in Candor appear to pinch out and are heavily filled with sediments. This may indicate that a different mechanism is responsible for breaking apart the mesa blocks when they are orders of magnitude smaller than those found in Hydraotes or Hydraspis.

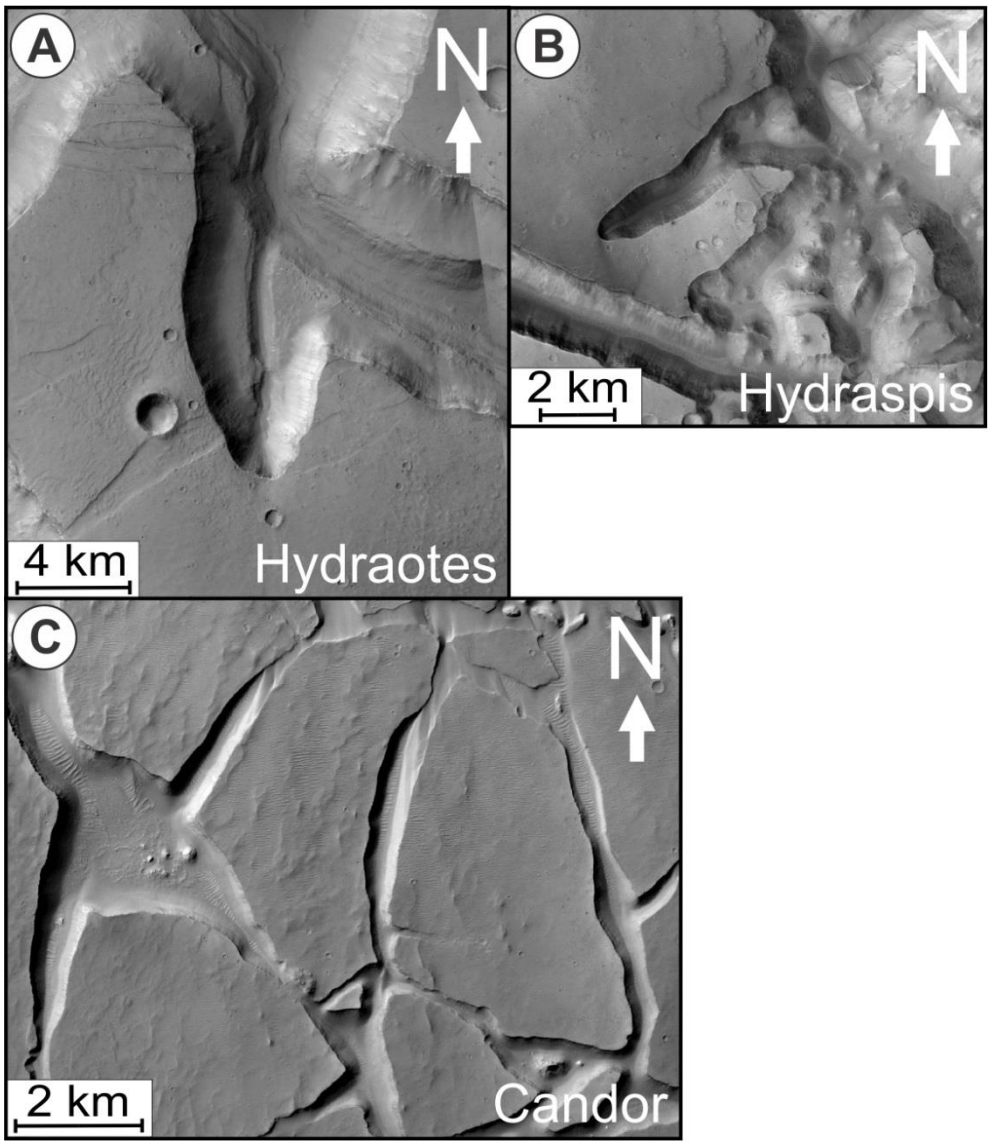

Figure 5-12 Sapping channels in Hydraotes (A) and the Hydraspis crater pair (B), compared with the mesas in Candor (C).

5.5.2 Lack of Mesa Terraces

No terraces have been identified around the mesas within Candor Chaos. As mentioned earlier in the Chapter 3.0, the elevation of the terraces in Hydraotes range from -3,829 m down to -4,532 m, while the highest mesas in Candor Chaos are at an elevation of -4,100 m. The terraces in Hydraotes also form approximately 500 m to 1,000 m down from the tops of the mesas. Using Hydraotes as a guide, terraces may be

present around the mesas in Candor Chaos; however if they are, they would be buried. Other authors (Rodríguez, et al., 2011) have suggested that secondary chaotic terrains, like that of Candor Chaos, do not produce large outbursts of water during collapse like primary chaotic terrains (Hydraotes) do. There would therefore not be enough water to create a standing body of water to produce terraces.

5.5.3 Orientations and Distribution of Mesas

The mesa blocks within Candor Chaos show low dip values (majority <8°) similar to previously investigated chaotic terrains (Hydraotes and Hydraspis) which suggests that very little rotation has occurred during the collapse of the blocks. It is suggested that this is a function of the size of the blocks, large blocks having less available space to rotate. The largest blocks are also adjacent to one another, which appears to be a common feature of other chaotic terrains (Rodríguez, et al., 2011) including those studied here (Hydraotes & Hydraspis). The smaller mesa blocks have higher dips with the highest dips seen in three small mesas with dips ≥10°. This appears to be common in other chaotic terrains, with larger mesas having lower dips and the smallest mesas having higher dips. This is most likely caused by the rotation of sections as they break off of larger blocks.

The regional map of Valles Marineris (Tanaka, et al., 2014) shows many wrinkle ridges and grabens in the surrounding plateau so there is a strong tectonic influence which is lacking for other chaotic regions (Hydraotes). The dip direction of mesas within Candor Chaos aligns with the opening to Melas to the southeast, suggesting that the strong regional tectonics within Valles Marineris have little direct influence on them. The

east-west nature of the grabens of Valles Marineris do however control the position of the corridors between chasma, so there is an indirect influence on the mesas.

There appear to be several distinct zones of mesa blocks within the basin area. The central area is mostly large mesa blocks with a zone of small blocks to the east and another separate group of medium sized mesa blocks to the west, surrounded by smaller blocks (Figure 5-2). This may be the result of separate collapse centers within the basin.

5.5.4 Sedimentation and Morphology of the Basin

The morphology of Candor Chaos and the surrounding basin area is similar to other identified chaotic regions of Mars, which have been interpreted as secondary chaotic terrains (Rodríguez, et al., 2011). The basin floor between the mesas is smooth and generally inundated by aeolian sedimentation. The deepest sections of the basin (Figure 5-13) are located between several of the largest mesas, suggesting these areas are protected from post-collapse deposition. Mesas within Candor Chaos have not been completely covered by eroded ILD, so erosion rates must have declined since the formation of chaos, or wind is depositing sediment further away. These deep sections are however isolated points, and the largest area of lower elevation is in the southern portion of the basin leading to Melas Labes. This has been previously interpreted as an outflow channel for catastrophic flooding (Fueten, et al., 2014). The basin in this area has a floor dominated by cracks in the surface which may be caused by desiccation of the channel floor following draining.

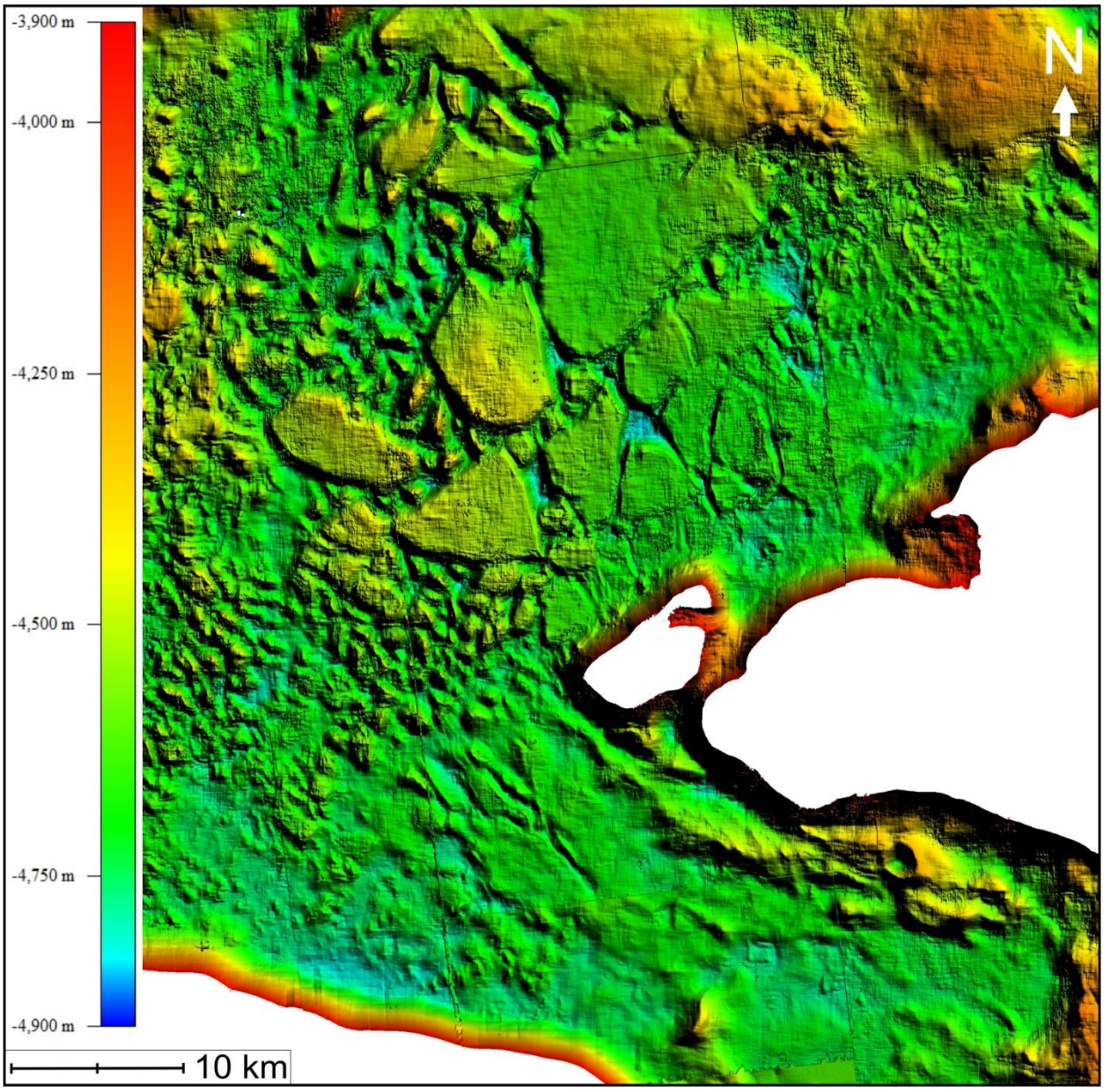

Figure 5-13 Zoomed DEM of Candor Chaos highlighting the deepest sections of the floor in blues.

5.5.5 Interior Layered Deposits within the Chaos

In the north/northeast part of the basin lies a large section of ILD resting on the floor of the basin next to a number of larger mesas (Figure 5-10:A). There are also light-toned deposits between mesas in the center of the chaos zone (Figure 5-10:C). This suggests that the mesas are indeed large rock units as ILD would not form next to

glaciers/ice packages (as interpreted by Gourronc et al. 2014). The large sections of ILD in the basin may be eroded material or part of the basal unit of the ILD east of Baetis Mensa (Figure 5-14). The smaller blocks within the chaotic terrain (Figure 5-10) may be remnants of the material deposited on top of sections of the floor of an ancient lake which is now exposed as the mesa tops.

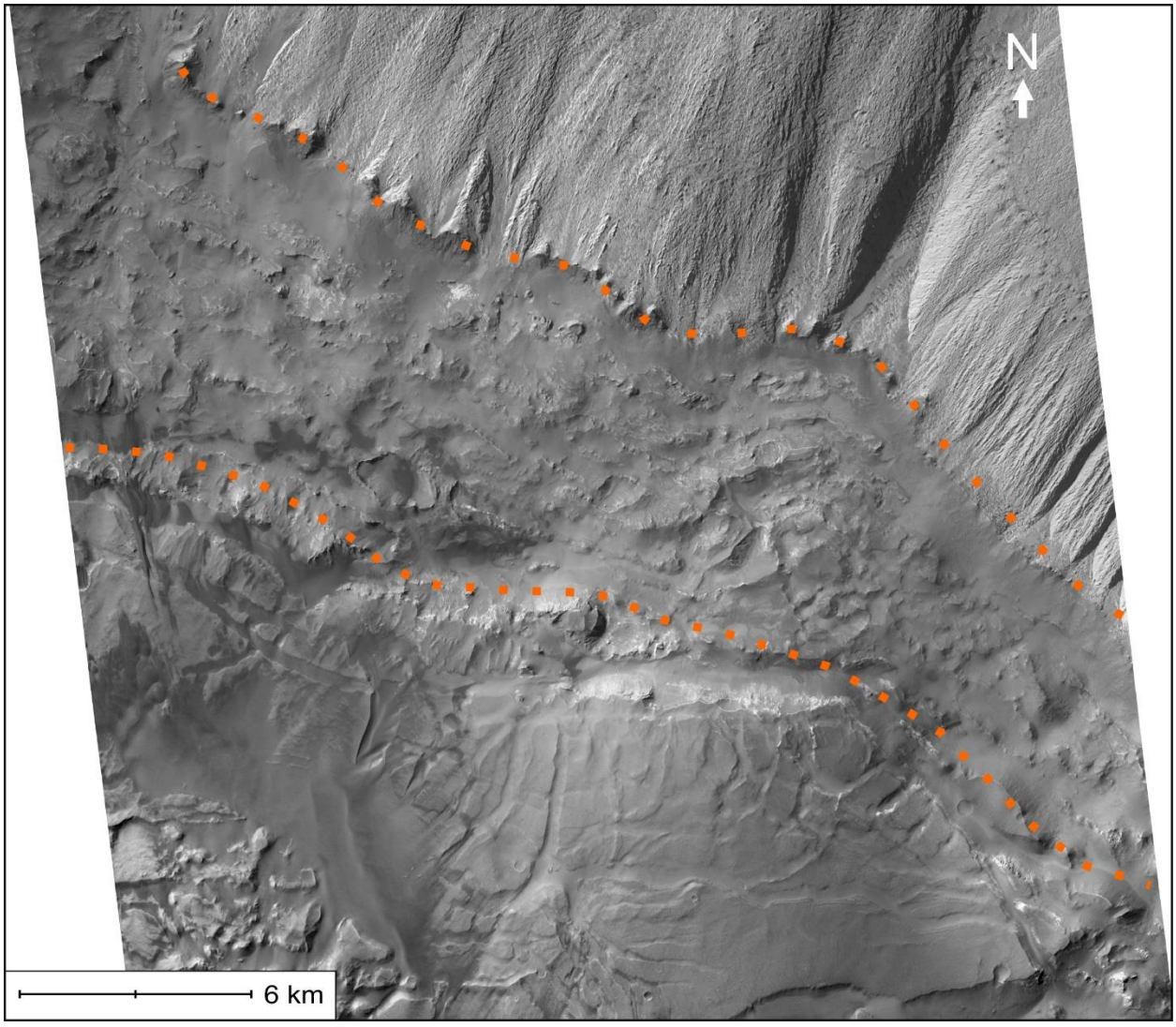

Figure 5-14 CTX image of the Eastern ILD and possible basal section separated by a channel, the sides of which are outlined in orange.

5.6 Candor Chaos Formation Model

A conceptual model (Figure 5-15) for the evolution of Candor Chaos was created along a north/south transect which simplifies Candor basin and the large ILDs within it.

5.6.1 Model Assumptions

Unlike for the previous chaotic terrains analyzed (Hydraotes & Hydraspis) there is no direct link between the chaos and surrounding plateau. This means there is no level of deposition that could be reasonably assumed, therefore a range of possibilities was plotted (Figure 5-11) which are taken from previously measured (Rodríguez, et al., 2011) chaotic terrains. It is also assumed that Candor basin was isolated for a span of time long enough to produce an ILD mound which would have taken up the majority of the central chasma covering the area of much of the current chaotic terrain. The topography of the basin is such that the elevation of the chaotic terrain is lower than the surrounding outlets, water would have therefore pooled in the basin. It is suggested that this remnant or later lake would have been the source of the collapse of the chaotic terrain. This assumes a localized water source like those of Hydraotes Chaos & the Hydraspis crater pair.

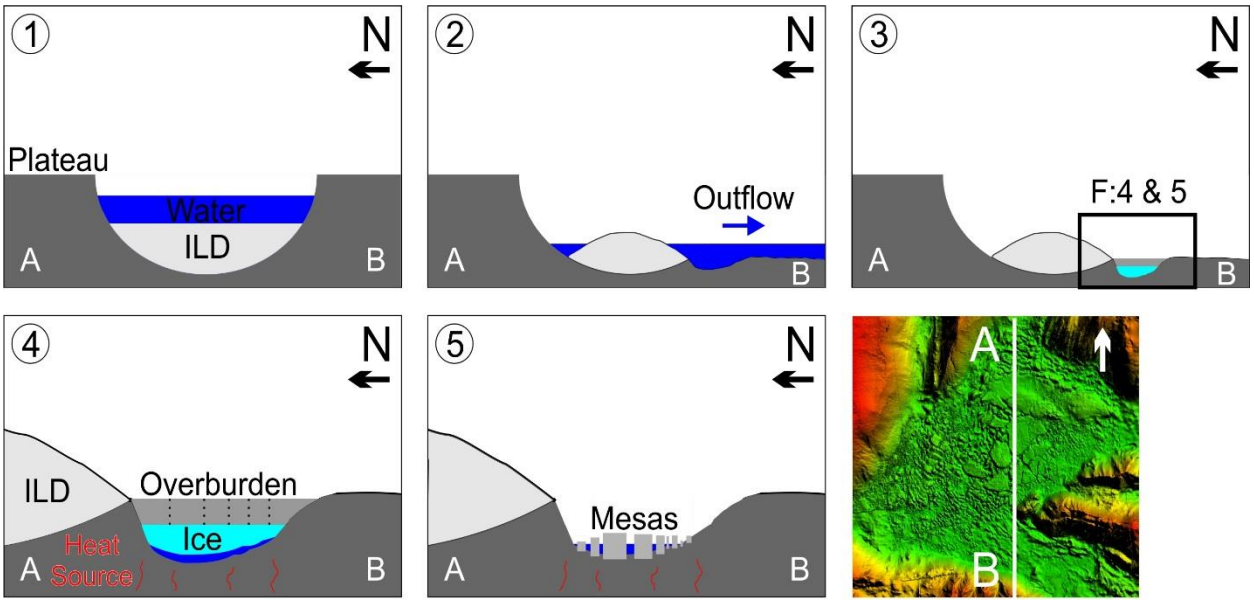

Figure 5-15 Cross sectional model along a north/south transect of Candor Chaos.

5.6.2 Model Description

The model begins following the initial subsidence (Schultz, 1998) of Candor Chasma but before it connected to Melas Chasma. Initially the chasma would have filled with water (Warner, et al., 2013; Fueten, et al., 2014; Schmidt, et al., 2018), either in liquid or solid form (Figure 5-15:1). Simultaneously sedimentation within that volume of water occurs (Figure 5-15:1). The ILDs within Candor have been shown to have fine layering (Fueten, et al., 2014) which has been interpreted as being evidence for lacustrine deposits (Figure 5-15:1). The lake which the ILDs were deposited in may have been stable over the time of ILD formation or thawed seasonally, with the end result of generating a large ILD mound in the center of Candor Chasma. At some point the plateau between Candor and Melas opened, similar to processes described by Warner, et al. (2013), allowing the draining of the lake within Candor (Figure 5-15:2).

The expulsion of water from Candor Chasma would have deeply incised the area immediately adjacent to the conduit to Melas (Figure 5-15:2), which is the current location of the chaotic terrain. Following the draining of water there would have been pooling within the areas of lowest elevation (between Figure 5-15:2 & 3). The much shallower remnant lake would have frozen and been quickly buried by local sediment (Figure 5-15:3).

External heating is most likely required (Figure 5-15:4) as the thickness of the overburden is not enough to cause a strong enough insulating effect for melting to occur. Evidence for volcanic activity in Coprates Chasma which postdated the draining of Valles Marineris (Hauber, et al., 2015) may have provided a heat source for melting of the now buried frozen lake. By this time enough material would have accumulated from a combination of sources including volcanic ashfall, ILD erosion, and plateau erosion. Melting of the subsurface ice causes instability in the overlaying rock as hydrofracturing begins to occur (Figure 5-15:4).

Collapse of the overlaying rock occurs as water breaches the surface (Figure 5-15:5). Unlike for Hydraotes Chaos & the Hydraspis crater pair, the amount of collapse is an order of magnitude less. This indicates that the amount of water reaching the surface is also much less. It is therefore assumed that there is very little flood generation if any, with the majority of water reaching the surface refreezing and sublimating.

Reference

Fueten, F., Flahaut, J., Stesky, R., Hauber, E., & Rossi, A. P. (2014). Stratigraphy and mineralogy of Candor Mensa, West Candor Chasma, Mars: Insights into the geologic history of Valles Marineris. *J. Geophys. Res. Planets*(119), 331-354. doi:10.1002/2013JE004557

Gourronc, M., Bourgeois, O., Mège, D., Pochat, S., Bultel, .. B., Massé, M., . . . Mercier, D. (2014). One million cubic kilometers of fossil ice in Valles Marineris: Relicts of a 3.5 Gy old glacial landsystem along the Martian equator. *Geomorphology, 204*, 235-255. doi:10.1016/j.geomorph.2013.08.009

Hauber, E., Brož, P., Rossi, A. P., & Michael, G. (2015). A Field of Small Pitted Cones on the Floor of Coprates Chasma Mars: Volcanism Inside Valles Marineris? *46th Lunar and Planetary Science Conference.*

Komatsu, G., Geissler, P. E., Strom, R. G., & Singer, R. B. (1993). Stratigraphy and erosional landforms of layered deposits in Valles Marineris, Mars. *J. Geophys. Res., 98*(E6), 11,105-11,121.

Lucchitta, B. K. (1999). Geologic map of Ophir and central Candor Chasmata (MTM -05072) of Mars. *U.S. Geological Survey Geologic Investigations Series I-2568*. Retrieved from https://pubs.usgs.gov/imap/i2568/

Lucchitta, B. K., & Ferguson, H. M. (1983). Chryse Basin Channels: Low-Gradient and Ponded Flows. *Journal of Geophysical Research, 2(15)*, 553-568.

Rodríguez, J. A., Kargel, J. S., Tanaka, K. L., Crown, D. A., Berman, D. C., Fairén, A. G., . . . Sasaki, S. (2011). Secondary chaotic terrain formation in the higher outflow channels of southern circum-Chryse, Mars. *Icarus, 213*, 150-194. doi:10.1016/j.icarus.2010.09.027

Schmidt, G., Fueten, F., Stesky, R., Flahaut, J., & Hauber, E. (2018). Geology of Hebes Chasma, Mars: 1. Structure, Stratigraphy, and Mineralogy of the Interior Layered Deposits. *Journal of Geophysical Research: Planets, 123*, 2893-2919. doi:10.1029/2018JE005658

Schultz, R. A. (1998). Multiple-process origin of Valles Marineris basins and troughs, Mars. *Planet. Space Sci., 46*, 827-829. doi:10.1016/S00320633(98)00030-0

Tanaka, K. L., & Hartmann, W. K. (2012). The Planetary Time Scale. In F. M. Gradstein, J. G. Ogg, M. Schmitz, & G. Ogg, *The Geologic Time Scale* (pp. 275-298). Elsevier.

Tanaka, K., Skinner, J. A., Dohm, J., Irwin, R. I., Kolb, E., Fortezzo, C., . . . Hare, T. (2014). Geologic map of Mars: U.S. Geological Survey Scientific Investigations Map 3292. *scale 1:20,000,000, pamphlet 43 p.* doi:https://dx.doi.org/10.3133/sim3292

Warner, N. H., Sowe, M., Gupta, S., Dumke, A., & Goddard, K. (2013). Fill and spill of giant lakes in the eastern Valles Marineris region of Mars. *Geology, 41*, 675-678. doi:10.1130/G34172.1

Chapter 6.0 : Juventae Chasma; Baetis Chaos

6.1 Introduction

Baetis Chaos is located north of Juventae Chasma (Figure 6-1, 6-2), it is connected to Juventae Chasma by at least two channels, with a third emptying just north of Baetis Chaos (Figure 6-2). Another unnamed chaos zone immediately east of Baetis Chaos will be referred to as the East Chaos. Baetis Chaos is approximately 3,052 km^2 while the East Chaos is approximately 865 km^2. The floor of Baetis Chaos is deepest next to the small southwestern channel (Figure 6-2), reaching a depth of -700 m below the global datum. The majority of the floor of the basin ranges from -400 down to -500 m, with the mesas and surrounding plateau reaching 1,000 m in elevation. The East Chaos has a basin elevation of 500 to 600 m above the global datum with a smoother floor than Baetis Chaos. The tops of the mesa blocks are slightly higher than those in Baetis Chaos at 1,100 m elevation.

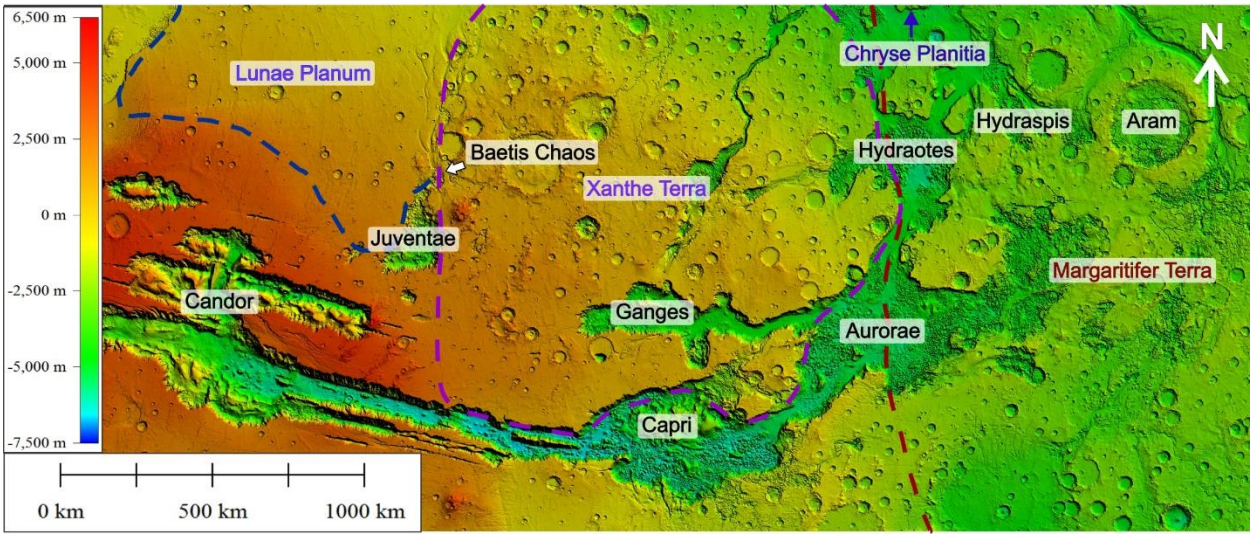

Figure 6-1 Overview of the area surrounding Juventae Chasma, the rough outline of Xanthe Terra (purple dashes) Margaritifer Terra (red dashes) and Lunae Planum (blue dashes) are shown.

The two chaotic zones share the major morphological features of other chaotic terrains: central mesa blocks separated by narrow channels, with knobs on the peripheries, all within a large depression. The largest mesas are 8 km across at the widest, making them similar in size to those seen in the Hydraspis crater pair and several smaller blocks in Hydraotes Chaos. Baetis Chaos has two inflow channels and several outflow channels (Figure 6-2) similar to Hydraotes Chaos. Unlike Hydraotes however the water flowing into Baetis Chaos was most likely solely sourced from Juventae Chasma, Hydraotes had the bulk of Valles Marineris as a potential source. The East Chaos appears to be a localized source of water with a single outflow channel at its northern end (Figure 6-2).

The plateau to the west of Baetis Chaos has a high density of approximately N-S wrinkle ridges, while the plateau is relatively featureless to the east (Rotto & Tanaka, 1995; Tanaka, et al., 2014). There is also a difference in lithologic units; those to the west are the “Early Hesperian Volcanic” unit while those to the east of Baetis Chaos are “Middle Noachian Highland” (Tanaka, et al., 2014).

Baetis Chaos and the East Chaos are unique among those studied here because they are isolated from Valles Marineris but still drain into Chryse Planitia, with the outflow channel Maja Valles (Figure 6-2) following the border between Xanthe Terra and Lunae Planum (Figure 6-1). Juventae Chasma, which is the main water source for Maja Valles (Chapman, et al., 2003; Catling, et al., 2006; Harrison & Grimm, 2008), has a north/south long axis which is perpendicular to the general east/west trend of Valles Marineris making it unique among chasmata in the area.

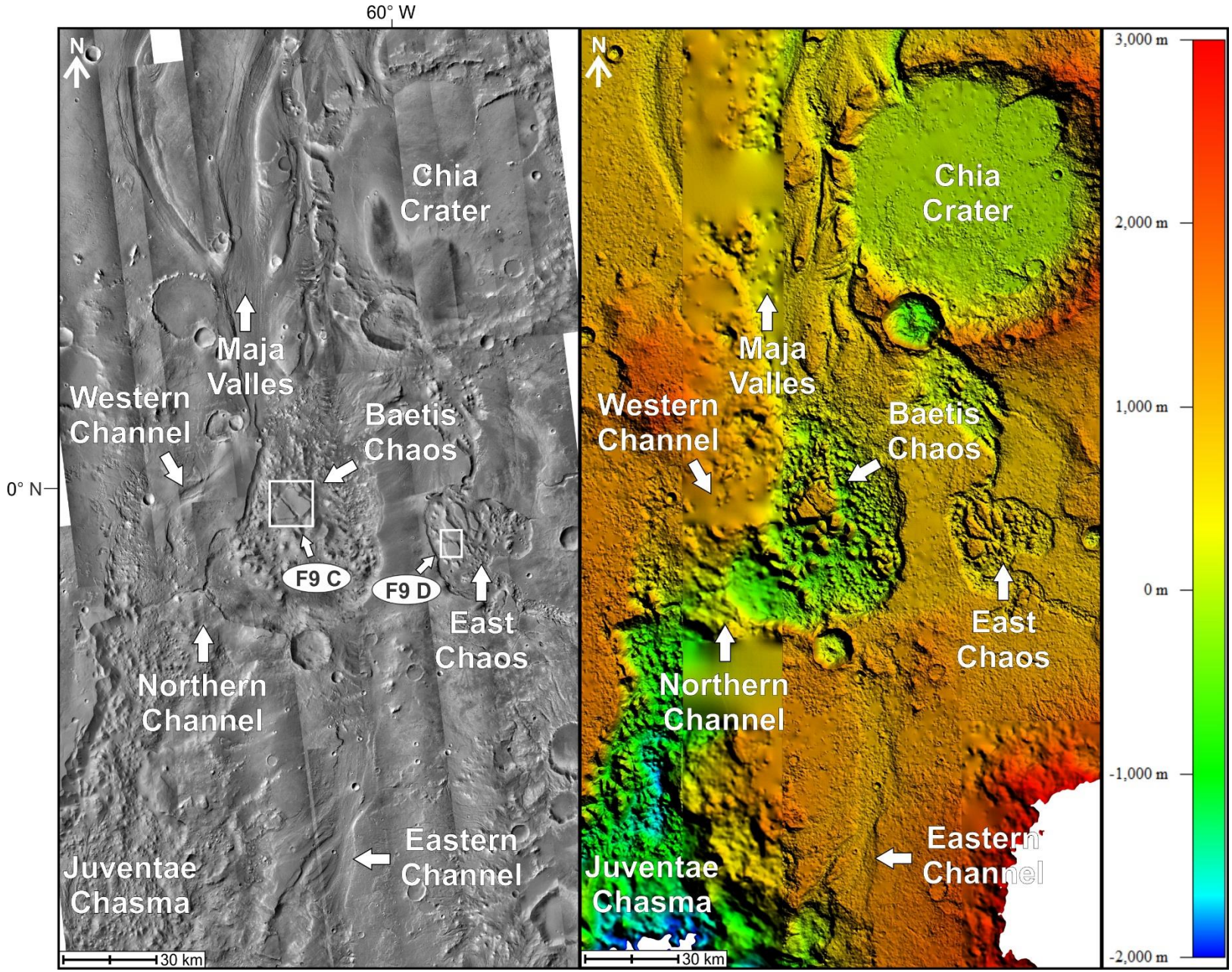

Figure 6-2 CTX composite (Left) and DEM composite (Right) generated with HRSC and CTX stereo pairs.

6.2 Previous Work

Previous studies have focused on the formation of Juventae Chasma and its Interior Layered Deposits (ILDs). Baetis Chaos to the north of Juventae Chasma and the East Chaos have not been studied in any detail to date.

Chapman et al. (2003) investigation of Juventae Chasma and Maja Valles suggests that a minimum of two periods of ILD formation exist, with one of those periods predating chaos formation in the northern section of Juventae Chasma (southwest of Baetis Chaos). They also identified megaripples (depositional bars) within Maja Valles which were taken as firm evidence for catastrophic flooding, with at least two periods of flooding indicated (Chapman, et al., 2003). Crater counting suggests that the youngest flood did not reach the full extent of Maja Valles or had very little effect on it, suggesting a significant drop in outflow volume over time (Chapman, et al., 2003). Formation of the ILDs in Juventae Chasma were suggested to be related to sub-ice volcanism (Chapman, et al., 2003). This would allow for a heat source to assist outflow of water from the chasma which increases in elevation northward to the outflow channel by 3 km (Chapman, et al., 2003).

Catling et al. (2006) studied the formation of the ILDs in Juventae Chasma. They also suggest that there are multiple ILD forming events (Chapman, et al., 2003). One of these ILD forming events predates the deposition of the Hesperian plateau basalts next to Juventae Chasma (Catling, et al., 2006). The composition of the ILDs using OMEGA data identified sulfates within the ILDs (Gendrin, et al., 2005), suggesting that the ILDs are sulfate-rich sedimentary rock (Catling, et al., 2006). The mechanism for the formation of the ILDs is suggested by Catling et al. (2006) to be evaporite deposits, or

dry deposition of volcanic sulfate aerosols accompanied by snow/ice deposition. Catling et al. (2006) suggest that ILDs are therefore easily eroded and estimates kilometers of material could have been eroded since the Hesperian. They also suggest that Juventae Chasma has undergone enlargement along the western wall which may still be actively collapsing. Large blocks identified in the southern basin were found to have dipping strata similar to that in the chasma walls (Catling, et al., 2006) giving further evidence of wall collapse in other areas of the chasma.

Coleman & Baker (2007) investigated a putative lake which formed in Juventae Chasma and overflowed northward into what would become Baetis Chaos. They then investigated the origins of outflow channels (Maja Valles) and their surface morphologies in and around Valles Marineris. They suggest that the floods which carved Maja Valles occurred during the mid-late Hesperian because they cut into Noachian and lower Hesperian surfaces. Fluvial incision during these floods could have triggered the collapse of the terrain and the formation of Baetis Chaos (Coleman & Baker, 2009). Streamlined islands are present in central Maja Valles and chaos development has occurred in several areas in Maja Valles (Coleman & Baker, 2009). In addition to the main channel between Juventae and Baetis Chaos a ‘western’ spillover channel was identified to the north separated by flood scoured plateau (Coleman & Baker, 2009).

Fueten et al. (2017) identify and describe four distinct ILD mounds within Juventae Chasma. They suggest that progressive widening of the chasma has occurred over geologic time (Catling, et al., 2006; Fueten, et al., 2017), with the ILDs forming in a much smaller basin than exists today (Fueten, et al., 2017). They also identify an

eastern outflow channel (Figure 2) which is 1.5 km higher than the northern channel and was therefore active first (Fueten, et al., 2017), bringing the number of major outflow channels northward out of Juventae Chasma to three. The opening of the northern channel was responsible for eroding the ILDs to their current levels (Fueten, et al., 2017) as lake levels dropped.

6.3 Methodology

For methods used, refer to Chapter 2.0 – Methodology above. This standard is used for each case study, except where otherwise indicated.

The DEM composite used for the area around Baetis Chaos is composed of CTX and HRSC. Orbits used are shown in Table 6-1. The entirety of the mesas in the Baetis Chaos and 70% of the basin floor are covered by CTX (20 m/pixel) the rest is HRSC (75m/pixel). The East Chaos is covered entirely by HRSC (50 m/pixel) the rest of the plateau is 75 m/pixel.

Table 6-1 Images used to create the composite DEM for the area around Baetis Chaos.

HRSC Orbit	CTX DEM Pairs
h1048_0000_da4_53 (50 m/pixel)	F04_037533_1813_XI_01N060W- F07_038443_1812_XI_01N060W
h1059_0000_da4_53 (75 m/pixel)	D10_031151_1812_XI_01N060W- P02_001957_1807_XN_00N060W

6.4 Results

6.4.1 Orientations Obtained with Augmented Visualization of Attitude (AVA)

An AVA (Figure 6-3) was produced for the chaotic area north of Juventae Chasma which includes Baetis Chaos and the East Chaos. The dips of every pixel were

calculated and are shown in Figure 6-4. The dip of the mesa block surfaces are separated into Baetis Chaos and the East Chaos (Figure 6-5). The surrounding plateau averages a dip of 2°. The dip of the steep sides of the mesa blocks was calculated using dips with values ranging from 17° - 40° to be consistent with previous analyses.

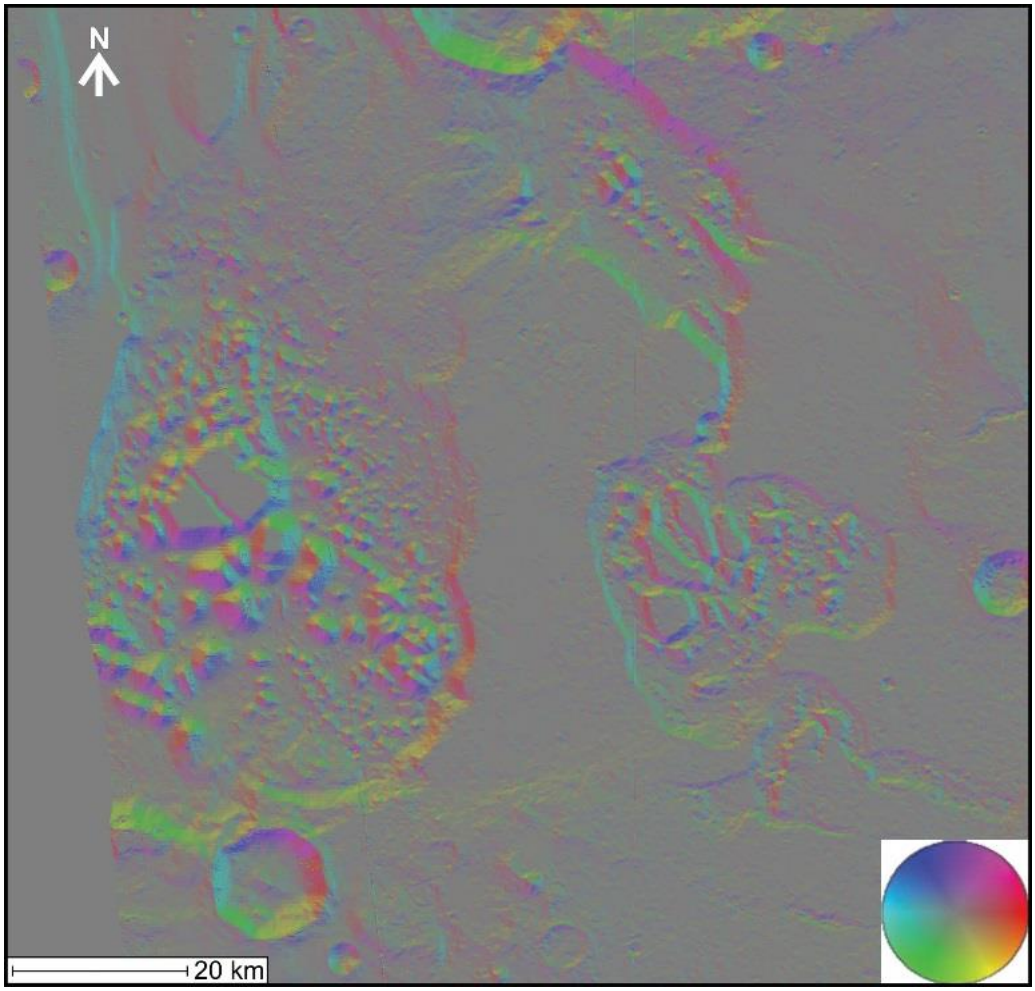

Figure 6-3 Colourized Augmented Visualization of Attitude (AVA) results using a colour coded stereonet.

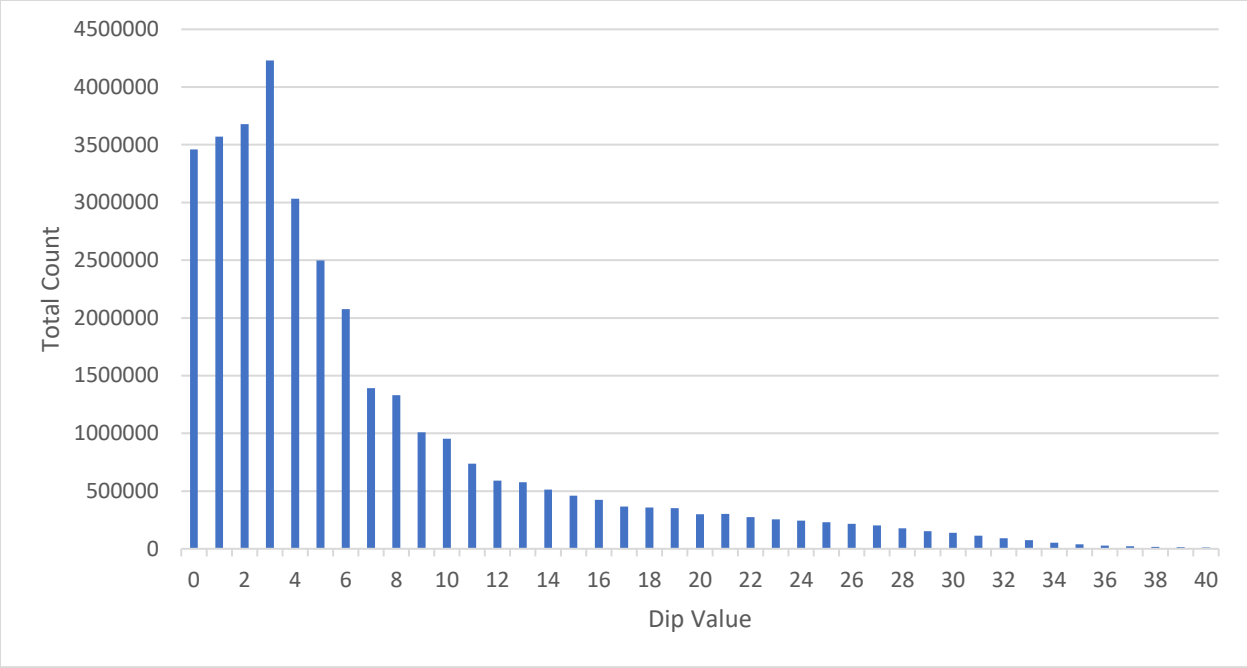

Figure 6-4 Dip value of all points calculated with the AVA of Baetis and surrounding area.

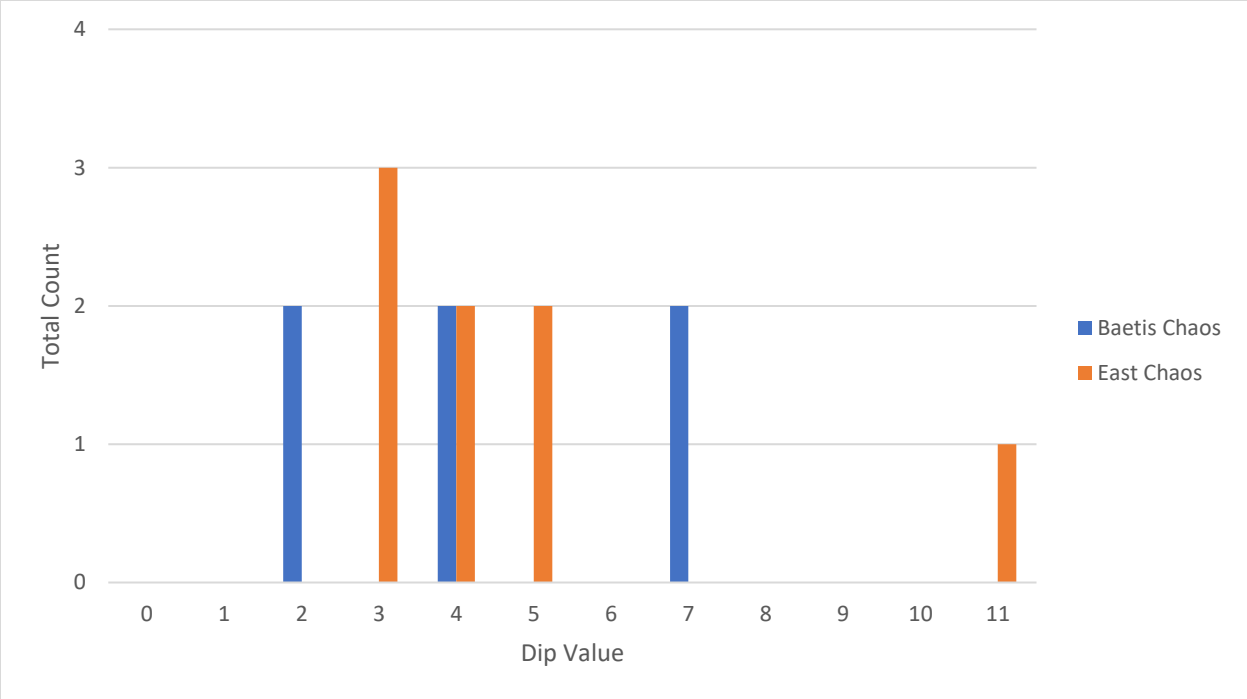

Figure 6-5 Average dip calculated for each mesa flat top within Baetis Chaos and the East Chaos. There are 6 mesas in the Baetis Chaos and 8 mesas in the East Chaos.

Figure 6-6 shows the strike values calculated using the AVA (Figure 6-3) for both basins. The mesas within Baetis Chaos show no strong preferred orientation (Figure 6-

6:A), while the mesas in the East Chaos show a southeast preferred strike (Figure 6-6:C). The steep sides of the mesas in Baetis Chaos also show no preferred orientation (Figure 6-6:B), while again the steep sides of the East Chaos mesas have a strong northwest/southeast orientation (Figure 6-6:D).

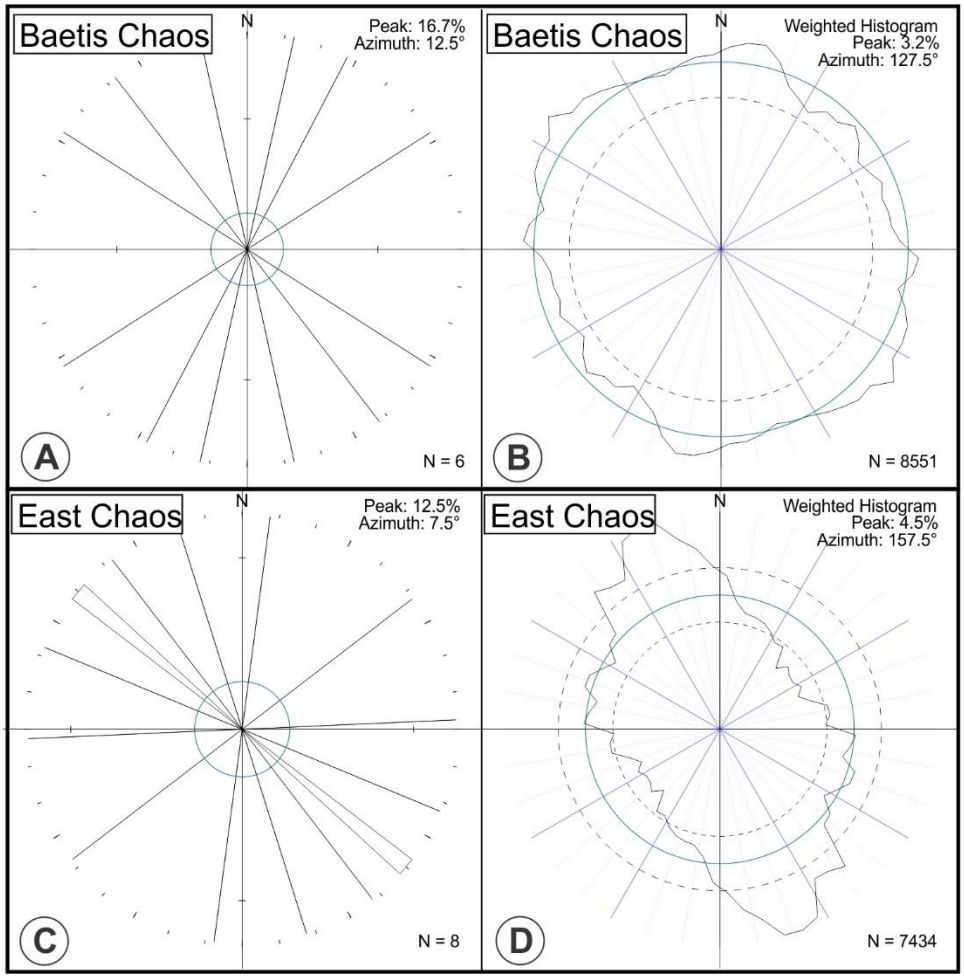

*Figure 6-6 A & C: Rose diagram of the strike for individual mesa tops within the Baetis Chaos and the East Chaos. B & D: Rose diagram of strike for all points within the two chaos regions that have dips from 17° - 40°. Due to computational limitations a histogram of all strike/dip value combinations with dips between 17-40 were used (360 strike values * 24 dip values = 8551 (Baetis) / 7434 (East) non-zero entries.*

6.4.2 Elevation and Distribution of Mesas

Figure 6-7 shows a contoured image of Baetis Chaos and the East Chaos, which includes the plateau region around them. Unlike the other chaotic terrain analyzed thus

far, the mesas within Baetis Chaos and the East Chaos are at a similar elevation to the surrounding plateau. The contouring is based on the major morphological groups: the surrounding plateau (red, orange, and yellow), the mesa blocks (isolated sections of orange and yellow), and the basin floors and outwash channels (greens). Both groups of mesas are clustered in the northwest section of their respective basins close to the outwash channels. The mesas within the East Chaos are higher in elevation than a large amount of the surrounding plateau suggesting uplift of the blocks or subsidence/erosion of the plateau.

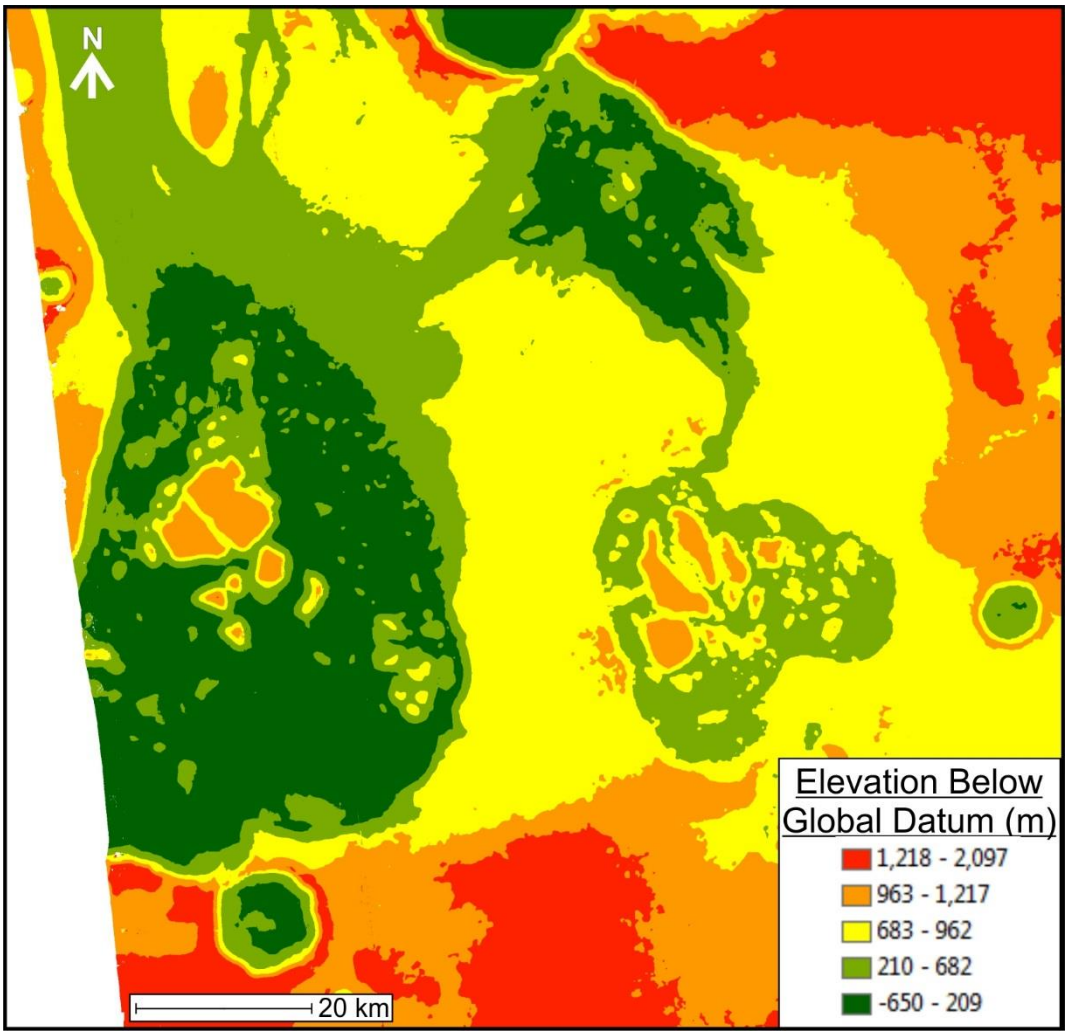

Figure 6-7 Manually set contoured DEM to allow for better visualization of Baetis Chaos and the East Chaos.

6.4.3 Orientation of Mesa Tops

The dips of the top surfaces of the mesa blocks and the surrounding plateau were calculated using the AVA (Figure 6-3). The rose diagrams (Figure 6-6) show no preferred orientation in Baetis Chaos, while the East Chaos shows a preferred southeast strike. Figure 6-8 shows that the mesas in the East Chaos are dipping away from the outwash channel.

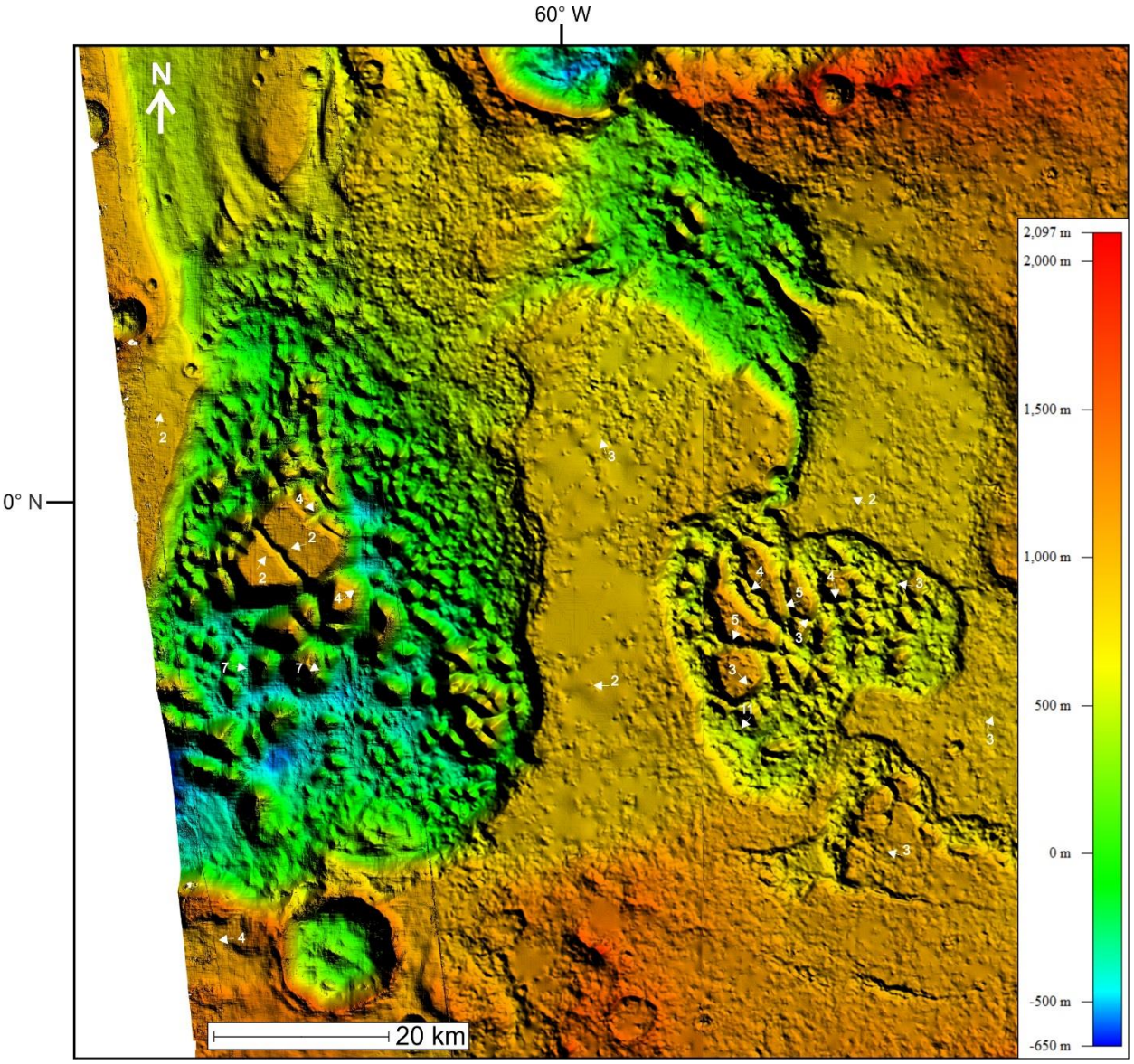

Figure 6-8 Composite DEM using HRSC and CTX, includes dip (numerical value) and dip direction (arrows) of mesa tops.

6.4.4 Calculation of Volume Loss

Volume loss was calculated similarly to Hydraotes Chaos and the Hydraspis crater pair however the mesas in Baetis Chaos and the East Chaos have not collapsed relative to the surrounding plateau. Two bounding surfaces were used for the respective basins. The elevation of those surfaces was taken from the highest points on the mesas in each basin (which are at or above the surrounding plateau elevation). Baetis Chaos

uses a surface at 1,180 m above the global datum and the East Chaos uses a surface at 1,220 m. The current basin floors were used as the bottom surfaces in the respective basins. The results of the calculation are shown in Table 6-2.

Table 6-2 Results of the volume loss calculation.

	Volume of Missing Material	Average Depth of the Basin
Baetis Chaos	3,200 km^3	1 km
East Chaos	400 km^3	0.5 km

6.5 Discussion

6.5.1 Differences with Hydraotes Chaos and the Hydraspis Crater Pair

The size of mesas within Baetis Chaos and the East Chaos are similar to those located in Hydraotes Chaos and the Hydraspis crater pair, but their elevation is at or higher than the surrounding plateau, suggesting no collapse. The basin floors of Baetis Chaos and the East Chaos are also several kilometers higher in elevation when compared with the other chaotic terrains previously mentioned.

6.5.2 Lack of Mesa Terraces

No mesa terraces can be identified in either Baetis Chaos or the East Chaos. This suggests no stable water bodies were present in either zone for long enough periods to produce them. The East Chaos outwash channel is at a lower elevation than

the chaos and would therefore not allow ponding in a lake. Baetis Chaos however is capable of containing a lake which would be 1 km deep at its deepest point.

Baetis Chaos is directly between the northern channel of Juventae Chasma and Maja Valles suggesting that a large volume of water must have flowed through it. This is similar to Hydraotes Chaos (Hydraotes has significantly more volume), however the mesas are not streamlined or completely removed as would be expected if catastrophic flooding were to occur. In Hydraotes Chaos this was addressed by ponding in a large lake which produced the terraces identified on many of the mesas therein. There are no terraces in Baetis Chaos, suggesting water did not pool as it did in Hydraotes Chaos even though the elevation of the outflow channel suggest that it could have, and yet it was still a major pathway for outflow from Juventae Chasma. For the mesas to remain intact the bulk volume of floods must have occurred on a surface above them prior to the removal of the material surrounding them in the basin. Another possibility would be if the entire surface were glaciated and only turbulent surface flow from Juventae Chasma was permitted northward to Maja Valles, the chaos having then formed following a warming period.

6.5.3 Orientation and Distribution of Mesas

Mesa blocks within Baetis Chaos and the East Chaos have very low dips (most <7°) which is the same for all chaotic terrains investigated here, suggesting that rotation is very minor in the creation of chaotic terrain. The larger mesas are also grouped together like they are in all chaotic terrains investigated; this is postulated to be the area of initial collapse. The mesas in these two chaos zones however have not collapsed

with respect to their surrounding plateau, in fact several mesas are higher in elevation than the plateau. The plateau immediately adjacent to the chaos has been previously interpreted as being a fluvially eroded surface (Coleman & Baker, 2009) and the surface morphologies agree with this hypothesis (Figure 6-2). This suggests that the original surface was higher in elevation before being eroded down by flooding.

6.5.4 Sedimentation of the Basin

Based on work by Rodríguez et al. (2011) Baetis Chaos and the East Chaos should be interpreted as secondary chaotic terrain using descriptions given by Coleman & Baker (2007, 2009). Like in other secondary chaotic terrains, the mesas have not undergone major collapse and have therefore most likely not produced any major flooding events during their creation. The problem with this interpretation is that the East Chaos has clearly produced flooding to erode a channel northward (Figure 6-2) as there is no other clear source of fluid. Baetis Chaos outflows into Maja Valles northward (Figure 6-2) which has been previously attributed entirely to Juventae Chasma outflow (Coleman & Baker, 2009).

Fueten et al. (2017) identified an abandoned channel in the northeast section of the wall of Juventae Chasma, referred to here as the eastern channel (Figure 6-2). This channel sits far above (1.2 – 1.5 km) (Fueten, et al., 2017) the main northern channel suggesting that it was active first (Fueten, et al., 2017) before water levels in Juventae Chasma dropped below it. Flooding of the eastern channel may have been responsible for the fluvial erosion of the plateau northwards, excavating volatiles in the subsurface and triggering the creation of secondary chaotic terrains where volatile concentrations

were highest. The activation of this channel most likely predates the collapse of the northern section of Juventae Chasma, which opened the northern channel, as the northern channel is significantly lower in elevation and would have received all outflow if it was available.

The western channel (Figure 6-2) is another abandoned channel, which circumvents Baetis Chaos entirely, suggesting that is was active before the creation of the secondary chaotic terrains. If the basin in Baetis Chaos had already formed as the lowest topography, it would have channeled all outflow towards it. The northern channel (Figure 6-2) has a deeply incised channel at its center suggesting that it was the last to flow as waters incised into the surface capturing all outflow northward out of Juventae chasma (Coleman & Baker, 2007; Coleman & Baker, 2009).

6.5.5 Sapping Channels

Sapping channels are present in Baetis Chaos and the East Chaos; however there are only several examples as there is a low number of mesas (Figure 6-2, 6-9). Sapping channels present in Baetis Chaos and the East Chaos have been filled with sediment (Figure 6-9:D) and some cut straight through blocks (Figure 6-9:C).

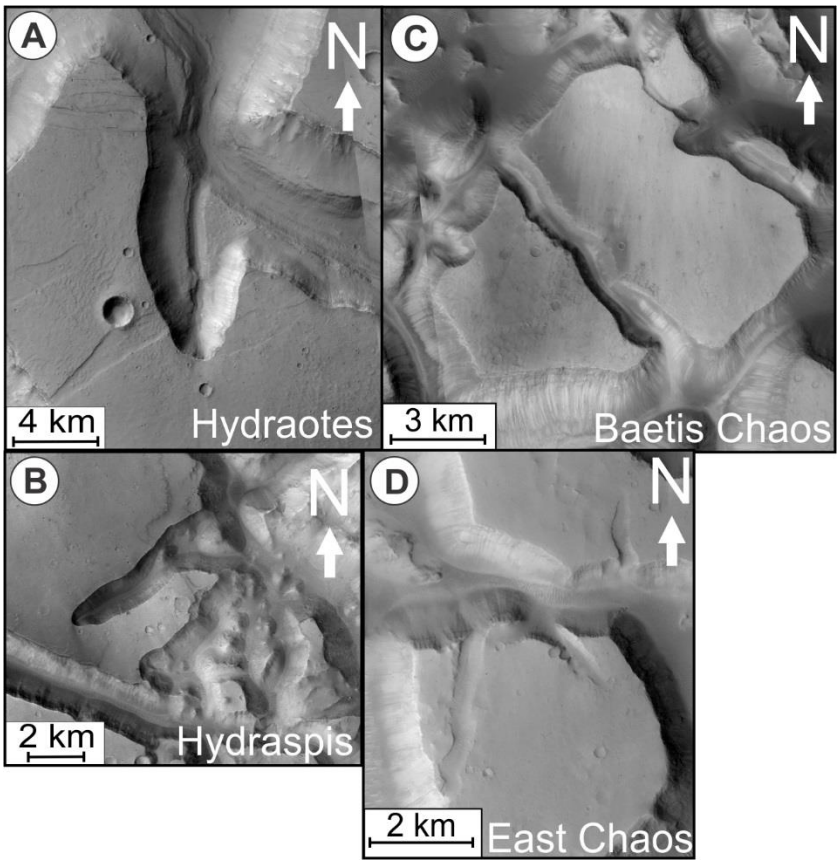

Figure 6-9 Comparison of sapping channels in Hydraotes (A), Hydraspis crater pair (B), Baetis Chaos (C)(Fig 2), and East Chaos (D)(Fig 2).

6.6 Origins of Juventae Chasma

Juventae Chasma has a general north-south long axis unlike the chasmata of Valles Marineris to the south or Hebes Chasma to the west. What is left of the ILDs, following erosion, within Juventae Chasma also trend north-south. Collapse of the plateau northwards into chaotic terrain within Juventae Chasma suggests a large volume of volatiles in the subsurface prior to collapse and expansion of the chasma. One of the ILD mounds in Juventae Chasma records thick, uninterrupted layering, suggesting a calm depositional environment (Fueten, et al., 2017), while the other mounds have evidence of soft sediment deformation and a wide range of layer thicknesses (Fueten, et al., 2017). The ILDs are a record of the environment in and around Juventae Chasma. The first mound to form would have done so in a much

smaller proto-Juventae and as the chasma widened through collapse outward other ILDs would be deposited with at least one following the creation of some of the northern chaos within Juventae Chasma, as it overlays blocks (Chapman, et al., 2003).

6.7 Baetis Chaos Formation Model

Conceptual models were created for the evolution of outflow from Juventae Chasma (Figure 6-10) and creation of Baetis Chaos (Figure 6-11).

6.7.1 Model Assumptions

The conceptual model for Juventae Chasma flooding and outflow carries several assumptions. It is assumed that the eastern channel out of Juventae Chasma was active first, based on its elevation above all other channels. Using the same reasoning it is also assumed that the western channel which circumvents Baetis Chaos was active before the basin within Baetis Chaos has formed. The northern channel which flows into Baetis Chaos most likely received the highest volume of water as the depth and width of the channel is the greatest and the channels into Maja Valles come from the northern end of Baetis Chaos. Based on the channels exiting Chia Crater to the north previous authors (Coleman & Baker, 2009) assumed that a large lake was present in Chia Crater. This lake was ultimately fed from Juventae Chasma outflow until the channel was dammed by an impact crater.

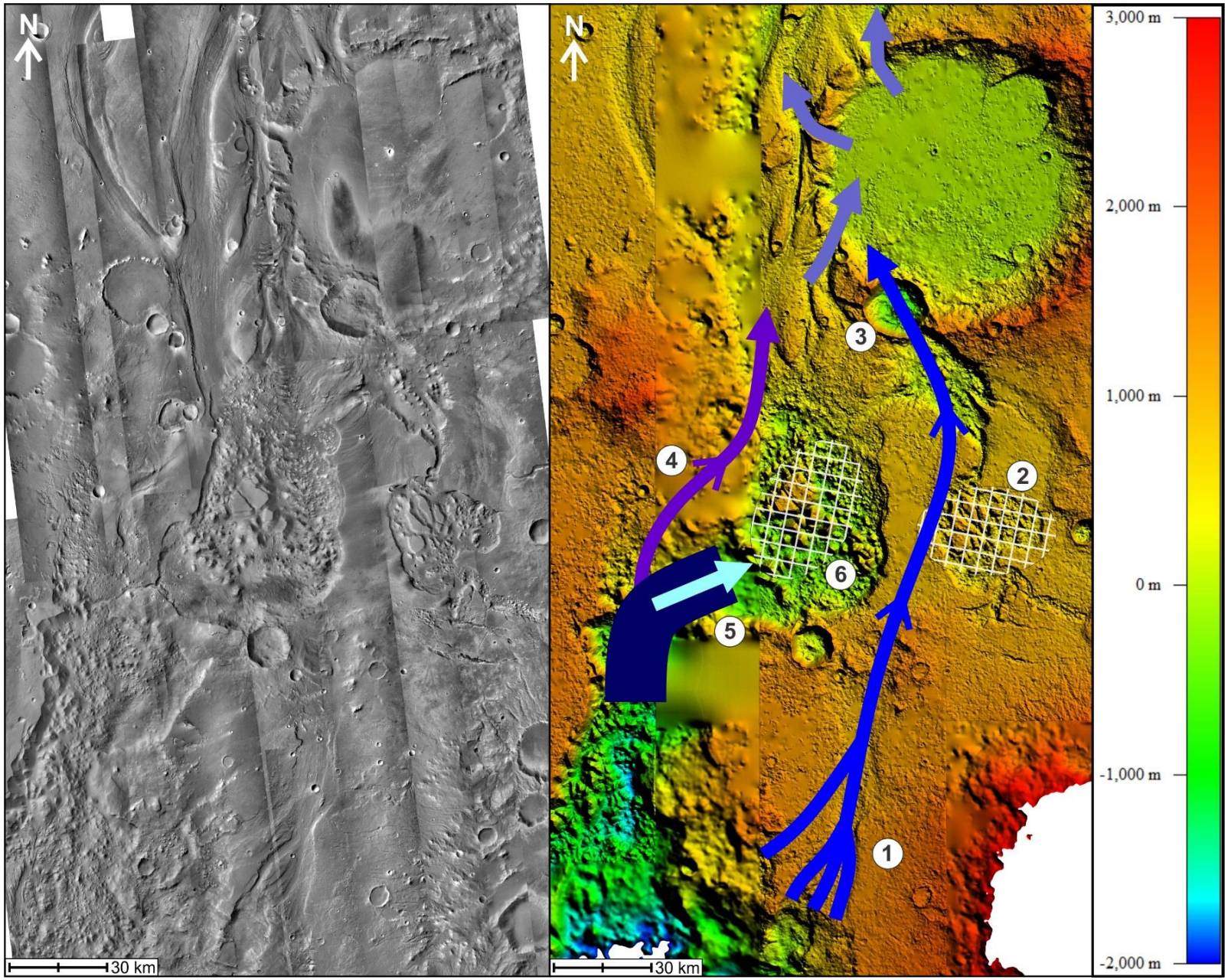

Figure 6-10 Model of relative timing of channel activation north out of Juventae Chasma. Relative age is given by the number; oldest (1) to youngest (6).

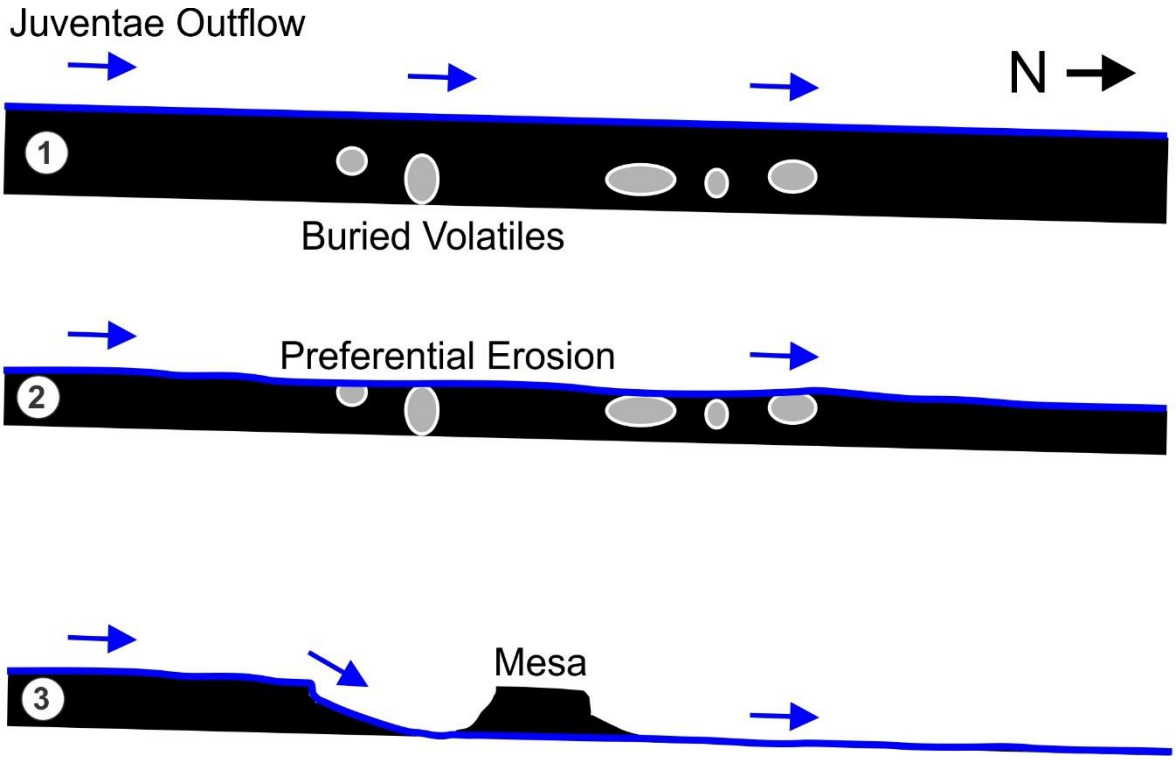

Figure 6-11 Conceptual model of secondary chaotic terrain formation for Baetis Chaos. 1) Erosion of the surface by water flow occurs. 2) Erosion of the surface exposes subsurface volatiles which preferentially erode. 3) Areas with comparatively low volatiles are resistant to erosion, leaving behind blocks which flooding flows around. Substantial flooding would erode blocks into streamlined islands, therefore those in Baetis Chaos must have been protected by ice, or low but sustained flooding volumes.

6.7.2 Model Description

The current elevation of the mesas within Baetis Chaos and the East Chaos are at or above their surroundings. It is therefore assumed no collapse has taken place when compared with other chaos regions like Hydraotes Chaos. A different mechanism for formation is therefore required to explain this (Figure 6-11). The concept model in Figure 6-11 is based on a previous model by Rodríguez et al. (2011) and shows the mechanism for the formation of secondary chaotic terrains in an outflow channel. Volatiles in the subsurface are the key to the formation of all chaotic terrains explored here, the major difference being the location and size of these high concentrations of volatiles. For the larger mesa chaotic terrains (Hydraotes and the Hydraspis crater pair)

the volatiles were in a large ice sheet under a large package of sediment. In Baetis Chaos and the East Chaos these high concentrations of volatiles were localized in pockets which got excavated by erosion. In this case flooding is assumed to have been responsible for this erosion, preferentially removing all material high in volatiles and leaving behind areas with comparably low concentrations (mesa blocks). The evolution of Juventae Chasma influenced the changing outflow channels and the creation of Baetis Chaos and the East Chaos. These areas of chaos still needed to have higher concentrations of volatiles in the subsurface to form, otherwise these two areas would simply be extensions of the channels and not large open basins with mesa blocks.

Figure 6-10 shows a relative timeline model of outflow from Juventae Chasma. Stages are labeled from oldest (1) to youngest (6). Outflow from the eastern channel begins when water levels in proto-Juventae begin to flow over the surrounding plateau (Figure 6-10:1). The flow erodes multiple channels which converge moving northwards. There are widespread eroded surfaces between Baetis Chaos and the East Chaos which have been previously interpreted as flooding surfaces (Coleman & Baker, 2009). It is hypothesized that a large amount of erosion of the plateau surface was a result of the activation of the eastern channel which scoured the surface northward to where it either produced the collapsed area adjacent to the southern rim of Chai Crater through volatile excavation, or simply exploited a pre-existing basin to drain into Chia Crater. During this time the East Chaos would have formed (Figure 6-10:2) in a similar fashion shown in Figure 6-11, this chaos zone would produce enough outflow to erode a small channel north towards Chai Crater.

Some time after this, flow from the eastern channel into Chai Crater would become blocked by an impact crater into the southern crater rim (Figure 6-10:3). By this time flow from the eastern channel was most likely low as there is no apparent outflow channels out of the south basin adjacent to Chai Crater. The majority of water from the first major floods out of Juventae Chasma would have therefore been drained into Chai Crater. Channels out of Chai Crater are labeled with arrows in Figure 6-10, however it is not known when these channels were active. Flooding from Juventae Chasma may have moved straight through the crater northwards, or more likely, it pooled into a lake (Coleman & Baker, 2009) which would eventually breach the crater rim in several areas.

It is assumed that collapse of the northern section of Juventae Chasma caused the cessation of flow in the eastern channel. The collapse increased the volume of Juventae Chasma which would drop water levels substantially, cutting off the eastern channel. Activation of the western channel followed the collapse of the northern section of Juventae Chasma (Figure 6-10:4). This channel completely circumvents what is now Baetis Chaos. For this reason, the basin of Baetis Chaos is assumed to have not been formed and that the channel exploited the path of least resistance northward.

The largest flooding event occurred through the northern channel (Figure 6-10:5). This channel was responsible for draining the majority of Juventae Chasma, heavily eroding the ILDs (Fueten, et al., 2017), and eroding surfaces downstream excavating volatiles in the subsurface, causing preferential erosion of those surfaces. This flooding most likely created Baetis Chaos (Figure 6-10:6) and the majority of Maja Valles northwards. Erosion along the western rim of Chai Crater by these channels most likely aided in the breaching of the Chai Crater rim and outflow followed. In the center of the

northern outflow channel there is a much narrower and deeper channel which would have captured and directed flow until its cessation (Figure 6-10:5 arrow).

References

Catling, D. C., Wood, S. E., Leovy, C., Montgomery, D. R., Greenberg, H. M., Glein, C. R., & Moore, J. M. (2006). Light-toned layered deposits in Juventae Chasma, Mars. *Icarus, 181*, 26-51. doi:10.1016/j.icarus.2005.10.020

Chapman, M. G., Hare, T. M., Russell, A. J., & Gudmundsson, M. T. (2003). Possible Juventae Chasma subice volcanic eruptions and Maja Valles ice outburst floods on Mars: Implications of Mars Global Surveyor crater densities, geomorphology, and topography. *J. Geophys. Res., 108*(E10), 5113. doi:10.1029/2002JE002009

Coleman, N. M., & Baker, V. R. (2009). Surface morphology and origin of outflow channels in Valles Marineris region. In D. M. Burr, P. A. Carling, & V. R. Baker (Eds.), *Megaflooding on Earth and Mars* (pp. 182-184). Cambridge University Press.

Coleman, N., & Baker, V. (2007). Evidence that a Paleolake Overflowed the Rim of Juventae Chasma, Mars. *Lunar and Planetary Science XXXVIII*.

Fueten, F., Novakovic, N., Stesky, R., Flahaut, J., Hauber, E., & Rossi, A. P. (2017). The Evolution of Juventae Chasma, Valles Marineris, Mars: Progressive Collapse and Sedimentation. *Journal of Geophysical Research: Planets*(122), 2223-2249. doi:10.1002/2017JE005334

Gendrin, A., Mangold, N., Bibring, J., Langevin, Y., Gondet, B., Poulet, F., . . . LeMouélic, S. (2005). Sulfates in Martian Layered Terrains: The OMEGA/Mars Express View. *Science, 307*(5715), 1587-1591. doi:10.1126/science.1109087

Harrison, K. P., & Grimm, R. E. (2008). Multiple flooding events in Martian outflow channels. *JGR, 113*, E02002. doi:10.1029/2007JE002951

Rodríguez, J. A., Kargel, J. S., Tanaka, K. L., Crown, D. A., Berman, D. C., Fairén, A. G., . . . Sasaki, S. (2011). Secondary chaotic terrain formation in the higher outflow channels of southern circum-Chryse, Mars. *Icarus, 213*, 150-194. doi:10.1016/j.icarus.2010.09.027

Rotto, S., & Tanaka, K. L. (1995). *Geologic/geomorphic map of the Chryse Planitia region of Mars.* USGS. doi:10.3133/i2441

Tanaka, K., Skinner, J. A., Dohm, J., Irwin, R. I., Kolb, E., Fortezzo, C., . . . Hare, T. (2014). Geologic map of Mars: U.S. Geological Survey Scientific Investigations Map 3292. *scale 1:20,000,000, pamphlet 43 p.* doi:https://dx.doi.org/10.3133/sim3292

Chapter 7.0 **: Discussion**

7.1 Introduction

This study analyzed several areas of chaotic terrain which drain into Chryse Planitia. Hydraotes Chaos and the Hydraspis crater pair are examples of primary chaotic terrains, while Candor Chaos, Baetis Chaos, and the East Chaos are examples of secondary chaotic terrains. These chaotic terrains were chosen due to morphological similarities which include smooth-topped mesas present in a large depression, though the formation mechanisms of the mesas and depressions are different. These smooth mesa surfaces allowed for the analysis of the orientation of blocks as well as their distribution in the chaotic terrains. This section will outline and discuss similarities and differences between the chaotic terrains analyzed.

7.2 Morphologic Similarities & Differences

Table 7-1 outlines the basic morphological properties of the different chaotic terrains studied.

Table 7-1 General morphological comparison of each chaotic terrain.

	Hydraotes Chaos	Hydraspis Crater Pair	Candor Chaos	Baetis & East Chaos
Are there central flat topped mesas surrounded by knobs?	Yes	Yes	Yes	Yes, few in number
Is the chaos in a large depression?	Yes	Yes, impact crater	Yes	Yes

Are there sapping channels?	Yes	Yes	No	Yes
Are there outflow channel/s?	Yes	Yes	Yes	Yes
Is there any evidence of volcanism?	Cinder Cones	None, proximity to Hydraotes Chaos	None, Proximity to Coprates Chasma	None, possible volcanic structure to the SE
What is the relationship between mesa and surrounding plateau?	Can trace plateau structures into chaos	Small spur and gully texture near the top of several SW blocks matches plateau morphology	Not part of the plateau, morphologically distinct	Same elevation as the surrounding plateau

One of the minor differences between the chaotic terrains is the presence or absence of sapping channels. This fact may be a function of the thickness of the blocks or the elevation of the original terrain. In Candor Chaos, it can not be reasonably assumed that the mesas represent the surface of the original plateau which has collapsed, as it is morphologically distinct and much further from the plateau than the other chaotic terrains. It is more likely that the area above Candor Chaos was covered by several kilometers of ILD, and so sapping channels would not have formed.

It is assumed in Hydraotes Chaos and the Hydraspis crater pair that sedimentation covered pre-existing depressions which were filled with ice. In the case of Hydraotes Chaos several faults can be followed from the existing plateau into the current mesas within the chaos zone. The Hydraspis crater pair has a weaker link to the

surrounding plateau as spur and gully textures observed on several mesas in the southern crater are similar to those observed in the surrounding plateau suggesting that they are made of a similar material. Nearby Aram Crater, which is significantly larger (Zegers, et al., 2010), has been previously suggested (Zegers, et al., 2010) to have been filled to just below the plateau prior to the formation of chaos and draining of the crater.

7.3 Need for Volcanism

Volcanism has been used to explain the formation of Chaotic Terrain in many previous studies (Komatsu, et al., 2000; Leask, et al., 2006; Rodriguez, et al., 2006; Meresse, et al., 2008). The presence of cinder cones in the case of Hydraotes Chaos shows that there was active volcanism in this area. The other chaotic terrains show no evidence of active volcanism with the possible exception of the chaos north of Juventae Chasma as there is a possible volcanic structure nearby. With the Zegers et al. (2010) subsurface lake destabilization model volcanic sources of heating are not necessary given a thick enough sediment package (500 m – 1,500 m) and a thick ice sheet (2 km at center). Evidence of cinder cones in nearby Coprates Chasma (Hauber, et al., 2015) may have provided heating for Candor Chaos, as this terrain is the least likely to fit the Zegers et al. (2010) model based on its morphology. The Hydraspis crater pair is near the limit of the Zegers et al. (2010) model with a sediment thickness ≥ 700 m and an estimated collapse depth of 1.45 km (assumed to be ice removed), a source of outside heating may therefore be required to trigger melting of the ice sheet. Secondary chaotic terrains like Baetis and the East Chaos do not require a source of outside heating

because their formation mechanism does not involve collapse, and instead relies on excavation of the surface by flooding. Volcanism as an outside heat source is therefore only required to produce primary chaotic terrains which have a depth of overburden and thickness of a subsurface ice sheet which is below the threshold (likely ~3 km of combined material) for melting caused by the difference between the thermal conductivity of the overburden and the basement.

7.4 Elevation Based Data

The basic elevation data of features identified within the chaotic terrains are recorded in Table 7-2. This table includes the location of terraces if present, the size of the mesas and their elevation, as well as the total depth of the chaotic terrains.

Table 7-2 Comparison of elevation data extracted from all chaotic terrains.

	Hydraotes Chaos	Hydraspis Crater Pair	Candor Chaos	Baetis & East Chaos
Terrace elevations	-3,829 m to -4,532 m Average -4,161 m	-2,985 m to -3,495 m Average -3,244 m	N/A	N/A
Formation level of terraces measured from mesa top	500 m – 1,000 m	200 m	N/A	N/A
Formation level of terraces measured from basin floor	≤ 500 m	≤ 500 m	N/A	N/A

Elevation of the base of mesas	-4.9 km	-3.9 km	-4.7 km	Baetis: -0.5 km East: 0.6 km
Total collapse depth	2.1 km	1.45 km	Unknown, estimated < 0.2 km	N/A
Mesa height	≥ 1.4 km	≥ 0.7 km	≥ 0.2 km	Baetis: ≥ 1.5 km East: ≥ 0.5 km

Terraces are only observed in two of the chaotic terrains studied here. On average the terraces in the Hydraspis crater pair are 1 km higher in elevation than those in Hydraotes Chaos. The terraces in the Hydraspis crater pair also form much closer to the surface of the mesas they are present on (200 m vs 500 – 1,000 m in Hydraotes). The terraces do form at a similar elevation relative to the basin floors suggesting a similar water depth in both chaotic terrains during terrace formation.

The thickness of the original ice layer is controlled by the amount of water/ice available and by the size of the sink to fill. The widest and deepest chaotic terrain examined here is Hydraotes Chaos, making it the largest sink. If one assumes the same availability of water for all examined chaotic terrains the largest ice sheet by volume would have formed in Hydraotes Chaos. Of the chaotic terrains that collapsed, Hydraotes Chaos also has the most mesa showing above the surface. Block thickness measurements are based on what is visible above the surface. The mesas are most likely thicker than this. In the case of Hydraotes Chaos the total collapse depth was calculated to be approximately ≤ 50% thicker than the mesa blocks while the Hydraspis crater pair the collapse depth is ≤ 100% thicker than the mesa blocks.

7.5 Volume Loss Comparison

The total volume loss calculated for the chaotic terrains studied is shown in Table 7-3, which also includes the average depth of each chaotic terrain as well as the estimated area used to calculate the average depth. Previous studies (Table 7-4) have estimated the volume of material excavated by water based on channel morphology adjacent to chaotic terrains. This gives an estimate of water produced by chaotic terrains, and thus a direct comparison to volume loss if the majority of that volume is water ice which it is assumed to be. Values are in cubic kilometers of ice which would be 8% less for liquid water.

Table 7-3 Comparison of chaotic terrains and their total volume loss.

	Hydraotes Chaos	Hydraspis Crater Pair	Candor Chaos	Baetis & East Chaos
Total Volume Loss	179,000 km^3	10,900 km^3	< 2,000 km^3	Baetis: 3,200 km^3 East: 400 km^3
Average Depth	2.10 km	1.45 km	< 0.5 km	Baetis: 1 km East: 0.5 km
Area of Chaotic Terrain	50,000 km^2	7,700 km^2	3,600 km^2	Baetis: 3,052 km^2

				East: 865 km^2

Table 7-4 Compilation of volume loss estimates by previous authors.

Area	Volume	Author
Hydraotes Chaos	117,000 km^3	Carr et al. (1987)
Simud & Tiu Valles	400,000 km^3 channel excavated by water	Carr et al. (1987)
Hydraspis Chaos	45,000 km^3	Carr et al. (1987)
Maja Valles	33,000 km^3 channel excavated by water	Carr et al. (1987)
Coprates	110,000 km^3 max lake	Harrison & Chapman (2008)
Aromatum	4,090 km^3 material removed 10,500 – 16,500 km^3 water generated	Leask et al. (2006)
Aram	30,000 – 120,000 km^3 water generated	Zegers & Roda (2012)
	93,000 km^3 water generated	Roda et al. (2014)

Circum-Chryse	300,000 km^3 individual floods 6,000,000 km^3 total floods	Carr (1996) (as cited in Wang, et al., 2006)

Comparing the volume loss results shown in Table 7-3 with the total flood results estimated by Carr (1996) (as cited in Wang, et al., 2006) (Table 7-4) shows that all volumes are within the maximum volume for individual floods. This is interesting for Hydraotes Chaos as it is expected to have had multiple flooding events from the generation of the chaos but also an unknown incoming volume of water from Valles Marineris, including the possible lake in Coprates Chasma (Harrison & Chapman, 2008). This gives further support to the argument that Hydraotes was a large lake where water pooled before moving northward so floods would be numerous and over a long period of time (millions of years). If the volume of ice under proto-Hydraotes was instead a pressurized aquifer system, as other authors suggest for general chaos formation (Chapman & Tanaka, 2002; Chapman, et al., 2003; Coleman, 2003; Leask, et al., 2006), then the volume of water is expected to be much greater to account for the collapse depth and removal of material. Using the study of Aromatum (Leask, et al., 2006) as a reference, this argument would suggest a volume in excess of 2 – 3 times greater than calculated (360,000 – 540,000 km^3) and a source aquifer with a surface area ~25 times the size of Hydraotes Chaos (1,250,000 km^2). Using these estimates Hydraotes Chaos would have produced enough water to erode Simud and Tiu Valles (the main outflow channels northward out of Hydraotes) without any input from Valles Marineris or the numerous other channels nearby. Comparing the results of Hydraotes with the study by Carr et al. (1987) which used Viking photogrammetric measurements,

shows a ~65% estimated increase in volume loss which is mostly taken up by the removal of the subsurface ice sheet, and most likely a minor increase from improved data (Viking compared with HRSC and CTX). With either value used, the excavated channels of Simud and Tiu Valles require more water than what could be produced by the formation of Hydraotes alone. If most of the subsurface water needed to erode Hydraotes comes from a buried ice sheet then Hydraotes is a significant contributor to the excavation of Simud and Tiu Valles, but it cannot be the only contributor.

The Hydraspis crater pair can also be compared with the study by Carr et al. (1987) which suggests 45,000 km^3 of material is eroded from all Hydraspis Chaos. The Hydraspis crater pair makes up approximately 1/3 of the area of Hydraspis Chaos so it is expected to produce a significant fraction of the total water (~24% compared with Carr et al. (1987)) needed to remove material from the area. In total it is estimated to be a minor source (< 6%) of flooding responsible for eroding the adjacent Tiu Valles, just north of Hydraotes Chaos.

The results for the chaotic terrains north of Juventae Chasma can also be compared to the previous study by Carr et al. (1987). They estimate the volume of Maja Valles (the channel leading north from Baetis Chaos) eroded by water to be 33,000 km^3. Baetis and the East Chaos zones could easily be eroded by this amount of water from the draining of Juventae Chasma (Chapman, et al., 2003; Catling, et al., 2006; Harrison & Grimm, 2008). It is possible that both chaos generated outflow (Leask, et al., 2006) through excavation of volatiles, however this would be minor compared with the volume required to excavate Maja Valles.

7.6 Lack of Regional Control

The chaotic terrains investigated in this study are all relatively close to Valles Marineris, with three chaos zones (Hydraotes, the Hydraspis crater pair, and Candor) directly linked through the canyon system. It was therefore initially hypothesized that the system of grabens and wrinkle ridges which formed the major structural features of the area would influence the collapse and possibly the location of chaotic terrain. This does not appear to be the case.

Hydraotes Chaos shows no strong regional trend in the surrounding plateau based on surficial investigation and USGS maps (Rotto & Tanaka, 1995; Tanaka, et al., 2014), showing that Valles Marineris has little effect on areas east of Coprates Chasma. The mesas show no preferred orientation of collapse, while the steep sides of the mesas are preferentially oriented towards the outflow channels. This preferred orientation of the steep sides is likely the result of erosion by flowing water. There is no current evidence of structural control on the outflow channels; if evidence existed is has been eroded away.

The Hydraspis crater pair also show no strong regional trend in the surrounding plateau. The chaos is however completely contained within two impact craters which could overprint any pre-existing regional trends. Any younger regional trends should be apparent. The mesas within the Hydraspis crater pair generally dip away from the crater rims, with the steep sides of the mesas having a weak trend towards the outflow channel.

Candor Chaos has strong regional trends being in the center of Valles Marineris. It is expected that the N/S trending wrinkle ridges or the E/W graben systems would

potentially have an effect on the collapse orientation. The mesas within Candor Chaos show a preferred dip towards the outflow channel into Melas Chasma, with a weak N/S trend for the steep sides of the mesas.

Baetis Chaos and the East Chaos north of Juventae Chasma have numerous N/S wrinkle ridges to the west in younger material and nothing to the east which is older (Tanaka, et al., 2014). Baetis Chaos shows no trend, while the East Chaos has a general SE trend away from its outflow channel. The steep sides of Baetis Chaos show no trend while the East Chaos has a NW/SE trend.

None of the chaotic terrains studied here show any strong evidence of regional control suggesting that the collapse of terrain is completely locally controlled. The steep sides of mesas tend to trend towards outflow channels which suggests that outflow of water towards these channels most likely eroded channels through the mesas, perhaps accelerated by sapping channel formation as water in the plateau moves downslope towards Chryse Planitia.

7.7 Role of the Global Ocean

The northern ocean model created by Citron et al. (2018) suggests a possible origin of water/ice for the generation of the chaotic terrains examined here. The interpreted Arabia shoreline (Citron, et al., 2018) indicates the possible extent of the early northern ocean reaching as far south as Hydraotes, and by close proximity the Hydraspis crater pair as well. The large lakes expected to have generated ILDs may have also come from this initial widespread presence of water either on the surface or in

the subsurface as groundwater reservoirs, giving possible sources of water for Juventae and Candor Chasma. It is expected that the majority of water on Mars is now locked up in the global cryosphere (Clifford, et al., 2010) and at the planet's polar caps, with little chance of significant reservoirs of deep groundwater below the cryosphere (Weiss & Head, 2017).

7.8 Global Cryosphere Relationship

The relationship between the global cryosphere and chaotic terrain has been examined by several authors (Chapman & Tanaka, 2002; Coleman, 2005; Andrews-Hanna & Phillips, 2007) who propose formation mechanisms which require a confined global aquifer system. This aquifer system is pressurized by surface loading or the downward movement of the cryosphere freezing front. Harrison & Grimm (2009) proposed that this aquifer system is compartmentalized locally instead of globally, which may explain why chaotic terrains form in specific areas and not all over Mars.

A study by Coleman (2005) investigated Aromatum Chaos and its outflow channel Ravi Valles. Coleman estimates that the global cryosphere is 700 – 1,000 m thick around Aromatum Chaos. The suggested mechanism to produce secondary chaotic terrains in Ravi Valles requires flooding to erode down through to the base of the cryosphere reaching the groundwater underneath the cryosphere causing it to breach through to the surface. This mechanism requires that flooding is waning in order to have less downward pressure on the groundwater. This formation mechanism also deviates from others (Rodríguez, et al., 2011) in that it is assumed that the formation of

the secondary chaos produces large enough floods to continue erosion down-slope where it excavates and triggers further secondary chaos.

7.9 Dark Competent Layer

Figure 7-1 shows examples of a dark competent layer which is a common feature present on the mesas and surrounding plateaus in all chaos zones studied here, with the exception of Candor Chaos which has no surrounding plateau. This feature is represented by a darker resistant layer just below the surface along the side walls of numerous mesas. A study by Beyer & McEwen (2005) suggests that this dark competent layer, shown in Figure 7-1 could be a flood basalt layer which they identified in Coprates and Capri Chasma which they expect are outcrops of flows covering a large area of Ophir and Aurorae Planum. The material above this layer may be less competent due to its lack of pore water/ice which has been lost by sublimation, or is simply less consolidated than the layers below. Table 7-5 shows the depth to the dark layer in each chaotic terrain. It is important to note that the surrounding plateaus of Hydraotes Chaos and the Hydraspis crater pair share the same elevation range. Baetis Chaos and the East Chaos have had their surrounding plateau eroded; however, the layer is present in the nearby plateau to the southwest, within Juventae Chasma. Candor Chaos shows no evidence of this dark layer in any nearby plateau. This dark layer is the same depth in the mesas as their respective plateaus, if this dark layer is a flood basalt layer similar to those investigated by Beyer & McEwen (2005) then it provides further evidence that the mesas were part of their surrounding plateau before collapsing.

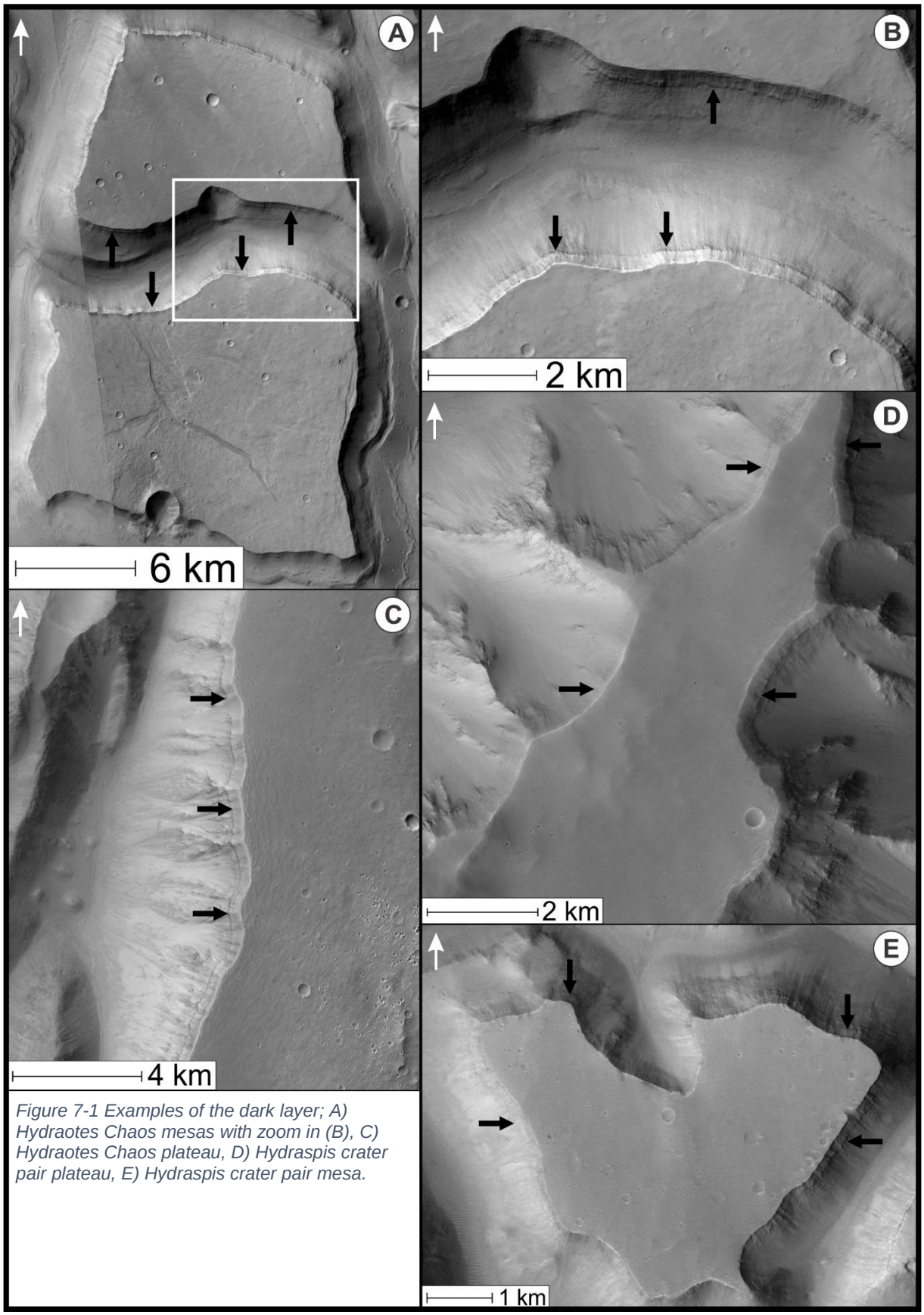

Figure 7-1 Examples of the dark layer; A) Hydraotes Chaos mesas with zoom in (B), C) Hydraotes Chaos plateau, D) Hydraspis crater pair plateau, E) Hydraspis crater pair mesa.

*Table 7-5 Accompanying measurements of depth to dark layer visible on mesa sides. Depth to the dark layer in the surrounding plateaus is within the same range. * Candor Chaos shows no dark layer on closest plateau walls.*

	Hydraotes Chaos	Hydraspis Crater Pair	Candor Chaos	Baetis & East Chaos
Depth to Dark Layer	150 – 200 m	200 – 250 m	25 – 50 m*	Ambiguous

7.10 Formation of Studied Chaotic Terrains

The formation of the chaotic terrains studied here, at the basic level requires the removal of subsurface material to produce mesas in a large depression. Some of these terrains are associated with large volumes of water being produced (Hydraotes & the Hydraspis crater pair) which require large localized reservoirs (ice sheets). Others did not produce large volumes of water (Candor, Baetis & East Chaos) and most likely had small or dispersed reservoirs (ice lenses) in the subsurface.

The formation mechanism for Hydraotes Chaos requires a pre-existing basin be partially filled with water/ice. Zegers et al. (2010) expect sedimentation rates of 1-10 mm/yr during the Noachian; however, filling of an Aram-sized basin (which is larger than Hydraotes Chaos) could still be achieved under lower rates of 0.01 mm/yr (Golombek & Bridges, 2000) over 200 Ma. This sediment covers the ice over millions of years until the thermal conductivity of the overburden becomes less that the basement triggering melting of the deepest parts of the ice. The melting triggers hydrofracturing of the overlying rock as pressures build. Runaway melting occurs as high-pressure water

reaches the surface and experiences a rapid drop in pressure from 30 MPa to 700 Pa (Zegers, et al., 2010), boiling the water.

Hydraotes Chaos closely matches the model parameters used by Zegers et al. (2010) for Aram Crater, which require 500 m – 1,500 m of sediment over top of a 2 km thick ice sheet to trigger melting without any external heat source.

The Hydraspis crater pair uses the same mechanism for collapse as Hydraotes Chaos but may require a difference source of heat to trigger melting. The Hydraspis crater pair is outside of the range of the Zegers et al. (2010) model parameters; requiring a thicker package of sediment to be deposited on top of the ice layer. Different environmental conditions from Hydraotes Chaos at the time of formation may also be possible; changes in surface heat flux, atmospheric pressure, or temperature, or different thermal properties of the overburden and basement. Another difference is that it is assumed that the initial 'basin' was a pair of impact craters but make no such assumption for Hydraotes Chaos. The central uplift in the crater pair may have caused the deepest area of ice to be present in a ring around the base of the peak, which would be the first place to experience melting as this area would be the most insulated from the surface. The overburden over this ring would collapse first, causing mechanical erosion on the overburden above the peak resulting in the rubble pile directly adjacent to the central peak.

Candor Chaos formed in an excavated basin following erosion from outflow, most likely from the opening of Candor Chasma into Melas Chasma. Ponded water/ice is buried by sediments over time. External heating melts the ice causing destabilization of the surface causing collapse. Low volumes of water generation are expected during

collapse. Candor Chaos does not conform to the Zegers et al. (2010) model parameters, therefore for subsurface melting to occur an external heat source is required.

Baetis Chaos and the East Chaos formed through the excavation of pre-existing areas of high concentrations of volatiles causing preferential erosion by outflow from Juventae Chasma. Multiple flooding events continue to erode material leaving behind the mesas which have low volatile concentrations (Rodríguez, et al., 2011). These two chaotic terrains also do not fit into the Zegers et al. (2010) model as the mesas are at or higher than the surrounding terrain, suggesting no collapse.

The major differences between the primary and secondary chaotic terrains is the scale of the collapse and the location of the collapse. Hydraotes Chaos and the Hydraspis crater pair have undergone significantly more collapse than the other chaotic terrains, which produced large enough volumes of water to erode the outflow channels leading from them. In the case of Hydraotes Chaos there is an assumption that flooding from the chaos produced some of the outflow channels, but evidence of this would have been overprinted by incoming flood waters from Valles Marineris. The secondary chaotic terrains of Candor Chaos, Baetis Chaos and the East Chaos, are present in outflow channels from external sources. Candor Chaos is inside the outflow channel which connects Ophir, Candor, and Melas Chasma together. Baetis and the East Chaos are inside the outflow channel between Juventae Chasma and Maja Valles. The erosion of these channels from external flood water is the trigger for the formation of these secondary chaotic terrains, while primary chaotic terrains are their own water source. An argument could be made that Hydraotes Chaos is inside an outflow channel with

external flood waters coming in causing erosion, however the size and shape of the chaos zone is many times greater than the channels leading into it, suggesting that the chaos formed independent of outside flooding.

7.11 Nature of Collapse

All chaotic terrains studied are expected to have collapsed except for Baetis/East Chaos which were produced by erosion, not collapse. The first evidence of possible collapse may be sapping channels which are early signs of water release from the subsurface. Sapping channels are formed through slope undercutting by release of groundwater. The largest volume of groundwater release is centered on the area/areas of deepest ice which melt first causing hydrofracturing to propagate from this starting location outwards as the ice melts. As larger blocks collapse, flexure in the surrounding plateau forces smaller blocks to break from the walls and collapse, the range of this effect is unknown, however in the Hydraspis crater pair it is stopped by the crater rims.

Hydraotes Chaos shows evidence of at least two distinct collapse events, with one major collapse responsible for most of the loss in elevation of the mesas, and the secondary collapse causing minimal collapse and little if any outflow. Candor Chaos shows possible zones of mesas which may indicate multiple collapse areas which have coalesced into a single larger zone. Baetis and the East Chaos have not undergone any collapse compared with their surroundings and instead the areas immediately adjacent to the mesas has been preferentially eroded by flooding.

7.12 The Role of Catastrophic Floods

Hydraotes Chaos covers a large area which has undergone major collapse and has at least two main outflow channels. Catastrophic flooding and erosion of the surface away from the chaos is expected to have occurred with the inflow of water from Valles Marineris aiding in the erosion of channels northwards, including Tiu and Simud Valles. This erosion is interrupted by periods of relative stability of the water depth to produce the terraces which surround many of the mesas in Hydraotes Chaos.

The northern rim of the Hydraspis crater pair has been breached by flooding and erosion produced by the collapse of the mesas within the crater pair. Flooding from this event also produced areas of secondary chaotic terrain northward along the outflow channel. Breaching of the northern rim of the crater led to the draining of the crater. Terrace formation may have occurred prior to the breaching of the northern crater rim but only in a small area in the southern portion.

Flooding is unlikely to have resulted from the collapse of Candor Chaos as very little collapse is expected to have occurred. The large outflow channels from Ophir and Candor Chasma towards Melas Chasma are most likely the result of lake draining following the linking of Valles Marineris, eroding a large portion of the ILDs (Komatsu, et al., 1993; Fueten, et al., 2014) of those chasmata, and not the result of flooding generated from subsurface ice melt.

Flooding from Juventae Chasma (Fueten, et al., 2017) produced Baetis and the East Chaos through erosion of volatiles in the subsurface. These volatiles could have been lenses of ice which would have added to flood waters. In the case of the East Chaos enough water was generated to produce an outflow channel northward. Baetis

Chaos may have also produced an outflow channel, but it has been overprinted by the draining of Juventae Chasma through Maja Valles.

7.13 Valles Marineris Link with Chaotic Terrain

Except for Baetis and the East Chaos, the chaotic terrains examined here are linked to Valles Marineris by other chasmata which eventually drain into Chryse Planitia. Draining of Valles Marineris would have had to pass through Hydraotes Chaos, and the Hydraspis crater pair drains into Tiu Valles, one of the outflow channels of Hydraotes Chaos. Candor Chaos is inside Valles Marineris proper, near the center. The chaotic terrains north of Juventae are not linked to Valles Marineris, however they do drain into the same basin. The majority of the chasmata east of Valles Marineris are filled with chaotic terrains, most of which are knobs with no large smooth-topped mesas.

7.14 Timing of Chaos Formation

Chaotic terrains are generally difficult to date directly due to the removal of material leading to a scarcity of impact craters. The chaotic terrains studied here may nevertheless be dated relative to one another. The oldest chaotic terrains are expected to be Hydraotes and the Hydraspis crater pair. It is assumed that Hydraotes Chaos had already formed prior to the linking of Valles Marineris and the subsequent floods which it generated. The formation of the Hydraspis crater pair and the collapse of the plateau north of it created a field of knobs in what is now Tiu Valles which have been eroded by

floods northward out of Hydraotes Chaos. This could mean that the Hydraspis crater pair is older than Hydraotes, or at least older than major floods north out of Hydraotes.

Table 7-6 compiles several important events in Martian geologic history including the possible timeframes when each of the four chaotic terrain regions formed. The first area to possibly be active is Tiu Valles, linked to Hydraspis. Pajola et al. (2016) place the activation of this channel north east of Hydraotes Chaos to be in the Middle Noachian. This is most likely before Hydraotes had formed as the activation is linked to outflow from Hydraspis (Pajola, et al., 2016), suggesting that the Hydraspis crater pair had formed or was in the process of forming. Activation of this channel may have affected the formation of Hydraotes Chaos, which likely formed some time after in the Late Noachian (Ori & Mosangini, 1998). The Hydraspis crater pair and Hydraotes Chaos would have formed in the period following the decline of the Arabia Ocean, before or during the early formation of the Deuteronilus Ocean, and during the accumulation of Tharsis. Opening and flooding from Hydraotes northward most likely occurred in the Early Hesperian (Tanaka, et al., 2014) following its formation. Major volcanic resurfacing of the planet was occurring during the end of the Noachian and start of the Hesperian (Carr & Head, 2010) which would have provided sedimentation to Hydraotes prior to its collapse.

Table 7-6 Table of major events on Mars, absolute age estimates and general age estimates of events. Proposed approximate formation of studied Chaotic Terrains in Chaotic Terrain column.

Absolute Ages		Relative Ages		Chaotic Terrain
Noachian				
4.55 Ga	Planet Formation (Carr & Head, 2010)	Early Noachian 4.55 Ga		
4.5-4.1 Ga	Dichotomy Formation (Carr & Head, 2010)			
4.0 Ga	Arabia Ocean Forms (Citron, et al., 2018)			
		Middle Noachian 3.93 Ga		
			Activation of Tiu Valles and Hydraspis Flooding (Pajola, et al., 2016)	Hydraspis Crater Pair
		Late Noachian 3.82 Ga		
			Hydraotes Forms (Upper Noachian) (Ori & Mosangini, 1998)	Hydraotes Chaos
			Valles Marineris Starts to Form (Carr & Head, 2010)	
Hesperian				
3.7 Ga	End of Heavy Bombardment (Carr & Head, 2010)	Early Hesperian 3.7 Ga	Major Volcanic Resurfacing (Carr & Head, 2010)	
3.7 Ga	Tharsis mostly Accumulated (Carr & Head, 2010)		Flooding north from Hydraotes (Tanaka, et al., 2014)	
			Candor Forms (Lucchitta, 1999)	
3.6 Ga	Deuteronilus Ocean Forms (Citron, et al., 2018)	Late Hesperian 3.6 Ga		
3.33 Ga	Juventae Forms (Gross, et al., 2009)		ILD in Candor Forms (Lucchitta, 1999)	
3.33 - 2.18 Ga	Maja Floods (Gross, et al., 2009)		Maja Floods (Coleman & Baker, 2007)	Baetis Chaos
3.3 - 3.2 Ga	Final Floods in Simud and Tiu Valles (Pajola, et al., 2016)			
3.3 - 3.0 Ga	ICC Stabilizes (Weiss & Head, 2017)		Valles Marineris Mostly Complete (Carr & Head, 2010)	
3.1 Ga	Draining of Capri-Eos Lake into Aurorae (Warner, et al., 2013)		Candor Drains (Lucchitta, 1999; Fueten, et al., 2014)	Candor Chaos
Amazonian				
3.0 Ga		Early Amazonian 3.0 Ga		
2.5 Ga	Aram Crater Floods into Ares Valles (Warner, et al., 2009)			

Flooding of Maja Valles occurred between 3.33 – 2.18 Ga (Gross, et al., 2009) most likely in the Late Hesperian (Coleman & Baker, 2007), suggesting that Juventae Chasma had already formed and was releasing flood waters north, carving out Baetis Chaos and the East Chaos. The linking of Valles Marineris likely occurred by the end of the Late Hesperian (Carr & Head, 2010) while the draining of the Capri-Eos lake into Aurorae Chaos was also occurring around 3.1 Ga (Warner, et al., 2013). It is likely that Candor Chasma was also linked by this time (Lucchittas, 1999; Fueten, et al., 2014) allowing much of Valles Marineris to flush through into Capri-Eos and then into Aurorae. The final and possibly largest floods of Simud and Tiu Valles north of Hydraotes Chaos have been dated to 3.3 – 3.2 Ga (Pajola, et al., 2016), placing it very close to the possible timing of the linking and draining of Valles Marineris. The linking and draining of the lake in Candor Chasma would produce Candor Chaos sometime by the end of the Hesperian.

The formation of the chaotic terrains studied here are spread over a period of nearly a billion years of Martian history (Middle Noachian to the end of the Late Hesperian). The Hydraspis crater pair and Hydraotes Chaos had most likely formed before or during the early stages of formation of Valles Marineris in the Noachian, while Baetis and Candor Chaos most likely formed by the time that Valles Marineris was mostly complete in the Late Hesperian. Formation of these chaotic terrains and the lakes/floods associated with them shows that water was available and stable on the surface at least episodically from the Noachian to the beginning of the Amazonian in the region around Valles Marineris.

7.15 Conclusions

The formation mechanisms for both primary and secondary chaotic terrains suggested here require substantial volumes of water/ice in the subsurface. According to Citron et al. (2018), the estimated southern reaches of the early Northern Ocean would have reached Hydraotes Chaos and the Hydraspis crater pair, filling any pre-existing basins, or filling craters in a water-rich environment. This event would produce high volume, localized water sources, which also coincides with the formation of primary chaotic terrains. The secondary chaotic terrains of Candor, Baetis, and the East Chaos, are removed from the estimated reaches of the northern ocean (Citron, et al., 2018). The estimated lake volume required to produce the large ILD mounds of Ophir and Candor Chasma would provide the required subsurface water for Candor Chaos to form. Baetis and the East Chaos require disseminated water in the subsurface, with pockets of high and low concentrations. Areas of high concentration were eroded by flooding, and areas of low concentration produced the mesas.

The chaotic terrains studied here vary in location, size, and volume of flooding produced; however, several general statement about these chaotic terrains can be made. Our findings demonstrate that: 1) Chaotic terrains require a large isolated volume of subsurface water/ice to form, 2) The largest chaotic terrains do not require external sources of heating to trigger melting, 3) Water within the cryosphere is likely heterogeneously distributed, in agreement with the conclusions of Harrison & Grimm (2009), and is related to the position of ancient basins/craters and oceans, 4) Collapse of chaotic terrain is not regionally controlled and there is little evidence that collapse occurs strongly in any direction, 5) Chaotic terrains are not the sole source of flooding

for the excavation of the larger outflow channels, 6) The chaotic terrains studied here did not form at the same time; it is likely that there are several periods of chaos formation spanning the history of Mars.

7.16 Limitations & Future Research

Resolution of imagery for individual chaotic terrains varied from 20 m/pixel to 50 m/pixel, with a small proportion of 75+ m/pixel. The biggest limitation for this study was areas with no DEM coverage. The Hydraspis crater pair and the Juventae Chasma northern channel have no accurate DEM coverage, being covered only by interpolated MOLA data which completely smooths any topography that could be there. Filling these gaps with CTX DEM would be ideal, and would allow for measurements of width, depth, and volume of the spillway between Juventae Chasma and Baetis Chaos. Better coverage of the southwestern mesas in the Hydraspis crater pair would give more accurate orientation measurements, but this would most likely not have a significant impact on the data shown here. CTX DEM coverage of Hydraotes Chaos and the Hydraspis crater pair would require 20 m/pixel resolution instead of the current 50 m/pixel (comparison can be made between Candor Chaos and Hydraotes Chaos DEMs) giving more accurate data but also the possibility of layer measurements within the terraces. HiRise data coverage of terraces and mesa sides would be ideal for measuring layering, and may tell us more about the environment the terraces formed in; were water levels stable, did they fluctuate, is there evidence of cyclicity?

The inclusion of CRISM data may be useful in future research if there are changes in mineralogy within and between chaotic terrains. Some chaos (Hydraotes

Chaos) contain remnants of plateau surfaces, while others do not (Candor Chaos). Is this reflected in the mineralogy? ILDs are also present in some chaotic terrains (Candor Chaos, the Hydraspis crater pair) which have a different suite of mineralogy than chaos. It would also be interesting to see if the terraces have a different mineralogy from the mesa tops.

Future studies should also include chaotic terrains outside the Circum-Chryse Basin area to see if the formation models used here are applicable across Mars or are localized. Continued comparison of the different types of chaotic terrains (Primary, Secondary, and FFCs) is definitely recommended to get a full picture of chaotic terrain on Mars.

References

Andrews-Hanna, J. C., & Phillips, R. J. (2007). Hydrological modeling of outflow channels and chaos regions on Mars. *JGR, 112*(E08001). doi:10.1029/2006JE002881

Beyer, R. A., & McEwen, A. S. (2005). Layering stratigraphy of eastern Coprates and northern Capri Chasmata, Mars. *Icarus, 179*, 1-23. doi:10.1016/j.icarus.2005.06.014

Carr, M. H., & Head, J. W. (2010). Geologic history of Mars. *Earth and Planetary Science Letters, 294*, 185-203. doi:10.1016/j.epsl.2009.06.042

Carr, M. H., Wu, S. S., Jordan, R., & Schafer, F. J. (1987). Volumes of Channels, Canyons and Chaos in the Circum-Chryse Region of Mars. *Lunar and Planetary Science Conference*, *XVIII*, p. 155.

Catling, D. C., Wood, S. E., Leovy, C., Montgomery, D. R., Greenberg, H. M., Glein, C. R., & Moore, J. M. (2006). Light-toned layered deposits in Juventae Chasma, Mars. *Icarus, 181*, 26-51. doi:10.1016/j.icarus.2005.10.020

Chapman, M. G., & Tanaka, K. L. (2002). Related Magma–Ice Interactions: Possible Origins of Chasmata, Chaos, and Surface Materials in Xanthe, Margaritifer, and Meridiani Terrae, Mars. *Icarus, 155*, 324-339.

Chapman, M. G., Hare, T. M., Russell, A. J., & Gudmundsson, M. T. (2003). Possible Juventae Chasma subice volcanic eruptions and Maja Valles ice outburst floods on Mars: Implications of Mars Global Surveyor crater densities, geomorphology, and topography. *J. Geophys. Res., 108*(E10), 5113. doi:10.1029/2002JE002009

Citron, R. I., Manga, M., & Hemingway, D. J. (2018). Timing of oceans on Mars from shoreline deformation. *Nature, 555*. doi:10.1038/nature26144

Clifford, S. M., Lasue, J., Heggy, E., Boisson, J., McGovern, P., & Max, M. D. (2010). Depth of the martian cryosphere: revised estimates and implications for the existence and detection of subpermafrost groundwater. *J. Geophys. Res., 115*(E7). doi:10.1029/2009JE003462

Coleman, N. M. (2003). Aqueous flows carved the outflow channels on Mars. *J. Geophys. Res., 108*(E5), 5039. doi:10.1029/2002JE001940

Coleman, N. M. (2005). Martian megaflood triggered chaos formation, revealing groundwater depth, cryosphere thickness, and crustal heat flux. *JGR, 110*, E12S20. doi:10.1029/2005JE002419

Coleman, N., & Baker, V. (2007). Evidence that a Paleolake Overflowed the Rim of Juventae Chasma, Mars. *Lunar and Planetary Science XXXVIII*.

Fueten, F., Flahaut, J., Stesky, R., Hauber, E., & Rossi, A. P. (2014). Stratigraphy and mineralogy of Candor Mensa, West Candor Chasma, Mars: Insights into the geologic history of Valles Marineris. *J. Geophys. Res. Planets*(119), 331-354. doi:10.1002/2013JE004557

Fueten, F., Novakovic, N., Stesky, R., Flahaut, J., Hauber, E., & Rossi, A. P. (2017). The Evolution of Juventae Chasma, Valles Marineris, Mars: Progressive Collapse and

Sedimentation. *Journal of Geophysical Research: Planets*(122), 2223-2249. doi:10.1002/2017JE005334

Golombek, M. P., & Bridges, N. T. (2000). Erosion rates on Mars and implications for climate change: Constraints from the Pathfinder landing site. *Journal of Geophysical Research, 105*(E1), 1841-1853. doi:10.1029/1999JE001043

Gross, C., Wendt, L., Dumke, A., & Neukum, G. (2009). Further Evidence for Multiple Flooding Events at Juventae Chasma and Maja Valles, Mars. *40th Lunar and Planetary Science Conference.*

Harrison, K. P., & Chapman, M. G. (2008). Evidence for ponding and catastrophic floods in central Valles Marineris, Mars. *Icarus, 198*, 351-364. doi:10.1016/j.icarus.2008.08.003

Harrison, K. P., & Grimm, R. E. (2008). Multiple flooding events in Martian outflow channels. *JGR, 113*, E02002. doi:10.1029/2007JE002951

Harrison, K. P., & Grimm, R. E. (2009). Regionally compartmented groundwater flow on Mars. *Journal of Geophysical Research, 114*(E4). doi:10.1029/2008JE003300

Hauber, E., Brož, P., Rossi, A. P., & Michael, G. (2015). A Field of Small Pitted Cones on the Floor of Coprates Chasma Mars: Volcanism Inside Valles Marineris? *46th Lunar and Planetary Science Conference.*

Komatsu, G., Geissler, P. E., Strom, R. G., & Singer, R. B. (1993). Stratigraphy and erosional landforms of layered deposits in Valles Marineris, Mars. *J. Geophys. Res., 98*(E6), 11,105-11,121.

Komatsu, G., Kargel, J. S., Baker, V. R., Strom, R. G., Ori, G. G., Mosangini, C., & Tanaka, K. L. (2000). A chaotic terrain formation hypothesis: Explosive outgas and outflow by dissociation of clathrate on Mars. *Lunar Planet. Sci. Conf. XXXI.* abstract 1434.

Leask, H. J., Wilson, L., & Mitchell, K. L. (2006). Formation of Aromatum Chaos, Mars: Morphological development as a result of volcano-ice interactions. *JGR, 111*(E08071). doi:10.1029/2005JE002549

Lucchitta, B. K. (1999). Geologic map of Ophir and central Candor Chasmata (MTM -05072) of Mars. *U.S. Geological Survey Geologic Investigations Series I-2568*. Retrieved from https://pubs.usgs.gov/imap/i2568/

Meresse, S., Costard, F., Mangold, N., Masson, P., & Neukum, G. (2008). Formation and evolution of the chaotic terrains by subsidence and magmatism: Hydraotes Chaos, Mars. *Icarus, 194*, 487-500. doi:10.1016/j.icarus.2007.10.023

Ori, G. G., & Mosangini, C. (1998). Complex depositional systems in Hydraotes Chaos, Mars' An example of sedimentary process interactions in the Martian hydrological cycle. *JGR, 103*(E10), 22,713-22,723.

Pajola, M., Rossato, S., Baratti, E., Mangili, C., Mancarella, F., McBride, K., & Coradini, M. (2016). The Simud–Tiu Valles hydrologic system: A multidisciplinary study of a possible site for future Mars on-site exploration. *Icarus, 268*, 355-381. doi:10.1016/j.icarus.2015.12.049

Roda, M., Kleinhans, M. G., Zegers, T. E., & Oosthoek, J. H. (2014). Catastrophic ice lake collapse in Aram Chaos, Mars. *Icarus, 236*, 104-121. doi:http://dx.doi.org/10.1016/j.icarus.2014.03.023

Rodríguez, J. A., Kargel, J. S., Tanaka, K. L., Crown, D. A., Berman, D. C., Fairén, A. G., . . . Sasaki, S. (2011). Secondary chaotic terrain formation in the higher outflow channels of southern circum-Chryse, Mars. *Icarus, 213*, 150-194. doi:10.1016/j.icarus.2010.09.027

Rodriguez, J. A., Kargel, J., Crown, D. A., Bleamaster III, L. F., Tanaka, K. L., Baker, V., . . . Komatsu, G. (2006). Headward growth of chasmata by volatile outbursts, collapse, and drainage: Evidence from Ganges chaos, Mars. *Geophysical Research Letters, 33*(L18203). doi:10.1029/2006GL026275

Rotto, S., & Tanaka, K. L. (1995). *Geologic/geomorphic map of the Chryse Planitia region of Mars.* USGS. doi:10.3133/i2441

Tanaka, K., Skinner, J. A., Dohm, J., Irwin, R. I., Kolb, E., Fortezzo, C., . . . Hare, T. (2014). Geologic map of Mars: U.S. Geological Survey Scientific Investigations Map 3292. *scale 1:20,000,000, pamphlet 43 p.* doi:https://dx.doi.org/10.3133/sim3292

Wang, C., Manga, M., & Hanna, J. C. (2006). Can freezing cause floods on Mars? *Geophysical Research Letters, 33*(L20202). doi:10.1029/2006GL027471

Warner, N. H., Sowe, M., Gupta, S., Dumke, A., & Goddard, K. (2013). Fill and spill of giant lakes in the eastern Valles Marineris region of Mars. *Geology, 41*, 675-678. doi:10.1130/G34172.1

Warner, N., Gupta, S., Muller, J., Kim, J., & Lin, S. (2009). A refined chronology of catastrophic outflow events in Ares Vallis, Mars. *Earth and Planetary Science Letters, 288*, 58-69. doi:10.1016/j.epsl.2009.09.008

Weiss, D. K., & Head, J. W. (2017). Evidence for stabilization of the ice-cemented cryosphere in earlier martian history: Implications for the current abundance of groundwater at depth on Mars. *Icarus*(288), 120-147. doi:10.1016/j.icarus.2017.01.018

Zegers, T. E., & Roda, M. (2012). Chaotic Terrains on Mars: testing the subsurface lake hypothesis. *Rend. online Soc. Geol. It., 22*, 243-246.

Zegers, T. E., Oosthoek, J. H., Rossi, A. P., Blom, J. K., & Schumacher, S. (2010). Melt and collapse of buried water ice: An alternative hypothesis for the formation of chaotic terrains on Mars. *Earth and Planetary Science Letters, 297*, 496-504. doi:10.1016/j.epsl.2010.06.049

Appendix 1 – Complete List of Reference

Anderson, R. C., Dohm, J. M., Golombek, M. P., Haldemann, A. F., Franklin, B. J., Tanaka, K. L., . . . Peer, B. (2001). Primary centers and secondary concentrations of tectonic activity through time in the western hemisphere of Mars. *JGR, 106*(E9), 20,563-20,585.

Andrews-Hanna, J. C., & Phillips, R. J. (2007). Hydrological modeling of outflow channels and chaos regions on Mars. *JGR, 112*(E08001). doi:10.1029/2006JE002881

Andrews-Hanna, J. C., Zuber, M. T., & Banerdt, W. B. (2008). The Borealis basin and the origin of the martian crustal dichotomy. *Nature, 453*(7199), 1212-1216.

Baker, V. R., Hamilton, C. W., Burr, D. M., Gulick, V. C., Komatsu, G., Luo, W., . . . Rodriguez, J. A. (2015). Fluvial geomorphology on Earth-like planetary surfaces: A review. *245*, 149-182. doi:10.1016/j.geomorph.2015.05.002

Bamberg, M., Jaumann, R., Asche, H., Kneissl, T., & Michael, G. G. (2014). Floor-Fractures Craters on Mars - Observations and Origin. *Planetary and Space Science, 98*, 146-162.

Beyer, R. A., & McEwen, A. S. (2005). Layering stratigraphy of eastern Coprates and northern Capri Chasmata, Mars. *Icarus, 179*, 1-23. doi:10.1016/j.icarus.2005.06.014

Beyer, R. A., Alexandrov, O., & McMichael, S. (2018). The Ames Stereo Pipeline: NASA's open source software for deriving and processing terrain data. *Earth and Space Science, 5*. doi:10.1029/2018EA000409

Brož, P., Čadek, O., Hauber, E., & Rossi, A. P. (2015). Scoria cones on Mars: Detailed investigation of morphometry based on high-resolution digital elevation models. *JGR: Planets, 120*, 1,512-1,527. doi:10.1002/2015JE004873

Carr, M. H., & Head, J. W. (2003). Oceans on Mars: An assessment of the observational evidence and possible fate. *Journal of Geophysical Research: Planets, 108*(E5).

Carr, M. H., & Head, J. W. (2010). Geologic history of Mars. *Earth and Planetary Science Letters, 294*, 185-203. doi:10.1016/j.epsl.2009.06.042

Carr, M. H., Wu, S. S., Jordan, R., & Schafer, F. J. (1987). Volumes of Channels, Canyons and Chaos in the Circum-Chryse Region of Mars. *Lunar and Planetary Science Conference*, *XVIII*, p. 155.

Catling, D. C. (2009). Atmospheric evolution, Mars. *Encyclopedia of Paleoclimatology and Ancient Environments*, 66-75.

Catling, D. C., Wood, S. E., Leovy, C., Montgomery, D. R., Greenberg, H. M., Glein, C. R., & Moore, J. M. (2006). Light-toned layered deposits in Juventae Chasma, Mars. *Icarus, 181*, 26-51. doi:10.1016/j.icarus.2005.10.020

Chapman, M. G., & Tanaka, K. L. (2002). Related Magma–Ice Interactions: Possible Origins of Chasmata, Chaos, and Surface Materials in Xanthe, Margaritifer, and Meridiani Terrae, Mars. *Icarus, 155*, 324-339.

Chapman, M. G., Hare, T. M., Russell, A. J., & Gudmundsson, M. T. (2003). Possible Juventae Chasma subice volcanic eruptions and Maja Valles ice outburst floods on Mars: Implications of Mars Global Surveyor crater densities, geomorphology, and topography. *J. Geophys. Res., 108*(E10), 5113. doi:10.1029/2002JE002009

Citron, R. I., Manga, M., & Hemingway, D. J. (2018). Timing of oceans on Mars from shoreline deformation. *Nature, 555*. doi:10.1038/nature26144

Clifford, S. M., & Parker, T. J. (2001). The Evolution of the Martian Hydrosphere: Implications for the Fate of a Primordial Ocean and the Current State of the Northern Plains. *Icarus, 154*, 40-79. doi:10.1006/icar.2001.6671

Clifford, S. M., Lasue, J., Heggy, E., Boisson, J., McGovern, P., & Max, M. D. (2010). Depth of the martian cryosphere: revised estimates and implications for the existence and detection of subpermafrost groundwater. *J. Geophys. Res., 115*(E7). doi:10.1029/2009JE003462

Coleman, N. M. (2003). Aqueous flows carved the outflow channels on Mars. *J. Geophys. Res., 108*(E5), 5039. doi:10.1029/2002JE001940

Coleman, N. M. (2005). Martian megaflood triggered chaos formation, revealing groundwater depth, cryosphere thickness, and crustal heat flux. *JGR, 110*, E12S20. doi:10.1029/2005JE002419

Coleman, N. M., & Baker, V. R. (2009). Surface morphology and origin of outflow channels in Valles Marineris region. In D. M. Burr, P. A. Carling, & V. R. Baker (Eds.), *Megaflooding on Earth and Mars* (pp. 182-184). Cambridge University Press.

Coleman, N., & Baker, V. (2007). Evidence that a Paleolake Overflowed the Rim of Juventae Chasma, Mars. *Lunar and Planetary Science XXXVIII*.

Craddock, R. A., & Howard, A. D. (2002). The case for rainfall on a warm, wet early Mars. *JGR, 107*(E11), 5111. doi:10.1029/2001JE001505

Fanale, F. P., Postawko, S. E., Pollack, J. B., Carr, M. H., & Pepin, R. O. (1992). Mars: Epochal Climate Cahnge and Volatile History. In H. H. Kieffer, B. M. Jakosky, C. W. Snyder, & M. S. Matthews (Eds.), *Mars* (pp. 1135-1179). The University of Arizona Press.

Frey, H. V. (2006). Impact constraints on, and a chronology for, major events in early Mars history. *Journal of Geophysical Research: Planets, 111*(E8).

Fueten, F., Flahaut, J., Stesky, R., Hauber, E., & Rossi, A. P. (2014). Stratigraphy and mineralogy of Candor Mensa, West Candor Chasma, Mars: Insights into the geologic history of Valles Marineris. *J. Geophys. Res. Planets*(119), 331-354. doi:10.1002/2013JE004557

Fueten, F., Novakovic, N., Stesky, R., Flahaut, J., Hauber, E., & Rossi, A. P. (2017). The Evolution of Juventae Chasma, Valles Marineris, Mars: Progressive Collapse and Sedimentation. *Journal of Geophysical Research: Planets*(122), 2223-2249. doi:10.1002/2017JE005334

Gendrin, A., Mangold, N., Bibring, J., Langevin, Y., Gondet, B., Poulet, F., . . . LeMouélic, S. (2005). Sulfates in Martian Layered Terrains: The OMEGA/Mars Express View. *Science, 307*(5715), 1587-1591. doi:10.1126/science.1109087

Glotch, T. D., & Rogers, A. D. (2007). Evidence for aqueous deposition of hematite- and sulfate-rich light-toned layered deposits in Aureum and Iani Chaos, Mars. *Journal of Geophysical Research, 112*. doi:10.1029/2006JE002863

Golombek, M. P., & Bridges, N. T. (2000). Erosion rates on Mars and implications for climate change: Constraints from the Pathfinder landing site. *Journal of Geophysical Research, 105*(E1), 1841-1853. doi:10.1029/1999JE001043

Gourronc, M., Bourgeois, O., Mège, D., Pochat, S., Bultel, .. B., Massé, M., . . . Mercier, D. (2014). One million cubic kilometers of fossil ice in Valles Marineris: Relicts of a 3.5 Gy old glacial landsystem along the Martian equator. *Geomorphology, 204*, 235-255. doi:10.1016/j.geomorph.2013.08.009

Greeley, R., Kuzmin, R. O., Nelson, D. M., & Farmer, J. D. (2003). Eos Chasma, Mars: Regional setting for a potential landing site for astrobiology. *J. Geophys. Res., 108*(E12), 8083. doi:10.1029/2002JE002014

Greenberg, R., Hoppa, G., Tufts, B., Geissler, P., Riley, J., & Kadel, S. (1999). Chaos on Europa. *Icarus, 141*(2), 263-286.

Gross, C., Wendt, L., Dumke, A., & Neukum, G. (2009). Further Evidence for Multiple Flooding Events at Juventae Chasma and Maja Valles, Mars. *40th Lunar and Planetary Science Conference.*

Harrison, K. P., & Chapman, M. G. (2008). Evidence for ponding and catastrophic floods in central Valles Marineris, Mars. *Icarus, 198*, 351-364. doi:10.1016/j.icarus.2008.08.003

Harrison, K. P., & Grimm, R. E. (2008). Multiple flooding events in Martian outflow channels. *JGR, 113*, E02002. doi:10.1029/2007JE002951

Harrison, K. P., & Grimm, R. E. (2009). Regionally compartmented groundwater flow on Mars. *Journal of Geophysical Research, 114*(E4). doi:10.1029/2008JE003300

Hauber, E., Brož, P., Rossi, A. P., & Michael, G. (2015). A Field of Small Pitted Cones on the Floor of Coprates Chasma Mars: Volcanism Inside Valles Marineris? *46th Lunar and Planetary Science Conference.*

Head, J. W., Hiesinger, H., Ivanov, M. A., Kreslavsky, M. A., Pratt, S., & Thomson, B. J. (1999). Possible ancient oceans on Mars: evidence from Mars Orbiter Laser Altimeter data. *Science, 286*(5447), 2134-2137.

Jaumann, R., Neukum, G., Behnke, T., Duxbury, T., Eichentopf, K., Flohrer, J., . . . Hoffmann, H. (2007). The high-resolution stereo camera (HRSC) experiment on Mars Express: Instrument aspects and experiment conduct from interplanetary cruise through the nominal mission. *Planetary and Space Science, 55*(7-8), 928-952. doi:10.1016/j.pss.2006.12.003

Komatsu, G., Geissler, P. E., Strom, R. G., & Singer, R. B. (1993). Stratigraphy and erosional landforms of layered deposits in Valles Marineris, Mars. *J. Geophys. Res., 98*(E6), 11,105-11,121.

Komatsu, G., Kargel, J. S., Baker, V. R., Strom, R. G., Ori, G. G., Mosangini, C., & Tanaka, K. L. (2000). A chaotic terrain formation hypothesis: Explosive outgas and outflow by dissociation of clathrate on Mars. *Lunar Planet. Sci. Conf. XXXI.* abstract 1434.

Korteniemi, J., Aittola, M., Öhman, T., & Raitala, J. (2006). Floor-Fractured Craters on the Terrestrial Planets – The Martian Perspective. *Proceedings of the First International Conference on Impact Cratering in the Solar System, Eur. Space Agency Spec. Publ., SP-612*.

Leask, H. J., Wilson, L., & Mitchell, K. L. (2006). Formation of Aromatum Chaos, Mars: Morphological development as a result of volcano-ice interactions. *JGR, 111*(E08071). doi:10.1029/2005JE002549

Lucchitta, B. K. (1999). Geologic map of Ophir and central Candor Chasmata (MTM -05072) of Mars. *U.S. Geological Survey Geologic Investigations Series I-2568*. Retrieved from https://pubs.usgs.gov/imap/i2568/

Lucchitta, B. K., & Ferguson, H. M. (1983). Chryse Basin Channels: Low-Gradient and Ponded Flows. *Journal of Geophysical Research, 2(15)*, 553-568.

Lucchitta, B. K., & Ferguson, H. M. (1983). Chryse Basin channels: Low-gradients and ponded flows. *Journal of Geophysical Research: Solid Earth, 88*(S02), A553-A568. doi:10.1029/JB088iS02p0A553

Manker, J. P., & Johnson, A. P. (1982). Simulation of Martian Chaotic Terrain and Outflow Channels. *Icarus, 51*, 121-132.

Marinova, M. M., Aharonson, O., & Asphaug, E. (2008). Mega-impact formation of the Mars hemispheric dichotomy. *Nature, 453*(7199), 1216-1219.

Marra, W. A., Braat, L., Baar, A. W., & Kleinhans, M. G. (2014). Valley formation by groundwater seepage, pressurized groundwater outbursts and crater-lake overflow in flume experiments with implications for Mars. *Icarus, 232*, 97-117. doi:10.1016/j.icarus.2013.12.026

Melosh, H. J., & Vickery, A. M. (1989). Impact erosion of the primordial atmosphere of Mars. *Nature, 338*, 487-489.

Meresse, S., Costard, F., Mangold, N., Masson, P., & Neukum, G. (2008). Formation and evolution of the chaotic terrains by subsidence and magmatism: Hydraotes Chaos, Mars. *Icarus, 194*, 487-500. doi:10.1016/j.icarus.2007.10.023

Minin, M. (2015). Quantification and Extraction of Surface Features from Digital Terrain Models (Masters Thesis). Retrieved from http://dr.library.brocku.ca/handle/10464/7893

Ori, G. G., & Mosangini, C. (1998). Complex depositional systems in Hydraotes Chaos, Mars' An example of sedimentary process interactions in the Martian hydrological cycle. *JGR, 103*(E10), 22,713-22,723.

Pajola, M., Rossato, S., Baratti, E., Mangili, C., Mancarella, F., McBride, K., & Coradini, M. (2016). The Simud–Tiu Valles hydrologic system: A multidisciplinary study of a possible site for future Mars on-site exploration. *Icarus, 268*, 355-381. doi:10.1016/j.icarus.2015.12.049

Palumbo, A. M., Head, J. W., & Wordsworth, R. D. (2018). Late Noachian Icy Highlands climate model: Exploring the possibility of transient melting and fluvial/lacustrine activity through peak annual and seasonal temperatures. *Icarus, 300*, 261-286. doi:10.1016/j.icarus.2017.09.007

Parker, T. J., Gorsline, D. S., Saunders, R. S., Pieri, D. C., & Schneeberger, D. M. (1993). Coastal geomorphology of the Martian northern plains. *Journal of Geophysical Research: Planets, 98*(E6), 11061-11078.

Petroff, A. P., Devauchelle, O., Abrams, D. M., Lobkovsky, A. E., Kudrolli, A., & Rothman, D. H. (2011). Geometry of valley growth. *Journal of Fluid Mechanics, 673*, 245-254. doi:10.1017/S002211201100053X

Phillips, R. J., Zuber, M. T., Solomon, S. C., Golombek, M. P., Jakosky, B. M., Banerdt, W. B., . . . Hauck II, S. A. (2001). Ancient geodynamics and global-scale hydrology on Mars. *Science, 291*(5513), 2587-2591. doi:10.1126/science.1058701

Robbins, S. J., & Hynek, B. M. (2012). A new global database of Mars impact craters ≥1 km: 2. Global crater properties and regional variations of the simple-to-complex transition diameter. *Journal of Geophysical Research, 117*. doi:10.1029/2011JE003967

Roberts, J. H., & Zhong, S. (2006). Degree-1 convection in the Martian mantle and the origin of the hemispheric dichotomy. *Journal of Geophysical Research, 111*. doi:10.1029/2005JE002668

Roda, M., Kleinhans, M. G., Zegers, T. E., & Govers, R. (2016). Origin of circular collapsed landforms in the Chryse region of Mars. *Icarus, 265*, 70-78. doi:http://dx.doi.org/10.1016/j.icarus.2015.10.020

Roda, M., Kleinhans, M. G., Zegers, T. E., & Oosthoek, J. H. (2014). Catastrophic ice lake collapse in Aram Chaos, Mars. *Icarus, 236*, 104-121. doi:http://dx.doi.org/10.1016/j.icarus.2014.03.023

Rodriguez, J. A., Kargel, J. S., Baker, V. R., Gulick, V. C., Berman, D. C., Fairén, A. G., . . . Glines, N. (2015). Martian outflow channels: How did their source aquifers form, and why did they drain so rapidly? *Scientific Reports, 5*, 13404.

Rodríguez, J. A., Kargel, J. S., Tanaka, K. L., Crown, D. A., Berman, D. C., Fairén, A. G., . . . Sasaki, S. (2011). Secondary chaotic terrain formation in the higher outflow channels of southern circum-Chryse, Mars. *Icarus, 213*, 150-194. doi:10.1016/j.icarus.2010.09.027

Rodriguez, J. A., Kargel, J., Crown, D. A., Bleamaster III, L. F., Tanaka, K. L., Baker, V., . . . Komatsu, G. (2006). Headward growth of chasmata by volatile outbursts, collapse, and drainage: Evidence from Ganges chaos, Mars. *Geophysical Research Letters, 33*(L18203). doi:10.1029/2006GL026275

Rodriguez, J. A., Platz, T., Gulick, V., Baker, V. R., Fairén, A. G., J., K., . . . Glines, N. (2015). Did the martian outflow channels mostly form during the Amazonian Period? *Icarus, 257*, 387-395. doi:10.1016/j.icarus.2015.04.024

Rodriguez, J. A., Sasaki, S., Kuzmin, R. O., Dohm, J. M., Tanaka, K. L., Miyamoto, H., . . . Ferris, J. C. (2005). Outflow channel sources, reactivation, and chaos formation, Xanthe Terra, Mars. *Icarus, 175*, 36-57. doi:10.1016/j.icarus.2004.10.025

Rotto, S., & Tanaka, K. L. (1995). *Geologic/geomorphic map of the Chryse Planitia region of Mars.* USGS. doi:10.3133/i2441

Sato, H., Kurita, K., & Baratoux, D. (2010). The formation of floor-fractured craters in Xanthe Terra. *Icarus, 207*, 248-264. doi:10.1016/j.icarus.2009.10.023

Schmidt, G. (2015). Geology of Hebes Chasma, Valles Marineris, Mars (Masters Thesis). Retrieved from http://dr.library.brocku.ca/handle/10464/7326

Schmidt, G., Fueten, F., Stesky, R., Flahaut, J., & Hauber, E. (2018). Geology of Hebes Chasma, Mars: 1. Structure, Stratigraphy, and Mineralogy of the Interior Layered Deposits. *Journal of Geophysical Research: Planets, 123*, 2893-2919. doi:10.1029/2018JE005658

Schultz, P. H., & Gault, D. E. (1975). Seismic effects from major basin formations on the Moon and Mercury. *The Moon, 12*(2), 159-177.

Schultz, R. A. (1998). Multiple-process origin of Valles Marineris basins and troughs, Mars. *Planet. Space Sci., 46*, 827-829. doi:10.1016/S00320633(98)00030-0

Sharp, R. P., & Malin, M. C. (1975). Channels on Mars. *Geological Society of America Bulletin, 86*(5), 593-609. doi:10.1130/0016-7606(1975)86<593:COM>2.0.CO;2

Sharp, R. P., Soderblom, L. A., Murray, B. C., & Cutts, J. A. (1971). The Surface of Mars: Uncratered Terrains. *JGR, 76*(2).

Smith, D., Zuber, M., Frey, H., Garvin, J., Head, J., Muhleman, D., . . . Banerdt, W. (2001). Mars Orbiter Laser Altimeter: Experiment summary after the first year of global mapping of Mars. *Journal of Geophysical Research: Planets, 106*(E10), 23689-23722. doi:10.1029/2000JE001364

Tanaka, K. L., & Hartmann, W. K. (2012). The Planetary Time Scale. In F. M. Gradstein, J. G. Ogg, M. Schmitz, & G. Ogg, *The Geologic Time Scale* (pp. 275-298). Elsevier.

Tanaka, K. L., Isbell, N. K., Scott, D. H., Greeley, R., & Guest, J. E. (1988). The resurfacing history of Mars-A synthesis of digitized, viking-based geology. *Lunar and Planetary Science Conference Proceedings*, *18*, pp. 665-678.

Tanaka, K. L., Scott, D. H., & Greeley, R. (1992). Global Stratigraphy. In H. H. Kieffer, B. M. Jakosky, C. W. Snyder, & M. S. Matthews (Eds.), *Mars* (pp. 345-382). The University of Arizona Press.

Tanaka, K., Skinner, J. A., Dohm, J., Irwin, R. I., Kolb, E., Fortezzo, C., . . . Hare, T. (2014). Geologic map of Mars: U.S. Geological Survey Scientific Investigations Map 3292. *scale 1:20,000,000, pamphlet 43 p.* doi:https://dx.doi.org/10.3133/sim3292

Wang, C., Manga, M., & Hanna, J. C. (2006). Can freezing cause floods on Mars? *Geophysical Research Letters, 33*(L20202). doi:10.1029/2006GL027471

Warner, N. H., Sowe, M., Gupta, S., Dumke, A., & Goddard, K. (2013). Fill and spill of giant lakes in the eastern Valles Marineris region of Mars. *Geology, 41*, 675-678. doi:10.1130/G34172.1

Warner, N., Gupta, S., Muller, J., Kim, J., & Lin, S. (2009). A refined chronology of catastrophic outflow events in Ares Vallis, Mars. *Earth and Planetary Science Letters, 288*, 58-69. doi:10.1016/j.epsl.2009.09.008

Weiss, D. K., & Head, J. W. (2017). Evidence for stabilization of the ice-cemented cryosphere in earlier martian history: Implications for the current abundance of groundwater at depth on Mars. *Icarus*(288), 120-147. doi:10.1016/j.icarus.2017.01.018

Wordsworth, R. D., Kerber, L., Pierrehumbert, R. T., Forget, F., & Head, J. W. (2015). Comparison of “warm and wet” and “cold and icy” scenarios for early Mars in a 3-D climate model. *JGR: Planets, 120*, 1,201-1,219. doi:10.1002/2015JE004787

Wordsworth, R., Forget, F., Millour, E., Head, J. W., Madeleine, J. B., & Charnay, B. (2013). Global modelling of the early martian climate under a denser CO2 atmosphere: Water cycle and ice evolution. *Icarus, 222*, 1-19. doi:10.1016/j.icarus.2012.09.036

Zegers, T. E., & Roda, M. (2012). Chaotic Terrains on Mars: testing the subsurface lake hypothesis. *Rend. online Soc. Geol. It., 22*, 243-246.

Zegers, T. E., Oosthoek, J. H., Rossi, A. P., Blom, J. K., & Schumacher, S. (2010). Melt and collapse of buried water ice: An alternative hypothesis for the formation of chaotic terrains on Mars. *Earth and Planetary Science Letters, 297*, 496-504. doi:10.1016/j.epsl.2010.06.049